学　位　論　文

2007年度

光　延　　聖

目　次

1. 主論文

The partition behaviors of antimony and arsenic in soil-water system under various redox conditions

（酸化還元状態が変化する環境でのアンチモンおよびヒ素の水—土壌分配挙動に関する研究）

Satoshi Mitsunobu

2. 公表論文

(1) Takahashi Y, Ohtaku N, Mitsunobu S, Yuita K, Nomura M, Determination of the As(III)/As(V) ratio in soil by X-ray absorption near-edge structure (XANES) and its application to the arsenic distribution between soil and water, *Anal. Sci.*, 19, 891-896, 2003.

(2) Mitsunobu S, Takahashi Y, Hirunuma R, Haba H, and Enomoto S, Coupling of ICP-MS and multitracer technique as a new method to investigate dynamics of various elements in soil-water system, *Chem. Lett.*, 34, 980-981, 2005.

(3) Mitsunobu S, Harada T, Hoshino K, and Takahashi Y, X-ray absorption study on the dominance of Sb(V) as secondary antimony species in soil, *Chem. Lett.*, 34, 1656-1657, 2005.

(4) Mitsunobu S and Takahashi Y, Study of the water solubility and sorption on particulate matters of phthalate in the presence of humic acid using ^{14}C labelled di-(2-ethylhexyl)phthalate, *Water, Air, and Soil Pollution*, 175, 99-115, 2006.

(5) Mitsunobu S, Harada T, and Takahashi Y, Comparison of antimony behavior with that of arsenic under various soil redox conditions, *Environ. Sci. Technol.*, 40, 7270-7276, 2006.

(6) Mitsunobu S, Takahashi Y, and Uruga T, Observation of chemical reactions at the solid-water interface by quick XAFS combined with a column reactor, *Anal. Chem.*, 78, 7040-7043, 2006.

(7) Mitsunobu S, Takahashi Y, and Sakai Y, Abiotic reduction of antimony(V) by green rust ($Fe_4(II)Fe_2(III)(OH)_{12}SO_4 \cdot 3H_2O$), *Chemosphere*, 70, 942-947, 2008.

公表論文

1. Takahashi Y, Ohtaku N, Mitsunobu S, Yuita K, Nomura M, Determination of the As(III)/As(V) ratio in soil by X-ray absorption near-edge structure (XANES) and its application to the arsenic distribution between soil and water, *Anal. Sci.*, 19, 891-896, 2003.
2. Mitsunobu S, Takahashi Y, Hirunuma R, Haba H, and Enomoto S, Coupling of ICP-MS and multitracer technique as a new method to investigate dynamics of various elements in soil-water system, *Chem. Lett.*, 34, 980-981, 2005.
3. Mitsunobu S, Harada T, Hoshino K, and Takahashi Y, X-ray absorption study on the dominance of Sb(V) as secondary antimony species in soil, *Chem. Lett.*, 34, 1656-1657, 2005.
4. Mitsunobu S and Takahashi Y, Study of the water solubility and sorption on particulate matters of phthalate in the presence of humic acid using ^{14}C labelled di-(2-ethylhexyl)phthalate, *Water, Air, and Soil Pollution*, 175, 99-115, 2006.
5. Mitsunobu S, Harada T, and Takahashi Y, Comparison of antimony behavior with that of arsenic under various soil redox conditions, *Environ. Sci. Technol.*, 40, 7270-7276, 2006.
6. Mitsunobu S, Takahashi Y, and Uruga T, Observation of chemical reactions at the solid-water interface by quick XAFS combined with a column reactor, *Anal. Chem.*, 78, 7040-7043, 2006.
7. Mitsunobu S, Takahashi Y, and Sakai Y, Abiotic reduction of antimony(V) by green rust ($Fe_4(II)Fe_2(III)(OH)_{12}SO_4 \cdot 3H_2O$), *Chemosphere*, 70, 942-947, 2008.

The partition behaviors of antimony and arsenic in soil-water system under various redox conditions

by

Satoshi Mitsunobu

Department of Earth and Planetary Systems Science,
Graduate School of Science,
Hiroshima University

Abstract

Antimony (Sb) is the 9th most exploited metal worldwide being mined each year. It is heavily used (> 10^5 tons annually worldwide) in non-metal products such as antimony trioxide (Sb_2O_3), primarily in flame retardants in many developed countries. In such countries, Sb concentrations can reach up to 100 times natural level in the proximity of anthropogenic sources, though the typical concentration of dissolved Sb in unpolluted waters are low and less than 1 μg/l. Thus, anthropogenic Sb pollution is often called the "developed-country type pollution" and recently has attained considerable importance in environmental chemistry. However, the geochemical and environmental behavior of Sb has been largely unknown, whereas those of As have been largely studied previously because of the importance as toxic metal. Antimony belongs to group 15 in the periodic table below arsenic (As). The most frequently observed species are Sb(III) and Sb(V) in the environmental samples. The behavior and toxicity of Sb in the environment depend on its oxidation state as is similar to that of As. Therefore, Sb analysis in environmental samples requires quantitative measurement of Sb(III) and Sb(V). The speciation of Sb and As in both solid and water phases were determined to understand the reaction of Sb in soil-water environment and to compare the Sb behavior with As examined in mine tailings (Ichinokawa mine, Ehime, Japan) as a natural system and in a soil-water system simulated in laboratory. In addition, the interaction of Sb with Fe(II)/Fe(III) hydroxide (green rust, GR) which is considered as a strong abiotic reducer occurring in soil and sediment was also studied to examine the potential of GR as a reductant of Sb(V). X-ray absorption fine structure (XAFS) and HPLC-ICP-MS were used for the speciation methods in solid and water phases, respectively.

Sb and As behaviors in soil-water systems under various redox conditions.

In the Ichinokawa soil and water systems, Sb was present dominantly as the oxidized form, Sb(V), over a wide redox range (from Eh = 360 to −140 mV, pH 8), while As was present as a mixture of As(III) and As(V). This finding was confirmed in the laboratory experiments. These results suggest that Sb(V) is a very stable form in the environment and that Sb is oxidized under more reductive condition than As. Combining the results of Fe and Mn XAFS analyses with a positive correlation among Sb, As, and Fe abundances in the soil, it is suggested that the host phases of Sb and As are amorphous Fe(III) hydroxide under all the redox conditions examined in the natural and synthetic systems. Direct speciations of Sb and As by their EXAFS analyses are also consistent with this finding. Under reducing condition, concentration of As in the soil water increased with Fe and Mn concentrations in both Ichinokawa and laboratory experiment systems. These results suggest that the As release from soil depends on (i) the reductive dissolution of Fe(III) hydroxide (= host-phase of As in soil) and (ii) the reduction of As(V) to As(III), since As(III) is more mobile than As(V). On the other hand, Sb abundance in soil water decreased under reducing condition and Sb in the soil water was predominantly in the oxidized form, Sb(V), opposite to the findings of As. In addition, Fe XANES analysis shows that Fe(III) hydroxide in the soil keeps its potential as adsorbent and

host-phase for Sb even under reducing condition, which suggests that the decline of Sb abundance in reducing soil water may be due to a change of Sb species. Microscopic observation of Ichinokawa soil grains using μ-XAFS shows that significant Sb(III) was locally observed at the rim of the Fe hydroxide particles, while Sb(III) was not observed at the core of the particle. In addition, a small amount of Sb(III) was observed both in soil and soil water phases under reducing condition in the bulk analysis. It is reported that the solubility of Sb(III) is much lower than that of Sb(V) Therefore, the findings obtained by the microscopic analysis suggest that Sb reduced to Sb(III) was precipitated on the mineral surface due to its low solubility and that the precipitates containing Sb(III) like Sb_2O_3 may cause the fixation of Sb to the solid phase under reducing condition.

Interaction of Sb(V) with GR.

Sb(V) is partly reduced by sulphate GR, suggesting that GR can be one of the important reducing agents for Sb(V) and that GR can influence the Sb mobility in suboxic environments where GR is formed. It was shown that Sb(V) is adsorbed to GR with an inner-sphere complex on the surface, and that the surface complex species is a mixture of edge- and corner-sharing complexes based on the EXAFS analysis. The conversion of "metastable" GR to magnetite and lepidocrocite was inhibited in the presence of Sb, showing the stabilization effect of GR Sb. The degree of stabilization increased with the increase in the Sb concentration in aqueous phase in the Sb concentration range in this study. This stabilization effect for GR was also reported for other oxyanions that are adsorbed to GR by the formation of inner-sphere complexes such as phosphate, arsenate, and silicate. Thus, it is suggested that the Sb inner-sphere complex to GR also contributes to the GR stabilization by Sb.

In this work, it was shown that the change of Sb solubility accompanied with the change of the oxidation state controls the partition behavior of Sb in soil-water system under various redox conditions. Actually, much lower Sb(III) solubility than Sb(V) (the difference > 10^5 order) controls the Sb partition behavior in soil-water system under reducing condition, while As(III) solubility is higher than As(V) in the case of As. Thus, to comprehend the fate and transport of Sb in aquatic environment, the determination of the "species", particular oxidation states, is much important. Comparing the behaviors of Sb and As in environment, the solubilities of Sb(III) and Sb(V) are wholly lower than those of As(III) and As(V), respectively. Since the solubility of Sb(III) is particularly lower than As(III) with more than 10^{10} order, the mobility of Sb in aqueous environment is largely different from that of As under redox condition where Sb(III) can occur. In addition, the different redox properties of Sb and As observed in present study is of great importance to an understanding of the behaviors of As and Sb and their fractionation in natural aquifer.

CONTENTS

CHAPTER 1 Introduction

This study focuses on the speciation of antimony (Sb) and arsenic (As) in both solid and water phases to understand the reaction of Sb and As in soil-water environment and to compare the Sb behavior with As under various redox conditions. First, the physicochemical properties, uses, toxicity, and occurrence of Sb or Sb compounds are summarized as Introduction section of the thesis based on the previous references. Next, the previous study for Sb geochemistry, environmental chemistry, and the objective of this study are also described in this chapter.

1-1 Antimony

A good deal of research on geochemical and biogeochemical processes in natural waters has been, and continues to be, devoted to trace elements, particularly transition metals. Rather less attention has been focused on the so-called metalloid elements. Among them, Sb is the one that has received the scientist attentions. Sb is a toxic element widely distributed in the lithosphere and mainly associated with As as sulfide or oxide. Antimony is a naturally occurring element. It belongs to the group 15 of the periodic table of the elements. Sb can exist in a variety of oxidation states (-III, 0, III, V) but it is mainly found in two oxidation states (III and V) in environmental, biological and geochemical samples. The relative abundance of Sb in different terrestrial systems is given in Table 1-1. According to the classical classification of Goldschmidt, Sb is a strong chalcophile element and as such mainly occurs in nature as Sb_2S_3 (stibnite) and Sb_2O_3 (valentinite or senarmontite), which is a transformation product of stibnite. These compounds of Sb are commonly found in ores of copper, silver, and lead. Sb is also a common component of coal and petroleum. Little information is available on the transformation and transport of Sb in the different environmental compartments. Even information on Sb speciation and total content in the various media is scarce and often contradictory. This lack of understanding of Sb behavior and fate in the environment hinders further research.

Table 1-1 Antimony abundance

Material	Sb[a]	Reference
Cosmic abundance	0.246[b]	Suess and Urey, 1956
C1 chondrites	0.142	Anderse and Grevesse, 1989
Mean crustal average	0.2	Taylor and McLennan, 1985
Upper continental crust	0.31	Wedepohl, 1995
Lower continental crust	0.30	Filella et al., 2002
Terrestrial abundance	0.7	Boyle and Jonasson, 1973
Basic rocks (basalt)	0.6	Turekian and Wedepohl, 1961
Granitic rocks	0.2	
Sedimentary rocks		
Shales	1-2	Turekian and Wedepohl, 1961
Carbonates	0.2	Turekian and Wedepohl, 1961
Deep sea clays	1	Turekian and Wedepohl, 1961

[a]All values in ppm, except for the cosmic abundance.

[b]Atomic abundance relative to Si (= 1,000,000) deduced from the following mean composition of meteorites: silicate = 100, sulfide = 7, metal = 10.6 parts per weight.

Table 1-2 Properties of the element antimony and arsenic[a].

Property (unit)	Sb	As
General		
Chemical series	metalloid	metalloid
Atomic number	51	33
Periodic table group	15	15
Bloch	p	p
Electronic configration		
Ground state electron configration	[Kr] 4d10 5s2 5p3	[Ar] 3d10 4s2 4p3
Shell structure	2. 8. 18. 18. 5	2. 8. 18. 5
Atomic mass (relative to ^{12}C = 12,000) (g)	121.75(3)	74.9216
Naturally occurring isotopes	^{121}Sb (57.21%) ^{123}Sb (42.79%)	^{75}As (100%)
Neutral radii (pm)		
Empirical atomic radius	145[b]	115[b]
Calculated atomic radius	133[c]	114[c]
Covalent radius	140	119
Electronegativity (Pauling unit)	2.05	2.18
Ionisation energies (kJ/mol)		
1st	834	947
2nd	1594.9	1798
3nd	2440	2735
4th	4260	4837
5th	5400	6043
6th	10400	12310

[a] When not explicity stated, values from Emsley (1992), Huheele et al. (1993), Greenwood and Earnshaw (1997), Lueth (1999), and Winter (2001)

[b] Slater (1964)

[c] Clementi and Raimondi (1963)

enrichments of Sb extending back to Roman times, indicating that the anthropogenic fluxes of this metal have exceeded natural ones for more than 2000 years. The present day enrichment factor is of the order of 70 times (for comparison, it is 20 for As, 130 for Pb) (Shotyk et al., 1996).

Sb is the ninth most exploited metal worldwide being mined each year. World reserves of Sb are in excess of 2 million tons and are located principally in Bolivia, China, Russia, South Africa, and Mexico (Carlin, 2000). Current world production of Sb is about 140,000 tons per year. Table 1-3 shows world mine production by the main producing countries in 1999. Stibnite, Sb_2S_3, is the most important ore of Sb and it occurs in large quantities in China, South Africa, Mexico, Bolivia, and Chile. Other sulfide ores include ullumanite (NiSbS), livingstonite ($HgSb_4S_8$), tetrahedrite (Cu_3SbS_3), wolfsbergite ($CuSbS_2$), and jamesonite ($FePb_4Sb_6S_{14}$). Indeed, complex ores containing Pb, Cu, Ag, and Hg are an important industrial source of Sb. Small amounts of oxide minerals formed by weathering are also known, e.g. valentinite (Sb_2O_3), cervantite (Sb_2O_4), and stibiconite ($Sb_2O_4 \cdot H_2O$), and minor finds of native Sb have occasionally been reported. Commercial ores have 5-60% Sb, and recovery methods depend on the grade. Low-grade sulfide ores (5-25% Sb) are volatilized as the oxide.

Sb compounds such as AlSb, GaSb, InSb is used in semiconductors for making infrared detectors, diodes and Hall-effect devices. The presence of Sb greatly increases the hardness and the mechanical strength of lead. Batteries, antifriction alloys, type-metal, small arms and tracer bullets, and cable sheathing are the main products containing Sb. Sb trioxide, Sb_2O_3, has many uses including as a flame-proof retardant and catalyst of textiles, papers, plastics and adhesives; as a paint pigment, ceramic opacifier, catalyst, mordant and glass decolouriser. Sb tetroxide, Sb_4O_8 is used as an oxidation catalyst, particularly for the oxidative dehydrogenation of olefins.

For years, the major industrial use of Sb was the production of alloys (Table 1-4). Nowadays, Sb is mostly used in large quantities as a flame retarding additive. The situation has largely evolved from the early 1950s when Sb was qualified as a "cheap metal which can be used in certain instances as a substitute for more expensive metals"

Table 1-3 World mine production of antimony by country in 1999 (Carlin, 2000).

Country	Sb production (metric tons)
Bolivia	5000
China	120,000
Kyrgyzstan	200
Russia	3000
South Africa	3000
Tajilistan	1200
USA	480
Other countries	5000
Total	138,000

Table 1-4 Some uses of antimony alloys.

Use	Sb/Pb batteries	Bearings	Ammunition	Solder	Type metal	Sheet pipe	Other metal	Non-metal products
Sb/tonnes	4143	365	216	121	68	55	144	6657
Percentage	35	3.5	1.8	1.0	0.6	0.5	1.2	56.5

(Latimer and Hildebrand, 1951). In 1999, the USA consumption of Sb was 36,480 tons domestic mine production plus secondary production from old scrap plus net import reliance) ▪ and the estimated distribution of Sb uses was as follows: flame retardants, 55%; transportation, including batteries, 18%; chemicals, 10%; ceramics and glass, 7%; and other, 10% (Carlin, 2000).

Sb is used in certain therapeutic agents against major tropical diseases, although in recent years, it has been increasingly replaced by other agents. Sb is still the treatment of choice for several tropical protozoan diseases, such as leishmaniasis, schistosomiasis, ascariasis, trypanosomasis and bilharziasis. Pentostam and Glucantime, pentavalent Sb-containing drugs, are widely used in the treatment of leishmaniasis ▪ (Berman, 1988). Sb compounds were once used in the treatment of syphilis.

Traditionally, the bulk of secondary Sb has been recovered as antimonial lead, most of which was generated and then also consumed by the battery industry. However, the current trend to avoid the use of Sb in lead alloys towards its use in fire-retardant treatments and other applications, which do not permit recycling, have caused lesser amounts of secondary Sb to be produced. This decrease in Sb recycling is of environmental concern.

Toxicity

Sb and its compounds were considered as pollutants of priority interest by the Environmental Protection Agency of the United States (USEPA, 1979) and the European Union (Council of the European Communities, 1976). The USEPA drinking water standards are: maximum contaminant level goal (MCLG) ▪ and maximum contaminant level (MCL), both 6 μg/L (USEPA, 1999). The European Union established a maximum admissible concentration of Sb in drinking water of 5 μg/L (Council of the European Union, 1998). Sb is on the list of hazardous substances under the Basel convention concerning the restriction of transfer of hazardous waste across borders (United Nations Environmental Program, 1999).

Sb has no known biological function and, like As, it is toxic. The toxicity of

inorganic Sb is assumed to be similar to that of As and also depends on the oxidation state; Sb(III) species are reported to be more toxic than Sb(V) forms (Bencze, 1994). Toxicities of Sb compounds are summarized in Table 1-5.

Sb is usually present at levels less than 1.0 μg/g in all human tissues. Lung, lymph nodes and hair contain the largest amounts (Fergusson, 1990; Emsley, 1991). Most of the work on the toxic effects of Sb has been focused on its uses in medicine or on occupational exposure. The small number of laboratory animal experiments have tended to involve forms of Sb, doses and routes of administration, which are not relevant to its possible effects as an environmental pollutant.

Occurrences in natural system

Sb is present in the aquatic environment as a result of rock weathering, soil runoff and anthropogenic activities. Typical concentrations of dissolved Sb in unpolluted waters are less than 1 μg/L. However, in the proximity of anthropogenic sources, concentrations can reach up to 100 times natural levels. Sb is present in substantial concentrations in precipitates from hot springs and boreholes and in geothermal waters. Concentrations ranging from 500 μg/L up to 10 wt% have been reported (Ritchie, 1961; Sabadell and Axtmann, 1975; Weissberg et al., 1979; Stauffer and Thompson, 1984). Field data are sparse on Sb pollution caused by the proximity of geothermal areas. Klein et al. (1975) suggested that, at that time, Sb weathering and mobilization from these areas might largely exceed mobilization from industrial operations but this hypothesis was not further investigated. Total concentrations of Sb present in aqueous and solid environmental samples can be readily determined using present day analytical techniques. This has primarily resulted from the development of microwave-digestion techniques for solid samples and NAA and plasma-based analyte detection systems. Both ICP-AES and ICP-MS techniques are nowadays widely used, with ICP-MS having less spectral interferences and a lower detection limit (pg/ml). Determination of Sb speciation still represents a challenging analytical problem. Data reported in the literature are almost exclusively based on hydride generation methods and often only oxidation state data are obtained. Antimony concentration values given in the following sections correspond to Sb contents in filtered samples (usually, 0.45 μm

Table 1-5 Acute toxicity of Sb compounds.

Sb compound		Target	Administration		(mg/kg-weight)	
Name	M Fotmula		Path		as Compounds	as Element
Antimony metal	Sb	Rat	Oral	LD_{50}	100	100
		Rat	Intra-abdominal injection	LD_{50}	100	100
Stibnite	SbH_3	Mouse	Inhalation	MLD	0.1 mg/m^3/4hr	-
		Rat	Intravenous injection	LD_{50}	8	7.81
Antimony trioxide	Sb_2O_3	Rat	Oral	LD_{50}	> 20000	> 16700
Antimony pentaoxide	Sb_2O_5	Rat	Intra-abdominal injection	LD_{50}	4000	3010
Antimony pentachloride	$SbCl_5$	Rat	Oral	LD_{50}	675	275
		Mankind	Inhalation	MLD	131 mg/m^3/4hr	-
Antimony trisulfide	Sb_2S_3	Rat	Intra-abdominal injection	MLD	1000	717
		Mankind	Inhalation	MLD	0.565 mg/m^3/4hr	-
Antimony pentasulfide	Sb_2S_5	Rat	Intra-abdominal injection	LD_{50}	1500	-
Antimony potassium tartarate	$K(SbO)C_4H_4O_6 \cdot (1/2)H_2O$	Mouse	Oral	LD_{50}	600	222
		Mouse	Intra-abdominal injection	LD_{50}	50	18.5
		Mouse	Intravenous injection	LD_{50}	42	15.7
		Mouse	Hypodermic injection	LD_{50}	55	20.1
		Rat	Oral	LD_{50}	115	42.0
		Rabit	Oral	LD_{50}	115	42.0
Antimony sodium tartarate	$Na(SbO)C_4H_4O_6 \cdot (1/2)H_2O$	Mouse	Intra-abdominal injection	LD_{50}	60	43.4
		Mouse	Intravenous injection	LD_{50}	25	-

pore size filters). The few studies where Sb contents in the particulate fraction are also given (Van der Weijden et al., 1989; Sinemus et al., 1992; Tanizaki et al., 1992a,b; Guieu et al., 1993; Jarvie et al., 2000) show that Sb exists almost exclusively in the dissolved fraction.

The distribution and speciation of Sb in freshwater systems have not been extensively studied. Concentrations range from a few ng/L to a few μg/L depending on location, thus reflecting the wide range of physical and chemical conditions existing in freshwater systems and the proximity of pollution sources (e.g. Mok and Wai, 1987, 1990; Mohammad et al., 1990; Ulrich, 1998).

Sb concentrations in sediments and soils are of the order of a few μg/g. Higher concentrations are directly related to anthropogenic sources, mainly proximity to smelting plants (O'Toole et al., 1971; Crecelius et al., 1974; Cawse et al., 1975; Ragaini et al., 1977; Ainsworth et al., 1990a; Asami et al., 1992). Elevated concentrations in sediments near the outfalls of sewage and fertilizer facilities have also been reported (Papakostidis et al., 1975; Grimanis et al., 1977). Unfortunately, not much is known about Sb mobility in soils. According to the Toxics Release Inventory (USEPA, 1998), Sb and Sb compounds releases to land and water in the US totaled 5.5 million kg from 1987 to 1993. These releases were nearly all on land (land: 5,456,079 kg, water: 150,029 kg). Sb fate in soils may thus be a key element in Sb cycling in the environment. The few data available points to an Sb accumulation near the soil surface, followed by a concentration decrease with depth (Ragaini et al., 1977; Ainsworth et al., 1990a). This indicates that the source is most probably atmospheric and that Sb is rather non-reactive in these media. Sb in geogenetically polluted soils is mostly immobile according to Hammel et al. (1998). It is possible that much of the Sb in contaminated soils remains as the non-reactive oxides when it is deposited in this form. On the other hand, Sb in contaminated soils does not seem to be readily bioavailable, its concentrations in invertebrates and the shrews that feed on them have been measured and no significant increase has been observed (Ainsworth et al., 1990b). High Sb concentrations are generally associated with high As concentrations in sulfide ores and the use of Sb concentration in soils has been proposed as pathfinder for gold,

confirming the chalcophilic nature of this element (Hawkes and Webb, 1962; Hale, 1981).

Relatively little is known about the origins and presence of Sb in waste and in waste incineration. During the last three years, there has been increasing interest in that topic. The thermal treatment of municipal waste is a useful tool for the study of the presence of Sb in waste. This is because the various product streams of waste incineration can be chemically analyzed and material balances prepared.

Several studies about the Sb content in various waste streams are available. Van der Beek et al. (1987) studied the Sb concentrations in collected municipal waste in Amsterdam, Arnhem and Rotterdam in the Netherlands. The study was concerned with typical small household waste (vegetables, fruits, paper, plastics, glass, bread, and carpet), in which an average concentration of 2.9 mg/kg for wet and 5.2 mg/kg for dry waste was determined.

Much higher values are reported by Hesseling (1987) for mixed waste fed to Dutch Waste Incineration Installation. Here, an average input concentration of 20 mg/kg was calculated. Antiomny is found in the slag, in the residues of the electrostatic precipitator (electrofilter) and in the fly ash. The concentrations are reported in Table 1-6, expressed in mg Sb per kg of original dry waste.

In this context, the work of Reimann (1989, 1995) is of great importance. The author carried out extensive chemical analyses of the various residues from the waste incineration plant at Bamberg, preparing mass balances for every single component (Reimann, 1989). In 1995, a special study was dedicated to Sb. The total average Sb concentration of the incoming waste was found to be 38 mg/kg (Reimann, 1995), which is considerably higher than the 20 mg/kg reported be Hesseling (1987).

Other sources report average Sb concentrations of 42±2 mg/kg and a range of 10-60 mg/kg (IAWG, 1995). All reported values are in the same order of magnitude, but there are important deviations from case to case. The data of the various are summarized in Table 1-6.

The different composition of the various input waste streams is most probably the reason for the discrepancies. The material burned in the waste incinerator at

Table 1-6 Antimony flows and concentrations in several urban/industrial waste incinerators. Data given in mg/kg original dry waste.

Waste stream	Netherlands	Bamberg	Switzerland (EAWAG)	IAWG (Internat.)
Bottom ash	13 ± 6	1 - 37	6 ± 2	3 -24
Electrofilter precipitate	6 ± 5	2 - 29	36 ± 2	7 - 36
Fly ash	1 ± 1	< 0.1	< 0.5	< 0.5
Total	20 ± 8	3 - 65	42 ± 3	10 - 60

Bembrg (Reimann, 1995) is well defined and consists of a mixture of 44% municipal waste, 43% industrial waste and 13% dewatered sludge. The exact composition of the other wastes in the Netherlands (Hesseling, 1987), in Switzerland and from the incinerator source (IAWG, 1995) was not reported, but it is likely that the share of industrial waste in Bemberg and in the Swiss example is higher than in the other two cases.

The Sb concentration in industrial waste, which yield and adequate explanation for the different Sb concentrations found in the various input waste stream. Additionally, it must be noted that the range of variation of all measured concentrations is very large. Reimann (1995) reported a bandwidth of 3 to 65 mg/kg for his average of 38 mg/kg Sb. This very large range is probably caused be the continuously changing composition of the solid refuse that is offered for incineration.

Interactions with inorganic ligands in solution chemistry

Both Sb(III) and Sb(V) ions hydrolyse easily in aqueous solution, thus making it difficult to keep Sb ions stable in solution except in highly acidic media. Since most of the techniques used for the study of solution equilibria (solubility measurements, potentiometry, voltammetry, spectroscopy) necessitate the use of macro amounts of reactants, relatively little information is available on the chemical species of Sb existing in aqueous solution, and their stability constants in particular.

(1) Hydroxyl

Sb usually exists as Sb(V) in solution under oxic conditions. As first pointed out by Pauling (1933), the coordination of Sb(V) with oxygen is quite different from that of As(V) and P(V). Based on its larger ionic radius and lower charge density, this author suggested that Sb should be octahedrally coordinated with oxygen in its compounds rather than tetrahedrally like As(V) and P(V) are. The $HSbO_3$ formulation has also been used. Antimonic acid cannot be isolated as a pure phase; it is a relatively strong acid that condenses to form polymers as the pH increases (Jander and Ostmann, 1962a,b; Ricca et al., 1965). SbO_2^+ is the species existing in solution under very acidic conditions and $[Sb(OH)_6]^-$ (or SbO_3^-) is the main species present in mildly acidic,

neutral, and alkaline conditions (Ricca and D'Amore, 1965). The Sb pentoxide, Sb_2O_5, is hardly soluble in water and generates the antimonate anion upon dissolution. Alkali metal hydroxoantimonate salts are also sparingly soluble in water (Blandamer et al., 1974).

The relatively low solubility of the Sb trioxide, Sb_2O_3, in water has traditionally limited the amount of physical and chemical evidence gathered on the actual structures of the ionic species formed by Sb(III) in solution. In the pH range 2–10, the solubility of Sb_2O_3 is independent of pH, thus indicating the formation of an undissociated substance, Sb hydroxide $Sb(OH)_3$ (or SbO(OH)), sometimes called meta-antimonious acid ($HSbO_2$). Sb(III) is present as SbO^+(or $Sb(OH)_2^+$) in acidic media and as $Sb(OH)^{4-}$ (or hydrated SbO_2^-) in basic media (Ahrland and Bovin, 1974; Antonovich et al., 1977). Species such as $SbOH^{2+}$ (Ahrland and Bovin, 1974; Antonovich et al., 1977) and $Sb_2(OH)_2^{4+}$ (Ahrland and Bovin, 1974) have also been reported. The free Sb^{3+} ion is stable in solution only at very high acidities.

Shoji et al. (1974) studied the hydrolysis of Sb(III) through solvent extraction with dithizone–carbon tetrachloride solutions and radiotracers. This technique allowed these authors to work at a trace concentration of Sb ($< 10^{-8}$ mol/l). Under these conditions, they found a monovalent ion, $Sb(OH)^{2+}$, and a neutral species, $Sb(OH)_3^0$, to be the predominant species in strongly acidic media and in the weakly acidic-neutral region, respectively. No evidence was found for the formation of any polymerized species.

(2) Chloride

Sb(III) chloride, which is often used as a standard substance for Sb(III), dissolves in strong HCl solutions. Successive chlorocomplexes, $SbCl_x^{[(x-)+3]+}$, are formed in solution depending on the chloride concentration present. Some authors have postulated the formation of the limiting species $SbCl_4^-$ (Bond and Waugh, 1970; Biernat et al., 1975), while others favor $SbCl_5^{2-}$ (Fridman et al., 1965; Kondziela and Biernat, 1975) or $SbCl_6^{3-}$ formation (Milne, 1975). Upon dilution, they extensively hydrolyze to SbOCl, which is not very soluble. It is important to point out that all the

studies involving Sb(III) and chloride have been performed in very acidic solutions that usually contained chloride concentrations much higher (up to 12 mol/l HCl) than those existing in seawater (≈ 0.7 mol/l Cl^-). According to Strohal et al. (1975), nonchloride-containing Sb(III) species may in fact predominate in seawater. Recently, extended X-ray absorption fine structure (EXAFS) of $SbCl_3$-containing solutions demonstrated the existence of aqueous inner sphere complexes of Sb(III)–chloride at 25°C (Oelkers et al., 1998). There is no evidence for any slow reaction occurring among Sb(III) species in HCl solutions.

Not many studies on Sb(V) interactions with chloride exist. Fridman et al. (1965) have shown, based on absorption data, that $SbCl_x^{[(x-)+5]+}$ species are only formed in strongly acidic solutions and that, in dilute acid solutions, hydrolyzed species such as $Sb(OH)Cl_5^-$ are most probably present. It has been suggested (Gilbert and Hume, 1973) that Sb(V) exists mainly as highly polymerised hydroxy-chloro complexes or as colloidal hydrous oxides in seawater but no evidence was produced. The kinetics of exchange of Sb between Sb(III) and Sb(V) in HCl solutions is rather slow (Neumann and Ramette, 1956). This has been attributed to one or more slow steps taking place in the parallel Sb(V) hydrolysis.

(3) Sulfide

Analytical chemists have known for many years that Sb(III) compounds are soluble in alkaline sulfide solutions (due to the formation of antimonites). Surprisingly, there is still considerable uncertainty regarding the stoichiometry of the species formed in these reactions. As mentioned above, the Sb–sulfide system has been the object of considerable attention due to its relevance for hydrothermal solutions. They differ widely from each other. Discrepancies among published results may be due to: (i) the somewhat wide range of Na_2S concentrations employed in the different studies; (ii) the oxidation in air of Sb(III) species, present in Na_2S solutions in equilibrium with stibnite, to Sb(V) species such as SbS_4^{3-}; (iii) solid phases other than the phases of interest being present in the experimental solutions (i.e. $Sb_2O_3(s)$); (iv) the nature of Sb_2S_3 used in the experiments, crystalline or amorphous (not always identified); and (v) the different

experimental pH ranges used (not always given). However, much of the difficulty in determining the speciation may be attributed to the inability of the traditionally used solubility and potentiometric methods to differentiate precisely among species with similar metal/S ratios (case of polymeric species). Stoichiometry often appears to have been simply assumed rather than proved. Moreover, most of the results do not apply to conditions existing in natural waters because the experimental concentrations used are too high and the pH ranges too basic. In particular, formation of polymerized species in real systems should be viewed with caution.

More recently, the application of spectroscopic methods, such as Raman spectroscopy (Wood, 1989; Gushchina et al., 2000) and EXAFS (Mosselmans et al., 2000; Sherman et al., 2000) has been attempted. One limitation of the Raman spectroscopic method is the need for a relatively high concentration of the scattering species. Moreover, the thioSb species do not give rise to very intense Raman lines and their concentration in solution is limited by the low solubility of stibnite. Thus, only solutions with relatively high Na_2S concentrations (>1 m or mol/l) and high pH (>12) result in sufficient concentration of thioSb species. This means that other possible species, which may be formed at more realistic environmental sulfide concentrations and pH values, will remain undetected. However, a conclusion of Wood's (1989) study merits attention, namely, that it is very unlikely for polymeric species to be present in solutions with Sb concentrations below 0.1 M. According to this author, probably no polymer was ever present in most of the studies. In an attempt to clarify Sb speciation in sulfidic solutions, ab initio quantum mechanical calculations were applied to Wood's Raman data by Tossell (1994). These calculations identified a different set of species as being those most probably formed in solution. An interesting point is that the Sb(V) species SbS_4^{3-} (four-coordinate Sb(V)) was found to show Raman peaks in aqueous solution (Mikenda and Preisinger, 1980) close to the values observed by Wood (1989) for sulfidic solutions in equilibrium with Sb_2S_3 (three-coordinate Sb(III)). It was commonly thought that only when the Sb source was pentavalent could Sb(V) compounds be observed, but EXAFS studies (Mosselmans et al., 2000; Sherman et al., 2000) have shown the formation of Sb(V) thioanions upon

dissolution of stibnite in deoxygenated aqueous NaHS solutions.

In some studies, the "solid phase" in equilibrium with the solution is not crystalline stibnite but some colloidal or amorphous Sb_2S_3. Thioantimonite complexes tend to condense to form large polymeric molecules, whose composition could be written as $(Sb_2S_3)\cdot nH_2S$ and whose stoichiometries approach that of Sb_2S_3 for large values of n. Consequently, the "equilibrium concentrations" measured in solubility studies using amorphous Sb sulfide are approximately one and a half orders of magnitude higher than those measured in the presence of crystalline stibnite (Krupp, 1988). It must be mentioned that systems containing colloidal species, often considered as a nuisance by the experimenters, are in fact closer to real anoxic water systems than systems with crystalline stibnite.

1-2 Previous study for Sb geochemistry and environmental chemistry

It is nowadays well recognized that the understanding of biogeochemical processes depends upon the knowledge of the chemical forms, or species, that are present in the natural environment. Despite this well-known requirement, the speciation of many elements in the natural environments is not adequately known. Sb is not an exception.

Speciation of Sb in water phases

Antimony occurs in two oxidation states in natural waters and, thus, its behavior can be affected by changes in the redox status of the aquatic environment. As pointed out above, studies on Sb speciation have mainly focused on the separation and identification of Sb(III) and Sb(V) species. Determination of tri-methylated Sb species has also received some attention.

Sb(V) is the predominant species present in oxygenated systems but thermodynamically unstable Sb(III) has also been detected in different marine water (Cutter, 1991; Cutter et al., 1991, 2001; Sun et al., 1993; Takayanagi and Michel, 1996; Cutter and Cutter, 1998), freshwater (Mohammad et al., 1990; Sun et al., 1993; Takayanagi and Cossa, 1997; Hou and Narasaki, 1999; Deng et al., 2000), groundwater

(Sun et al., 1993) and rain water (Cutter et al., 1991). This is in contrast with thermodynamic equilibrium predictions, which suggest that Sb(V) concentration should exceed Sb(III) by several orders of magnitude.

For thermodynamically unstable species to be present in water, mechanisms for their production and slow rates of interconversion must exist. Most authors invoke biological activity as the cause for Sb(III) presence. Although possible, a detailed analysis of published data shows that too often there is no proof to validate this hypothesis: Bertine and Lee, (1983) observed a surface enrichment of Sb(III) in Saanlich Inlet, Canada, and suggested that Sb(III) production occurs in the photic zone. Andreae and Froelich (1984) observed a maximum of Sb(III) in the surface mixed layer of the Baltic Sea and attributed it to the presence of biological activity in this layer. In the surface layer of this lake, Sb(III) and Sb(V) coexist at a similar concentration level. Only two studies are universally cited to support the biological origin of the presence of Sb(III) in oxic waters: Kantin (1983) and Andreae and Froelich (1984).

Persistence of Sb(III) in oxic waters requires kinetic stabilization. Cutter(1992) estimated a pseudo first-order rate constant of 0.008 day^{-1} (residence time =1/k = 125 days) for Sb(III) removal in oxic waters of the Black Sea. This rate includes all forms of removal (i.e., oxidation but also scavenging by adsorption to particles). A recent study, where Sb(III) was completely oxidized by amorphous iron (5 days) and manganese (3 days) oxyhydroxides, showed that Sb(III) can persist in an oxidizing environment for short periods of time (Belzile et al., 2001). Thus, the above rate constant should be considered as a maximum estimation because it was calculated at the suboxic–oxic interface of the Black Sea where the presence of manganese and iron oxides is likely to increase the rate. Possible stabilization of Sb(III) in natural aquatic systems by the presence of organic matter could not be discarded; Sb(III) oxidation is known to be prevented by some organic ligands such as tartaric acid (Sun et al., 1982; Abbasi, 1989).

The true speciation of Sb under anoxic conditions remains unclear. On the basis of thermodynamic calculations, Sb should be completely present in the trivalent form in the absence of oxygen. However, the occurrence of oxidized Sb species in anoxic waters has been reported in different systems. In the Saanich Inlet, Bertine and

Lee(1983) found that only about 50% of Sb exists as Sb(III)+Sb(III)-S. In the Baltic Sea, Sb(III) accounted for 44% of total inorganic Sb; only in the deepest sample did this percentage increase to 93%, more as a result of a decrease in total Sb rather than an increase in Sb(III) (Andreae and Froelich, 1984). In the Black Sea, Cutter (1991) reported that Sb(III) concentrations increased rapidly near the sulfide interface (up to 94% of total Sb).

A variety of mechanisms has been postulated to explain these results, including (i) delivery of Sb(V) on sinking detritus from oxic waters (Cutter, 1991, 1992), (ii) formation of thiocomplexes by the pentavalent element (Bertine and Lee, 1983; Andreae and Froelich, 1984), and (iii) advection of surface waters containing high concentrations of antimonate (Cutter, 1991). All these mechanisms must be coupled with relatively slow rates of reduction for As(V). Only one value for a pseudo first-order rate constant (0.0004 $year^{-1}$) for the reduction of antimonate has been estimated using Black Sea data by Cutter (1991).

Efficient removal of Sb has been observed close to the oxic–anoxic interface (Cutter et al., 1991). This has been attributed to the adsorption of Sb onto manganese and iron oxide particles. The very low concentrations of Sb detected in Lake Pavin at pH 7 and pe below 4.2 (Takayanagi and Cossa, 1997) have been attributed to the formation of insoluble Sb sulfide.

Speciation of Sb in solid phases

Very scarce information exists on Sb interaction with solid phase such as soil, sediment, and metal colloids compared with in water phase (Filella et al., 2002 and reference therein). Indirect indications of Sb affinity for different substrates in soils and sediments can be obtained by application of sequential extraction procedures. Over half of the Sb in non-contaminated Puget Sound muds appeared to be bound to extractable iron and Al compounds (oxalate extraction) (Crecelius et al., 1975). In two contaminated sediments near a copper smelter, < 20% Sb was bound to extractable iron and Al compounds and most of Sb was present in a rather chemically stable form, probably the slag particles (Crecelius et al., 1975). Application of a sequential selective

extraction procedure to a broad range of anaerobic American sediments (Sb content, 0.5–17.5 μg/g) revealed that most native (and added) sediment Sb was associated with relatively immobile (i.e. oxalate soluble) iron and Al compounds (Brannon and Patrick, 1985). When sediments were incubated with added Sb (addition of a 1000 μg/l solution of Sb potassium tartrate, followed by 45 days incubation at 20°C), significant amounts of Sb were also found in the interstitial water and in the "exchangeable" fraction (Brannon and Patrick, 1985). A sequential leaching technique was applied to forest soil (Oh horizon only) contaminated by Chernobyl fallout (Carbol et al., 1995). Results obtained showed that 50% of the Sb was present in the ionexchangeable fraction. Of the remaining Sb, about 25% was present in the organic fraction and the rest could be classified as strongly bound to soil grains, especially the silt–clay fraction. Abtimony was more loosely bound to Oh horizon material than ^{137}Cs. In contrast, application of a sequential extraction technique to soils situated near an Sb smelter showed that more than 60% of total Sb was present in the most refractory (1 h aqua regia, 100°C, extraction) form while less than 10% was either soluble or present in ion-exchangeable sites (Ainsworth and Cooke, 1991). Antimony was found mostly associated with amorphous and crystalline iron oxyhydroxides in bottom sediments of the Garonne River (Leleyter and Probst, 1999). Existing data seem to indicate that Sb is significantly associated with relatively immobile compounds in soils and sediments.

Both Sb(III) and Sb(V) appear to bind strongly to hydroxides of Fe and Mn and only weakly to clay minerals. Thanabalasingam and Pikering (1990) reported that the hydrous oxide of Mn, Fe, and Al avidity sorbed antimony from dilute (μmol/L) $Sb(OH)_3^0$ solutions, with uptake leveling off as the initial antimony concentration increased. Capacity values decreased along the sequence MnOOH > $Al(OH)_3$ > FeOOH. The amount sorbed by each substrate decreased gradually at pH values >6, as expected for anionic species. Addition of 0.4 mol/l CH_3COONa to the aqueous phase to minimize retention of weakly bound Sb had little effect on MnOOH uptake capacity (~160 μmol/kg at pH < 7) but retention dropped rapidly at higher pH. With the other two substrate, sorption capacity were (pH 6-7): ~45 μmol/kg FeOOH and ~33 μmol/kg $Al(OH)_3$, with Sb sorption tending to a peak in the pH 7-8 region. Adsorption of Sb(III) onto

ferrihydrite was described by Enders and Jekel (1996) in terms of the triple layer model; the formation of mono-(SO-$Sb(OH)_2$) and binuclear ($(SO)_2$-$SbOH$) complexes at the surface was assumed.

Sb(V) adsorption on high purity hematite was studied by emission Mössbauer spectroscopy (Ambe et al., 1986). Strong adsorption of Sb(V) ions was observed below pH 7, while the percentage adsorbed diminished abruptly above this pH value. However, most of the Sb ions adsorbed on hematite from solutions of pH 2–5 were not desorbed in alkaline conditions (5 days). Adsorption was interpreted in terms of electrostatic attraction and repulsion between the negativelycharged $Sb(OH)_6^-$ and the hematite (ZPC, pH 6.5–8.6).

Dzombak and Morel (1990) estimated adsorption constant values (diffuse layer model) for $SbO(OH)_4^-$ sorption on hydrous ferric oxide by using a Linear Free Energy Relationship (LFER) that correlates the logarithms of the surface complexation constants with the pK of the sorbing ion. By using a pK of 2.72 (no source given for this value), they obtained the following values for the intrinsic sorption constants: K_2^{int} ($\equiv FeOH^0 + SbO(OH)_4^- + H^+ = \equiv FeSbO(OH)_4 + H_2O$) = 8.4 and K_3^{int} ($\equiv FeOH^0 + SbO(OH)_4^- = \equiv FeOHSbO(OH)_4^-$) = 1.3.

1-3 Objective of this study

As stated in Section 1-1, it is considered that the behavior of Sb in the environment depends to a great extent on its oxidation state. The toxicity of inorganic Sb also depends on the oxidation state; Sb(III) is more toxic than Sb(V). Therefore, it is very important for Sb geochemistry and environmental chemistry to determine the Sb species in environmental samples. Many past studies of Sb speciation are limited to water samples using chromatography and voltammetry, and thus few studies have examined the speciation of Sb in solid phase such as soil and sediment samples. Moreover, since most of the Sb speciation in solid phase has been made on by indirect methods such as selective sequential extraction, there has been no direct information on Sb speciation of solid phase previously. Thus, Sb species in solid phase is still unclear

part in Sb environmental chemistry, however, the speciation of Sb in solid phase is essential to understand fully the behavior of Sb in solid-water system.

The objective of this study is the speciation of Sb and As in both solid and water phases to understand the reaction of Sb in aquatic environment in detail and to compare the Sb behavior with As examined in mine tailings in a natural system and in a solid-water system synthesized in laboratory (from Chapter 2 to 5). We particularly investigated the Sb and As behaviors when redox condition in the system varies focusing on "speciation" of Sb and As (oxidation state and host phase). Accordingly we employed X-ray absorption fine structure (XAFS) analysis for the Sb and As speciation, since *in situ* speciation by XAFS spectroscopy has proven to be a powerful tool for metal speciation in solid phases (Manceau et al., 1996), and XAFS has only rarely been applied to Sb speciation, with a prime focus on the determination of Sb complexation with chloride and sulfide in aqueous solutions (Oelkers et al., 1998; Mosslmans et al., 2000; Sherman et al., 2000). We also determined the oxidation states for Sb and As in water phase by chromatographic method and the obtained finding is combined with the Sb speciation in solid phase to understand in detail Sb and As behaviors in aquatic environmental system. Moreover, to understand kinetics and dynamics of the reactions for Sb and As in environment, I developed a new method using the time resolved XAFS to observe the reaction at solid-water interface as an additional objective of this study (Appendix 1).

The thesis is presented in 'paper format' — each chapter has been written to stand alone and is based on the papers published or submitted in a peer-reviewed publication except for Chapter 4 (Figure 1-1):

Chapter 2 describes Sb and As behaviors in soil-water system under various redox conditions examined in the system around Sb mine tailing (Ichinokawa mine, Ehime, Japan) and in the system simulated in laboratory, highlighting the Sb and As distributions in the system.

(*Published as* Mitsunobu, S., Harada, T., Takahashi, Y. Comparison of antimony behavior with arsenic under various soil redox conditions *to Environmental Science & Technology*; Mitsunobu, S., Harada, T., Hoshino, K., Takahashi, Y. X-ray Absorption

Study on the Dominance of Sb(V) as Secondary Antimony Species in Soil *to Chemistry Letters.*)

Chapter 3 provides the characterization of Fe hydroxides, host phases of Sb and As in the soil, in Ichinokawa soil using XAFS and Mössbauer spectroscopies, examining the morphology and structure order of Fe(III) hydroxides controlling As and Sb behaviors in soil-water system.

(*Submitted as* Mitsunobu, S., Sakai, Y., Takahashi, Y. Characterization of Iron(III) hydroxides in Arsenic_contaminated soil under various redox conditions by XAFS and Mössbauer spectroscopies *to Applied Geochemistry.*)

Chapter 4 describes a microscopic speciation of Sb and Fe in soil grains in Ichinokawa soil using μ-XAFS and electron probe micro analyzer (EPMA) to observe the spatial distribution of Sb(III)/Sb(V) in the soil grain and to understand the Sb behavior under reductive condition in detail.

Chapter 5 provides an interaction of Sb with Fe(II)/Fe(III) hydroxide (green rust) which is considered as a strong abiotic reducer occurring in soil and sediment, examining the reducing potential of green rust on Sb(V) and the detail of the reaction.

(*Published as* Mitsunobu, S., Takahashi, Y., Sakai, Y., Abiotic reduction of antimony(V) by green rust ($Fe_4(II)Fe_2(III)(OH)_{12}SO_4 \cdot 3H_2O$) *to Chemosphere*; *Submitted as* Mitsunobu, S., Takahashi, Y., Sakai, Y., Inumaru, K. Interaction of synthetic sulphate green rust with antimony(V) *to Environmental Science & Technology.*)

Chapter 6 presents the conclusions of the thesis.

Appendix 1 states a new method to observe the kinetics of various reactions at the solid-water interface using quick XAFS developed in the present work, applied to the oxidation reaction of As(III) by manganese oxide, a strong oxidizer in natural systems.

(*Published as* Mitsunobu, S., Takahashi, Y., Uruga, T. A new method to observe chemical reactions at the solid-water interface by quick XAFS combined with a column reactor *to Analytical Chemistry.*)

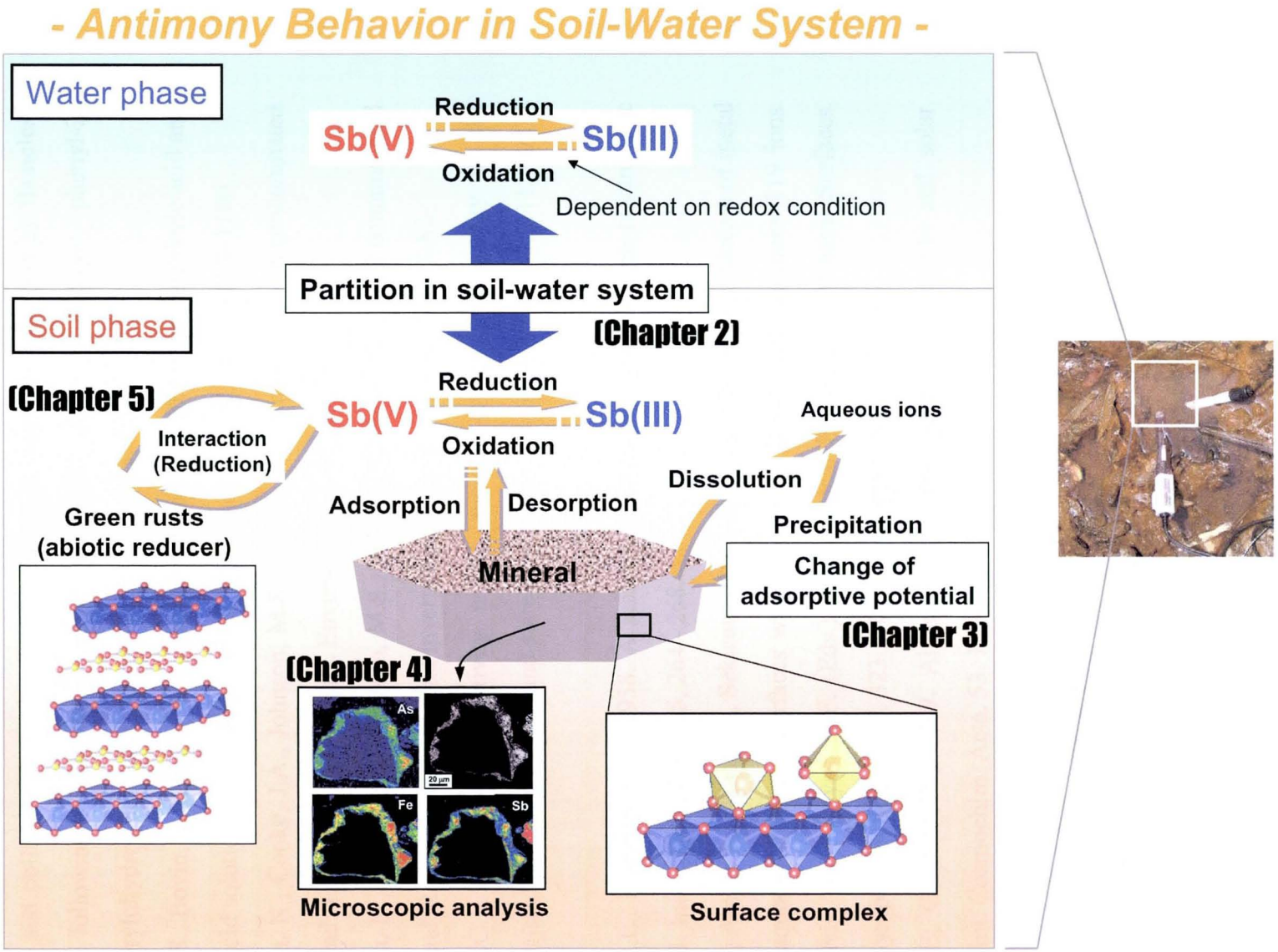

Figure 1-1. Schematic figure of Sb behavior and geochemical processes in soil-water system and the composition of this thesis. Each chapter number in the figure (ex. **Chapter 1**) corresponds the topic written in this thesis.

References

Abbasi, S.A., 1989. Sub-microdetermination of antimony(III) and antimony (V) in natural and polluted waters and total antimony in biological materials by flameless AAS following extractive separation with *N-p-* methoxy- phenyl-2-furylacrylohydroxamic acid. Anal. Lett. 22, 237–255.

Ahrland, S., Bovin, J.-O., 1974. The complex formation of Sb(III) in perchloric acid and nitric acid solutions. A solubility study. Acta Chem. Scand., A 28, 1089–1100.

Ainsworth, N., Cooke, J.A., Johnson, M.S., 1990a. Distribution of Sb in contaminated grassland: 1. Vegetation and soils. Environ. Pollut. 65, 65–77.

Ainsworth, N., Cooke, J.A., Johnson, M.S., 1990b. Distribution of Sb in contaminated grassland: 2. Small mammals and invertebrates. Environ. Pollut. 65, 79–87.

Allen, L.C., 1989. Electronegativity is the average one-electron energy of the valence-shell electrons in ground-state free atoms. J. Am. Chem. Soc. 111, 9003–9014.

Allred, A.L., Rochow, E.G., 1958. A scale of electronegativity based on electrostatic force. J. Inorg. Nucl. Chem. 5, 264– 268.

Ambe, F., Ambe, S., Okada, T., Sekizawa, H., 1986. In situ Mössbauer studies of metal oxide-aqueous solution interfaces with adsorbed cobalt-57 and antimony-119 ions. In: Davis, K.F., Hayes, K.F. (Eds.), Geochemical Processes at Mineral Surfaces. ACS Symposium Series, vol. 323. ACS, Washington, pp. 403–424.

Anders, E; Grevesse, N, 1989. Abundances of the elements: meteorite and solar. Geochim. Cosmochim. Acta. 53, 197-214.

Andreae, M.O., Froelich, P.N., 1984. Arsenic, antimony, and germanium biogeochemistry in the Baltic Sea. Tellus 36B, 101–117.

Antonovich, V.P., Nevskaya, E.M., Suvorova, E.N., 1977. Spectrophotometric determination of the hydrolysis constants of monomeric Sb(III) ions. Russ. J. Inorg. Chem. 22, 696– 699.

Asami, T., Kubota, M., Saito, S., 1992. Simultaneous determination of Sb and bismuth in soils by continuous hydride generation—atomic absorption spectrometry. Water,

Air, Soil Pollut. 62, 349–355.

Belzile, N., Chen, Y.-W., Wang, Z., 2001. Oxidation of antimony (III) by amorphous iron and manganese oxyhydroxides. Chem. Geol. 174, 379–387.

Bencze, K., 1994. Sb. In: Seiler, H.G., Sigel, A., Sigel, H. (Eds.), Handbook on Metals in Clinical and Analytical Chemistry. Marcel Dekker, New York, pp. 227–236.

Berman, J.D., 1988. Chemotherapy for leishmaniasis: biochemical mechanisms, clinical efficacy and future strategies. Rev. Infect. Dis. 10, 560–586.

Bertine, K.K., Lee, D.S., 1983. Antimony content and speciation in the water column and interstitial waters of Saanich Inlet. In: Wong, C.S., Boyle, E., Bruland, K.W., Burton, J.D., Goldberg, E.D.(Eds)., Trace Metals in Sea Water. NATO Adv. Res. Inst., Plenum, New York, pp. 21–38.

Biernat, J., Ziegler, B., ZralAko, M., Kondziela, P., 1975. Variability of some polarographically determined stability constants. A new kind of coordination: the dual complexation. J. Electroanal. Chem. 63, 444– 449.

Blandamer, M.J., Burgess, J., Peacock, R.D., 1974. Solubility of sodium hexahydroxoantimonate in water and in mixed aqueous solvents. J. Chem. Soc., 1084–1086 (Dalton). Bond, A.M., Waugh, A.B., 1970. AC polarography and its application to overcome the problem of DC polarographic maxima in the study of complex ions. Electrochim. Acta 15, 1471–1482.

Boyle, R.W., 1965. Geology, geochemistry, and origin of the lead–zinc–silver deposits of the Keno Hill–Galena Hill area, Yukon Territory. Geol. Surv. Can., Bull. 111, 302 pp.

Brannon, J.M., Patrick Jr., W.H. 1985. Fixation and mobilization of antimony in sediments. Environ. Pollut. 9B, 107– 126

Carbol, P., Skalberg, M., Skarnemark, G., 1995. Cesium and antimony behaviour in water and forest soil after the Chernobyl accident. Radiochim. Acta 69, 259– 270.

Carlin Jr., J.F., 2000. Sb. U.S. Geological Survey Mineral Commodity Summaries.

Crecelius, E.A., Bothner, M.H., Carpenter, R., 1975. Geochemistries of arsenic, antimony, mercury, and related elements in sediments of Puget Sound. Environ. Sci. Technol. 9, 325–333.

Crecelius, E.A., Johnson, C.J., Hofer, G.C., 1974. Contamination of soils near a copper smelter by arsenic, Sb and lead. Water, Air, Soil Pollut. 3, 337–342.

Cawse, P.A., Jones, I.S., Cox, G.W., 1975. Cultivation and multielementanalysis of vegetables and grass grown in soil contaminated with trace elements. AERE Report 8103 UK Atomic Energy Authority, Harwell Laboratories; cited in Ainsworth, N. and Cooke, J.A., 1991. Biological significance of Sb in contaminated grassland. Water, Air, Soil Pollut. 57–58, 193–199.

Clementi, E., Raimondi, D.L., 1963. Atomic screening constants from S.C.F. functions. J. Chem. Phys. 38, 2686–2689.

Council of the European Communities, 1976. Council Directive 76/464/EEC of 4 May 1976 on pollution caused by certain dangerous substances discharged into the aquatic environment of the Community. Official Journal L 129, 18/05/1976, pp. 23–29.

Council of the European Union, 1998. Council Directive 98/83/EC of 3 November 1998 on the quality of water intended for human consumption. Official Journal L 330, 05/12/1998, pp. 32–54.

Cutter, G.A., 1991. Dissolved arsenic and antimony in the Black Sea. Deep-Sea Res. 38, S825–S843.

Cutter, G.A., 1992. Kinetic controls on metalloid speciation in seawater. Mar. Chem. 40, 65–80.

Cutter, L.S., Cutter, G.A., San Diego-McGlone, M.L.C., 1991. Simultaneous determination of inorganic arsenic and antimony species in natural waters using selective hydride generation with gas chromatography-photoionization detection. Anal. Chem. 63, 1138–1142.

Deng, T.L., Chen, Y.-W., Belzile, N., 2000. Antimony speciation at ultra trace levels using hydride generation atomic fluorescence spectrometry and 8-hydroxyquinoline as an efficient masking agent. Anal. Chim. Acta 432, 293–302.

Dzombak, D.A., Morel, F.M.M., 1990. Surface Complexation Modeling. Hydrous Ferric Oxide. Wiley, New York, pp. 307– 312.

Elinder, C.-G., Friberg, L., 1986. Sb. In: Friberg, L., Nordberg, G.F., Vouk, V. (Eds.), Handbook on the Toxicology of Metals, 2nd edn. Elsevier, Amsterdam, pp. 26–42.

Emsley, J., 1991. The Elements, 2nd edn. Clarendon Press, Oxford 251 pp.

Enders, R., Jekel, M., 1996. Adsorption und Mitfällung von Antimon(III) bei der Hydroxid-fällung verschiedener Metalle. Von Wasser 86, 141– 155.

Fergusson, J.E., 1990. The Heavy Elements: Chemistry, Environmental Impact and Health Effects. Pergamon, Oxford, 614 pp. Gebel, T., 1997. Arsenic and Sb: comparative approach on mechanistic toxicology. Chem.-Biol. Interact. 107, 131–144.

Filella M., Belzile, N., Chen, Y.-W., 2002. Antimony in the environment: a review focused on natural waters II. Relevant solution chemistry. Earth-Sci. Rev. 59, 265-285.

Gilbert, T.R., Hume, D.N., 1973. Direct determination of bismuth and Sb in sea water by anodic stripping voltammetry. Anal. Chim. Acta 65, 451– 459.

Greenwood, N.N., Earnshaw, A., 1997. Chemistry of the Elements, 2nd edn. Pergamon, Oxford.

Guieu, C., Zhang, J., Thomas, A.J., Martin, J.M., Brun-Cottan, J.-C., 1993. Significance of atmospheric fallout on the upper layer water chemistry of the North-Western Mediterranean. J. Atmos. Chem. 17, 45–60.

Gushchina, L.V., Borovikov, A.A., Shebanin, A.P., 2000. Formation of Sb(III) complexes in alkali sulfide solutions at high temperatures: an experimental Raman spectroscopic study. Geochem. Int. 38, 510–513.

Hale, M., 1981. Pathfinder applications of arsenic, Sb and bismuth in geochemical exploration. J. Geochem. Explor. 15, 307–323.

Hammel, W., Steubing, L., Debus, R., 1998. Assessment of the ecotoxic potential of soil contaminants by using a soil-algae test. Ecotoxicol. Environ. Saf. 40, 173–176.

Hasseling, E.H.M. Investigation about the emissions from waste incinerator, 1987. TNO/MT Reports No. 87726-16068 and 8726-13611.

Hou, H.-B., Narasaki, H., 1999. Differential determination of antimony(III) and antimony(V) in river water by hydride-generation inductively coupled plasma mass spectrometry. Anal. Sci. 15, 911–914.

Huheey, J.E., Keiter, E.A., Keiter, R.L., 1993. Inorganic Chemistry: Principles of

Structure and Reactivity, 4th edn. Harper Collins, New York.

IAWG, 1995. An international perspective on characterization and management of residues from municipal solid waste incineration. Final Document-International Ash Working Group.

Jander, G., Ostmann, H.-J., 1962a. U¨ ber die Sauerstoffsa¨uren des Antimon(V). I. Messungen der Lichtabsorption und des Diffusionsvermo ¨gens on Antimonat(V)-lo¨sungen bei verschiedenen Wasserstoffionen-Konzentrationen. Z. Anorg. Allg. Chem. 315, 241–249.

Jander, G., Ostmann, H.-J., 1962b. U¨ ber die Sauerstoffsa¨uren des Antimon(V). II. Elektrochemische Titrationen. Z. Anorg. Allg. Chem. 315, 250–258.

Jarvie, H.P., Neal, C., Burton, J.D., Tappin, A.D., 2000. Patterns in trace element chemistry in the freshwater tidal reaches of the River Trent. Sci. Total Environ. 251/252, 317–333.

Kantin, R., 1983. Chemical speciation of antimony in marine algae. Limnol. Oceanogr. 28, 165–168.

Klein, D.H., Andren, A.W., Bolton, N.E., 1975. Trace element discharges from coal combustion for power production. Water, Air, Soil Pollut. 5, 71–77.

Krupp, R.E., 1988. Solubility of stibnite in hydrogen sulfide solutions, speciation, and equilibrium constants, from 25 to 350 °C. Geochim. Cosmochim. Acta 52, 3005–3015.

Latimer, W.M., Hildebrand, J.H., 1951. Reference Book of Inorganic Chemistry, 3rd edn. Macmillan, New York, p. 222.

Leleyter, L., Probst, J.-L., 1999. A new sequential extraction procedure for the speciation of particulate trace elements in river sediments. Int. J. Environ. Anal. Chem. 73, 109–128.

Lueth, V.W., 1999. Sb: element and geochemistry. In: Marshall, C.P., Fairbridge, R.W. (Eds.), Encyclopedia of Geochemistry. Kluwer Academic Publishers, Dordrecht, pp. 15–16.

Manceau, A., Boisset, M.C., Sarret, G., Hazemann, J.L., Mench, M., Cambier, P., Prost, R., 1996. Direct determination of lead speciation in contaminated soils by EXAFS spectroscopy. Environ. Sci. Technol. 30, 1540 ▪ 1552.

Mikenda, W., Preisinger, A., 1980. Vibrational spectra of Na_3SbS_4, $Na_3SbS_4 \cdot 9H_2O$ (Schlippe's salt) and $Na_3SbS_4 \cdot 9D_2O$. Spectrochim. Acta 36A, 365– 370.

Milne, J.B., 1975. Spectrophotometric studies of Sb(III) in hydrochloric acid solutions. Can. J. Chem. 53, 888– 893.

Mohammad, B., Ure, A.M., Reglinski, J., Littlejohn, D., 1990. Speciation of Sb in natural waters: the determination of Sb(III)and Sb(V) by continuous flow hydride generation–atomic absorption spectrometry. Chem. Speciation Bioavailability 3, 117–122.

Mok, W.-M., Wai, C.M., 1987. Simultaneous extraction of trivalent and pentavalent Sb and arsenic species in natural waters for neutron activation analysis. Anal. Chem. 59, 233–236.

Mok, W.M., Wai, C.M., 1990. Distribution and mobilization of arsenic and Sb species in the Coeur d'Alene River, Idaho. Environ. Sci. Technol. 24, 102–108.

Mosselmans, J.F.W., Helz, G.R., Pattrick, R.A.D., Charnock, J.M., Vaughan, D.J., 2000. A study of speciation of Sb in bisulfide solutions by X-ray absorption spectroscopy. Appl. Geochem. 15, 879–889.

Nakamura, K., Kinoshita, S., Takatuki, S., 1996. The origin and behavior of lead, cadmium, and Sb in MSW incinerator. Seminar on cycle and stabilization technologies of MSW incineration residues, March 5-8, Kyoto Research Park, Japan.

Nash, M.J., Maskall, J.E., Hill, S.J., 2000. Methodologies for determination of Sb in terrestrial environmental samples. J. Environ. Monit. 2, 97–109.

Neumann, H.M., Ramette, R.W., 1956. Kinetics of the hydrolysis of hexachloroantimonate(V). J. Am. Chem. Soc. 78, 1848–1851.

Oelkers, E.H., Sherman, D.M., Ragnarsdottir, K.V., Collins, C., 1998. An EXAFS spectroscopic study of aqueous Sb(III)-chloride complexation at temperatures from 25 to 250°C. Chem. Geol. 151, 21– 27.

Onishi, H., 1969. Sb. In: Wedepohl, K.H. (Ed.), Handbook of Geochemistry, vol. 2/4. Springer, Heidelberg, pp. 51-B-1– 51-O-3.

Onishi, H., Sandell, E.B., 1955. Notes on the geochemistry of Sb. Geochim. Cosmochim. Acta 8, 213–221.

O'Toole, J.J., Clark, R.G., Malaby, K.L., Tanger, D.L., 1971. Environmental trace element survey at a heavy metals refining site. ANS Meeting, University of Missouri, Columbia. Cited in: Peterson, P.J., Benson, L.M. and Zieve, R., 1981. Metalloids. In: Lepp, N.W. (Ed.), Effect of Heavy Metal Pollution on Plants. Effects of Trace Metals on Plant Function, vol. 1. Applied Science Publishers, London, pp. 279–342.

Pauling, L., 1933. The formulas of antimonic acid and the antimonates. J. Am. Chem. Soc. 55, 1895– 1900.

Ragaini, R.C., Ralston, H.R., Roberts, N., 1977. Environmental trace metal contamination in Kellogg, Idaho, near a lead smelting complex. Environ. Sci. Technol. 11, 773–781.

Reimann, D.O, 1989. Heavy metals in domestic refuse and their distribution in incinerator residues. Waste Man. Res. 7, 57-62.

Reimann, D.O., 1995. Sb (Sb) – im Abfall sowie quantitativer Vergieich zu weiteren Restabfallinghaltstoffen (Sb) in waste and a quantitative comparison with other waste constituents). Kurzbericht UO1/539/A/AM.

Ricca, B., D'Amore, G., Bellomo, A., 1965. Ricerche sugli antimoniati acidi. Ann. Chim. (Rome) 46, 491–507.

Ritchie, J.A., 1961. Arsenic and Sb in some New Zealand thermal waters. N. Z. J. Sci. 4, 218–229.

Sabadell, J.E., Axtmann, R.C., 1975. Heavy metal contamination from geothermal sources. Environ. Health Perspect. 12, 1–7.

Sanderson, R.T., 1988. Principles of electronegativity. Part I. General nature. J. Chem. Educ. 65, 112–118.

Sherman, D.M., Ragnarsdottir, K.V., Oelkers, E.H., 2000. Sb transport in hydrothermal solutions: and EXAFS study of Sb(V) complexation in alkaline sulfide and sulfide – chloride brines at temperatures from 25°C to 300°C at Psat. Chem. Geol. 167, 161–167.

Shoji, H., Mabuchi, H., Saito, N., 1974. Solvent extraction studies of the hydrolysis of Sb(III) in tracer concentrations. Bull. Chem. Soc. Jpn. 47, 2502– 2507.

Shotyk, W., Cheburkin, A.K., Appleby, P.J., Fankhauser, A., Kramers, J.D., 1996. Two

thousand years of atmospheric arsenic, Sb, and lead deposition recorded in an ombrotrophic peat bog profile, Jura Mountains, Switzerland. Earth Planet. Sci. Lett. 145, E1–E7.

Sinemus, H.-W., Kleiner, J., Stabel, H.-H., Radziuk, B., 1992. Combination of flow injection hydride generation and sequestration on a graphite tube for the automated determination of Sb in potable and surface waters. J. Anal. At. Spectrom. 7, 433–437.

Slater, J.C., 1964. Atomic radii in crystals. J. Chem. Phys. 41, 3199–3204.

Stauffer, R.E., Thompson, J.M., 1984. Arsenic and Sb in geothermal waters of Yellowstone National Park, Wyoming, USA. Geochim. Cosmochim. Acta 48, 2547–2561.

Strohal, P., Huljev, D., Lulic′, S., Picer, M., 1975. Sb in the coastal environment, North Adriatic. Estuarine Coastal Mar. Sci. 3, 119– 123.

Suess, H.E., Urey, H.C., 1956. Abundances of the elements. Rev. Mod. Phys. 28, 53–74.

Sun, Y.C., Yang, J.Y., 1999. Simultaneous determination of arsenic(III, V), selenium(IV,VI), and antimony(III,V) in natural water by coprecipitation and neutron activation analysis. Anal. Chim. Acta 395, 293–300.

Takayanagi, K., Michel, P., 1996. Semi-automated determination of dissolved antimony in seawater and sediment pore water.

Bunseki Kagaku 45, 1115–1120.

Takayanagi, K., Cossa, D., Martin, J.-M., 1996. Antimony cycling in the western Mediterranean. Mar. Chem. 54, 303–312. Takayanagi, K., Cossa, D., 1997. Vertical distributions of Sb(III) and Sb(V) in Pavin Lake, France. Water Res. 31, 671–674.

Tanizaki, Y., Shimokawa, T., Nakamura, M., 1992a. Physicochemical speciation of trace elements in river waters by size fractionation. Environ. Sci. Technol. 26, 1433–1444.

Tanizaki, Y., Shimokawa, T., Yamazaki, M., 1992b. Physicochemical speciation of trace elements in urban streams by size fractionation. Water Res. 26, 55–63.

Taylor, S.R.; McLennan, S.M., 1985. The continental crust: its composition and

evolution. Blackwell Scientific Publ., Oxford, England, 312 pp.

Thanabalasingam, P., Pickering, W.F., 1990. Specific sorption of antimony (III) by the hydrous oxides of Mn, Fe, and Al. Water, Air, Soil Pollut. 49, 175– 185.

Tossell, J.A., 1994. The speciation of Sb in sulfidic solutions: a theoretical study. Geochim. Cosmochim. Acta 58, 5093– 5104.

Turekian, K.K., Wedepohl, K.H., 1961. Distribution of the elements in some major units of the Earth's crust. Geol. Soc. Am. Bull. 72, 175–192.

Ulrich, N., 1998. Speciation of Sb(III), Sb(V), and trimethylstiboxide by ion chromatography with inductively coupled plasma atomic emission spectrometric and mass spectrometric detection. Anal. Chim. Acta 359, 245–253.

United States Environmental Protection Agency, 1979. Water Related Fate of the 129 Priority Pollutants, vol. 1. USEPA, Washington, DC, USA, EP-440/4-79-029A.

United States Environmental Protection Agency, 1998. Toxics Release Inventory. USEPA, Washington, DC, USA, Doc. 745-R-00-007.

United Nations Environmental Program, 1999. Basel Convention on the Control of Transboundary Movements of Hazardous Wastes and Their Disposal (with amended Annex I and two dditional Annexes VIII and IX, adopted at the fourth meeting of the Conference of the Parties in 1998). SBC No. 99r001. UNEP, Geneva.

Van de Beek, A.I.M., Cornelissen, A.A.J., Aalders, T.G., 1989. Fysisch en chemisch onderzoek aan huishoudelijk afval van 1987, inclusief batterijen (Physical and chemical studies on municipal waste of 1987, including batteries). Report No. 738505007, Dutch National Institute of Public Health and Environmental Protection.

Van der Weijden, C.H., de Lange, G.J., Middelburg, J.J., van der Sloot, H.A., Hoede, D., Shofiyah, S., 1989. Geochemical characteristics of Kau Bay water. Neth. J. Sea Res. 24, 583–589.

Wedepohl, K.H., 1995. The composition of the continental crust. Geochim. Cosmochim. Acta 59, 1217–1232.

Weissberg, B.G., Browne, P.R.L., Seward, T.M., 1979. Ore metals in active geothermal systems. In: Barnes, H.L. Ed., Geochemistry of Hydrothermal Ore Deposits. Wiley, New York, pp. 738–780.

Winter, M., 2001. WebElementsk (www.webelements.com). University of Sheffield and WebElements, UK.

Wood, S.A., 1989. Raman spectroscopic determination of the speciation of ore metals in hydrotermal solutions: I. Speciation of Sb in alkaline sulfide solutions at 25 °C. Geochim. Cosmochim. Acta 53, 237– 244.

CHAPTER 2

Distributions of Sb and As in soil-water system under various redox conditions

Introduction

Antimony (Sb) is a toxic element widely distributed in the lithosphere and mainly associated with arsenic (As) as sulfide or oxide. Antimony can be introduced to the aquatic environment through natural processes, such as rock weathering and volcanic activity (Wedepohl, 1995). In general, the natural abundance of Sb in soil is low (< 1 mg kg^{-1}) and in freshwater ranges from 10^{-6} to 10^{-9} g dm^{-3} (Filella et al., 2002). However, elevated concentrations of Sb in both soil and water can be found near Sb mines and in areas contaminated by human activities. Antimony compounds are considered to be pollutants of priority interest by the United States Environmental Protection Agency (UESPA, 1979) and the European Union (Council of European Community, 1976). Antimony belongs to group 15 of the periodic table, below As, and can exist in four oxidation states (–III, 0, III, V), though Sb(III) and Sb(V) are the most frequently encountered species in the environment. The behavior of Sb in the environment depends to a great extent on its oxidation state. The toxicity of inorganic Sb is assumed to be similar to that of As and also depends on the oxidation state; Sb(III) is more toxic than Sb(V) (Picard and Bosco, 2003). Therefore, Sb analysis in environmental samples requires quantitative measurement of Sb(III) and Sb(V) to assess its toxicity. Many past studies of Sb speciation are limited to water samples using high performance liquid chromatography (HPLC) and voltammetry, but few studies have examined the speciation of Sb in solid phase. However, speciation of Sb in solid phase such as soil and sediment is essential to understand fully the behavior of Sb in solid-water systems. Although Sb is occasionally found with Fe, Mn, and Al oxides (Clecelius et al., 1975; Brannon and Patrick, 1985) or with organic carbon (El Bilali et al., 2002), the geochemical behavior of Sb in sediment is still largely unknown.

The aim of this study is the speciation of Sb and As in both solid and water phases to understand the reaction and dynamics of Sb in soil-water environment and to compare the Sb behavior with As in the soil-water system. Accordingly, we employed

X-ray absorption fine structure (XAFS) analysis to determine directly the Sb and As species (oxidation state and host phase), while we also determined the Sb(III)/Sb(V) and As(III)/As(V) ratios in soil water by HPLC-ICP-MS for the soil-water system contaminated by mine water and in a soil-water system synthesized in laboratory.

Materials and Methods

Ichinokawa soil samples. Ichinokawa soil and soil water samples containing Sb were collected in October 2005 around the Ichinokawa mine pit (33.53N, 133.12E), Ehime, Japan, which was formerly one of the largest Sb (stibnite: Sb_2S_3) mines (Bancroft, 1988, Figure 2-1). The sampling site was soil under flooded condition (water layer: a few cm) located at about 5 m downward from the mine pit. The soil samples are contaminated soil in the mine area and contain Sb, As, and Se. To allow us to observe the oxidation states under various redox conditions, soil water and soil samples were collected at different depths. At first, the Eh and pH were measured in-situ by a Pt electrode (Fujiwara Sci., EHS-120) and a glass electrode (Horiba, D-51), respectively, by inserting the electrodes to each depth. Pore water (soil water) was extracted at four depths (1, 3, 6, and 9 cm) by soil water samplers (Fujiwara Sci., FV-448) and filtrated through 0.45 μm membrane filters. Subsequently, soil samples were collected from four depth ranges (0-3, 3-6, 6-9, and 9-12 cm) successively from the top layer with a plastic spatula. Below the soil lay bedrock at a depth of about 15 cm at the sampling site. Collected soil and soil water samples were immediately sealed in polystyrene bottles and kept at 4°C during transportation to our laboratory. In the laboratory, before all measurements, the soil samples were passed through a 500 μm stainless steel sieve to remove large organic particles and gravel fractions and then homogenized. To minimize air-oxidation, this procedure was immediately undertaken at about 0-5°C. Aliquots of the homogenized soil were packed into polyethylene bags for XAFS analysis, and stored at −20°C to avoid change of the oxidation states before analysis. The Sb(III)/Sb(V) and As(III)/As(V) ratios in the pore water samples were measured by HPLC-ICP-MS on the sampling day. Residual soil water samples were acidified to 2 wt.% HNO_3 by adding concentrated HNO_3.

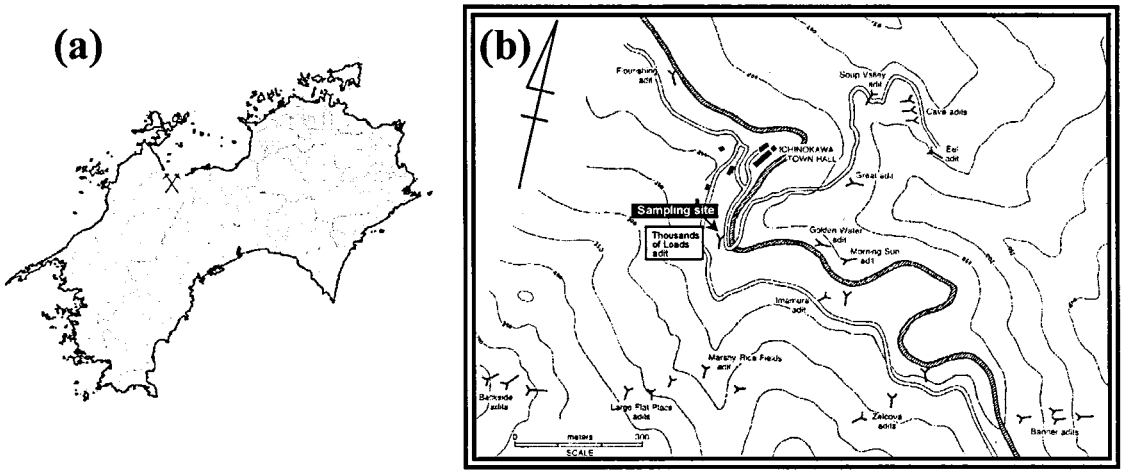

Figure 1. Location map of Ichinokawa mine (a) and topographical map around the sampling site in Ichinokawa mine (b) (Bancroft, 1988, modified).

Laboratory (soil incubation) experiments. Soil incubation experiments were based on a method in the literature (Mitsunobu et al., 2005; Takahashi et al., 2003). The soil used was fine textured Gray Lowland soil, from paddy fields in the National Institute of Agro-Environmental Science (Tsukuba, Japan), which was air-dried, homogenized, and sieved (2 mm) before use. Major element compositions of the soil were reported in Takahashi et al. (2003), while Sb and As abundances were 796 μg kg^{-1} and 10.2 mg kg^{-1}, respectively. Laboratory experiments were on 10.0 g of the soil, which was put into a 50 mL polystyrene tube with Milli-Q water. To promote reductive conditions in the system, 0.01 g of D(+)–glucose (Wako, Japan) was added. Subsequently, 2.0 mg of Sb(V) and As(V) was added to the system as a solution prepared by dissolution of $K[Sb(OH)_6]$ (Wako, Japan) and KH_2AsO_4 (Wako, Japan), respectively. To observe the oxidation state of Sb and As under various redox conditions, the total amount of water in the soil was varied, noted as the degree of water saturation (W_S). After incubation for 7 days at 25°C, soil and soil water samples were collected for further analyses.

Water and soil analyses. Total Fe, Mn, Sb, and As abundances in the water samples were measured by graphite-furnace atomic absorption spectroscopy (Shimadzu AA6650) for Fe and ICP-MS (VG; PQ-3) for other elements. The precision of the measurement was better than 5% for Fe, Mn, Sb, and As. Concentrations of major elements in soil samples were measured by X-ray fluorescence spectrometry (XRF; Rigaku ZSX-101e) as described in Kanazawa et al. (2001). Antimony and As concentrations in soil samples were determined using the standard addition method by XRF. The results of major element abundance are summarized in Table 2-1. Micrometer-scale distribution of Sb and S were examined by Electron Probe Micro Analyzer (EPMA) (JEOL JXA-8200) to observe whether stibnite mineral was contained in the Ichinokawa soil samples. In addition, mineral compositions were analyzed by X-ray diffractometer (XRD; MAC Sci., M18XHF). Based on the XRD and EPMA analyses, stibnite was not present in the soil samples studied. The major minerals in all soil samples were kaolinite, quartz, and mica.

XAFS measurement and data analysis. Antimony K-edge XAFS spectra were

Table 2-1. Concentrations of various elements in soil samples around Ichinokawa mine and soil used in laboratory experiments.

Depth (cm)	0-3	3-6	6-9	9-12	[d]R_{Fe}^2	[e]R_{Mn}^2	[c]paddy soil
As (mg kg^{-1})	1450	1160	1270	1960	0.72	0.90	10.2
Sb (mg kg^{-1})	9150	8870	10600	11200	0.72	0.64	0.796
SiO_2 (%)	56.18	55.88	59.45	49.85			59.5
TiO_2 (%)	0.56	0.52	0.58	0.49			0.85
Al_2O_3 (%)	12.12	11.81	14.44	12.86			17.8
[a]Fe_2O_3 (%)	6.20	5.60	6.76	7.53			7.19
[b]MnO (%)	0.72	0.54	0.69	0.90			0.10
MgO (%)	1.01	0.97	1.22	1.14			1.05
CaO (%)	0.67	0.52	0.88	1.10			1.19
Na_2O (%)	1.11	1.19	1.43	1.05			1.37
K_2O (%)	2.25	2.20	2.69	2.32			1.76
P_2O_5 (%)	0.10	0.09	0.14	0.16			0.20

a. Total iron as Fe_2O_3.

b. Total manganese as MnO.

c. Element abundances originally contained in soil used in laboratory experiment.

d. Square of correlation coefficient to Fe in natural soil samples.

e. Square of correlation coefficient to Mn in natural soil samples.

measured at the beamline BL01B1 at SPring-8 (Hyogo, Japan) with a Si(311) double-crystal monochromator and two mirrors. The K-edge XAFS spectra of As, Fe, and Mn were obtained at the beamline BL12C in the Photon Factory, KEK (Tsukuba, Japan) with a Si(111) double-crystal monochromator and a bent cylindrical mirror. All spectra were collected in the fluorescence mode using a Lytle detector or a 19-element Ge semiconductor detector. The measurements were carried out at room temperature under ambient air conditions.

EXAFS (extended X-ray absorption fine structure) data were analyzed by REX2000 (Rigaku Co. Ltd.). The oscillation was extracted from the original spectrum by a spline smoothing method. E_0 was set at the edge inflection point for all the samples studied. The Fourier transformation of the $k^3\chi(k)$ EXAFS oscillation from k space to r space was performed in a range 3.0–11.0 $Å^{-1}$ to obtain a radial distribution function (RSF) for Sb and As. The inversely Fourier filtered data were analyzed with a usual curve fitting method. Theoretical phase shift and amplitude functions employed in this fitting procedure were extracted from FEFF 7.0 (Zabinsky et al., 1995). For this procedure, As-O and As-Fe phase shifts and amplitude functions were extracted from the structure of scorodite ($FeAs^{V}O_4 \cdot 2H_2O$) (Kitahama et al., 1975). Sb-O and Sb-Fe phase shifts and amplitude functions were extracted from the structure of tripuhyite ($FeSb^{V}O_4$) (Berlepsch et al., 2003). Error estimates of the fitted parameters in bond distance and coordination number were ±0.02 Å and ±20%, respectively.

Preparation of model compounds for XAFS. Ferrihydrite was prepared by hydrolysis of ferric nitrate at pH 7.5 and 20 ±2°C according to Schwertmann and Cornell (1991). The product was characterized as the two-line ferrihydrite by XRD. δ-MnO_2 was prepared by the oxidation of Mn(II) ion by permanganate following the procedures of Murray (1974). A 1.0 M $Mn(NO_3)_2$ solution (7 ml) was slowly added to 400 ml of a stirred 35 mM KOH solution, containing 4.2 mmol $KMnO_4$. The XRD diffraction analysis of the dried samples gave broad, diffuse reflection peaks, characteristic of δ-MnO_2. A suspension of ferrihydrite or δ-MnO_2 was made by adding 0.20 g of each phase to 10 ml of Milli-Q water. Ferrihydrite and δ-MnO_2 were equilibrated with 100 mg kg^{-1} Sb and As, respectively, at pH 7.9 and 25 ±1°C under ambient air conditions for

72 h. Each suspension of As and Sb was separated by filtration using 0.2 μm hydrophilic PTFE membrane filters to recover a viscous paste, which was kept at –20°C until XAFS analysis. The filtrate was analyzed for the concentrations and oxidation states of dissolved As and Sb species by ICP-MS. The final molar Sb/Fe and Sb/Mn ratios of the samples are 0.013 and 0.018 for ferrihydrite and δ-MnO_2, respectively, while those for As/Fe and As/Mn ratios 0.028 and 0.020, respectively.

HPLC-ICP-MS. The Sb(III)/Sb(V) and As(III)/As(V) ratios in soil water were determined by HPLC-ICP-MS. The operation condition is summarized in Table 2-2. The pump and oven used were a Pu-2089 Plus (JASCO) and a Co-2065 Plus (JASCO), respectively. The experimental conditions were the same as those described by Krachler and Emons (2001). An anion exchange column (Hamilton PRP X-100) was used at 40°C. The mobile phase was a 20 mM EDTA (Wako, Japan) solution at pH 4.7. The flow rate was 0.25 ml min^{-1}. Two standard solutions of Sb(III) and Sb(V) were prepared by dissolving appropriate amounts of potassium antimony tartrate (Wako, Japan) and $KSb(OH)_6$, respectively, in Milli-Q water. The standard solutions of As(III) and As(V) were prepared from potassium salts, $KAsO_2$ and KH_2AsO_5, respectively.

Results and Discussion

Eh and pH conditions. Eh values decreased monotonically from 360 to –140 mV with depth in the Ichinokawa soil samples (Figure 2-2a). In the laboratory experiment samples, Eh also decreased with the increase in the amount of water (Figure 2-2b). These results show that the redox condition became reductive in the soil, since oxygen supply diminishes with depth or with the amount of water (Mitsunobu et al., 2005; Takahashi et al., 2004). The pH values of the soil water were relatively uniform with depth and water saturation levels.

Concentrations of Fe, Mn, Sb, and As in soil. Both Fe and Mn concentrations in Ichinokawa soil samples increase slightly with depth (Table 2-1). Antimony and As concentrations in soil also increased slightly with depth and a good correlation is

Table 2-2
Operation condition for HPLC-ICP-MS instrument.

HPLC	
Column	Hamilton PRP-X100 (250 mm × 4.1 mr
Mobile phase	20 mM EDTA at pH 4.7
Flow rate	1.0 mL/min
Injection volume	100 µL
Column temperature	40 °C
ICP-MS	
Forward rf power	1360 W
Auxiliary Ar flow	0.86 L/min
Nebulizer Ar flow	0.83 L/min
Data acquisition mode	Time resolved analysis
Integration time	20 ms
Isotopes monitored	^{121}Sb and ^{123}Sb
Total analysis time	600 s

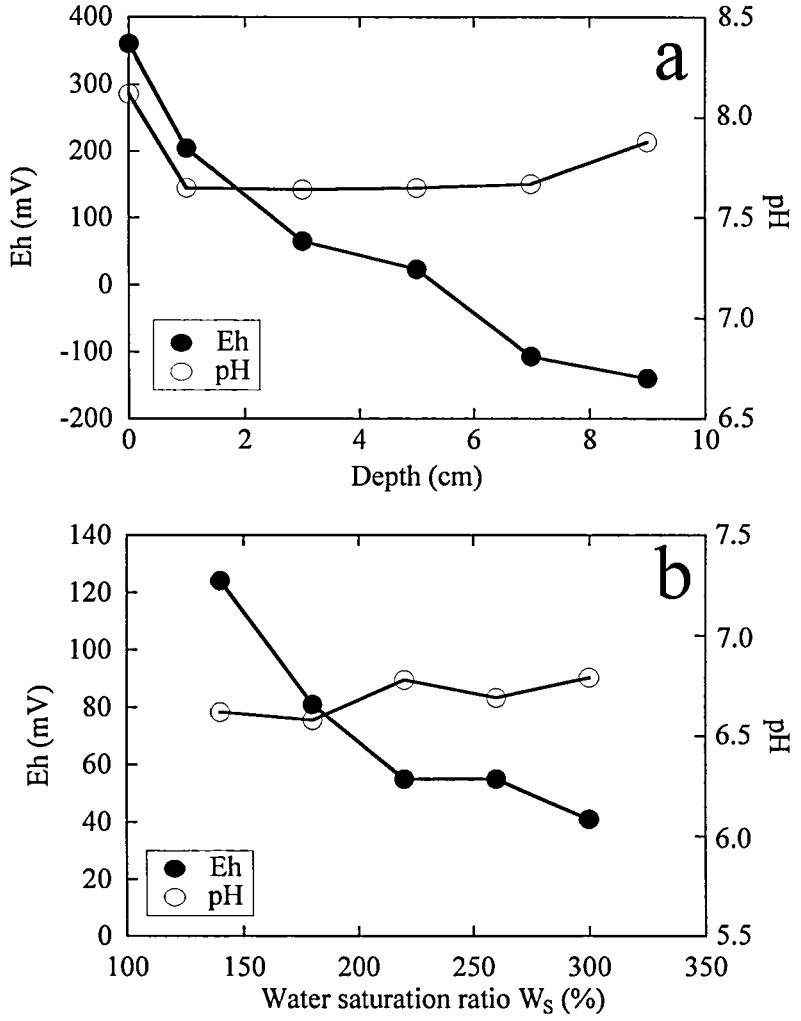

Figure 2-2. Eh and pH variations (a) with depth in Ichinokawa soil-water system around Ichinokawa mine and (b) with water amount (W_S) in the laboratory experiment. The Eh and pH were measured by a Pt electrode (Fujiwara Sci., EHS-120) with a AgCl reference electrode (Fujiwara Sci., 4400-0.65C) and a glass electrode (Horiba, D-51), respectively.

observed between As and Sb concentrations. The Sb and As concentrations correlate well also with Fe and Mn concentrations in soil (R_{Fe}^2 = 0.72, R_{Mn}^2 = 0.64 for Sb; R_{Fe}^2 = 0.72, R_{Mn}^2 = 0.90 for As), though the correlation coefficients are based on only 4 samples. These results suggest that the behaviors of Sb and As are closely related to those of Fe and Mn in the soil profile.

XANES analyses for Fe and Mn. It has often been shown that Fe(III) hydroxide and Mn(IV) oxide can be the host phases in soil for various trace elements, including Sb and As, due to their large surface areas, high adsorptive capacities and large abundances in soil (Brannon et al., 1985; Langmuir, 1997). Therefore, trace element distribution in such environments is often governed by Fe(III) hydroxide and Mn(IV) oxide, which may cause the moderate correlation among distributions of Fe, Mn, As, and Sb in our soil samples.

Characterization of Fe species in the soil profile was by X-ray absorption near-edge structure (XANES) at the Fe K-edge (Figure 2-3a). Features around the absorption edge of all the soil samples showed little variation and they are mostly similar to that of ferrihydrite within the depth profile. Using the pre-edge shift mainly due to change of Fe(II)/Fe(III) ratios, average oxidation state of Fe can be estimated (Bajt et al., 1994; Wilke et al., 2001). The Fe pre-edge structure around 7.110 keV was simulated by combination of Gaussian and spline functions. Figure 2-3a shows the simulation of Fe pre-edge peaks for Ichinokawa soil samples. Fe(II)/Fe(III) ratio does not show large variation with the depth and Fe(III) fraction in the soil samples are more than 80% within the depth profile. These results suggest that the major oxidation state of Fe is Fe(III) and that Fe is mainly present as Fe(III) hydroxide like ferrihydrite at all depths and can perform as a strong sorbent of Sb and As in the soil-water system. Similar results were obtained by Fe K-edge EXAFS (Figure 2-4).

On the other hand, Mn K-edge XANES spectra of soil samples varied greatly with depth (Figure 2-3b). The overall shapes of Mn K-edge XANES spectra of soil samples changed drastically at a depth of 6-9 cm. In addition, the pre-edge peak around 6.539 keV, which is closely related to the Mn(IV)/Mn(II) ratio, was simulated by method similar to that in the case of Fe (Figure 2-3a) following Wilke et al. (2001) and

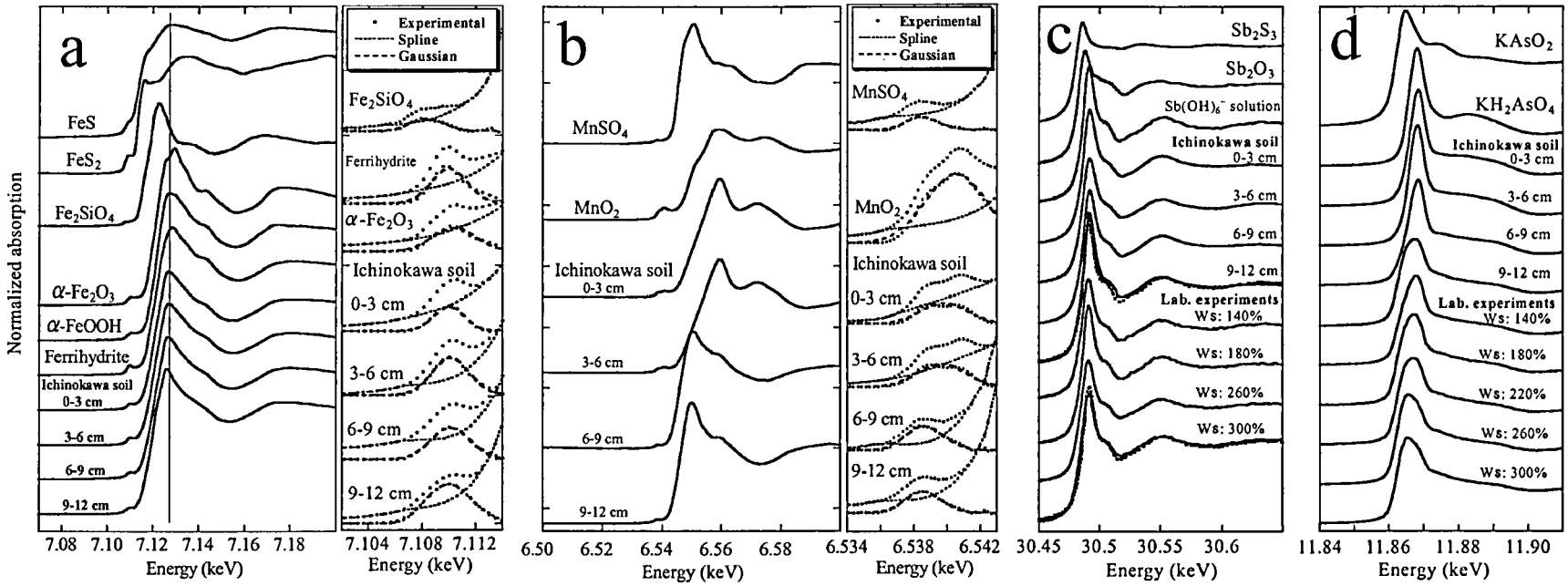

Figure 2-3. (a) Normalized Fe K-edge XANES spectra of the reference materials (FeS, FeS_2, Fe_2SiO_4, α-Fe_2O_3, α-FeOOH, and Ferrihydrite) and Fe in the natural soil samples from the Ichinokawa mine tailing. A line is drawn to indicate the absorption maximum of a soil sample at 0-3 cm depth. (b) Normalized Mn K-edge XANES spectra of the reference materials ($MnSO_4$ and MnO_2) and Mn in the Ichinokawa soil samples. In the pre-edge structures shown in (a) and (b), circles show experimental values while the solid curve indicates the spectrum resulting from the subtraction of the spline curve (dotted curve) by the simulation conducted according to Schulze et al. (1995). The solid curve was simulated by a Gaussian function, indicated as a dashed curve. (c) Normalized Sb K-edge XANES spectra of the reference materials (Sb_2S_3, Sb_2O_3, and $Sb(OH)_6^-$ solution), Sb in soil samples in the laboratory experiments, and in the Ichinokawa soil samples. Some spectra were overlapped with the spectrum of $Sb(OH)_6^-$ shown by dotted curves for comparison. (d) Normalized As K-edge XANES spectra of the reference materials ($KAsO_2$ and KH_2AsO_4), As in solid samples in the laboratory experiments, and in the Ichinokawa soil samples.

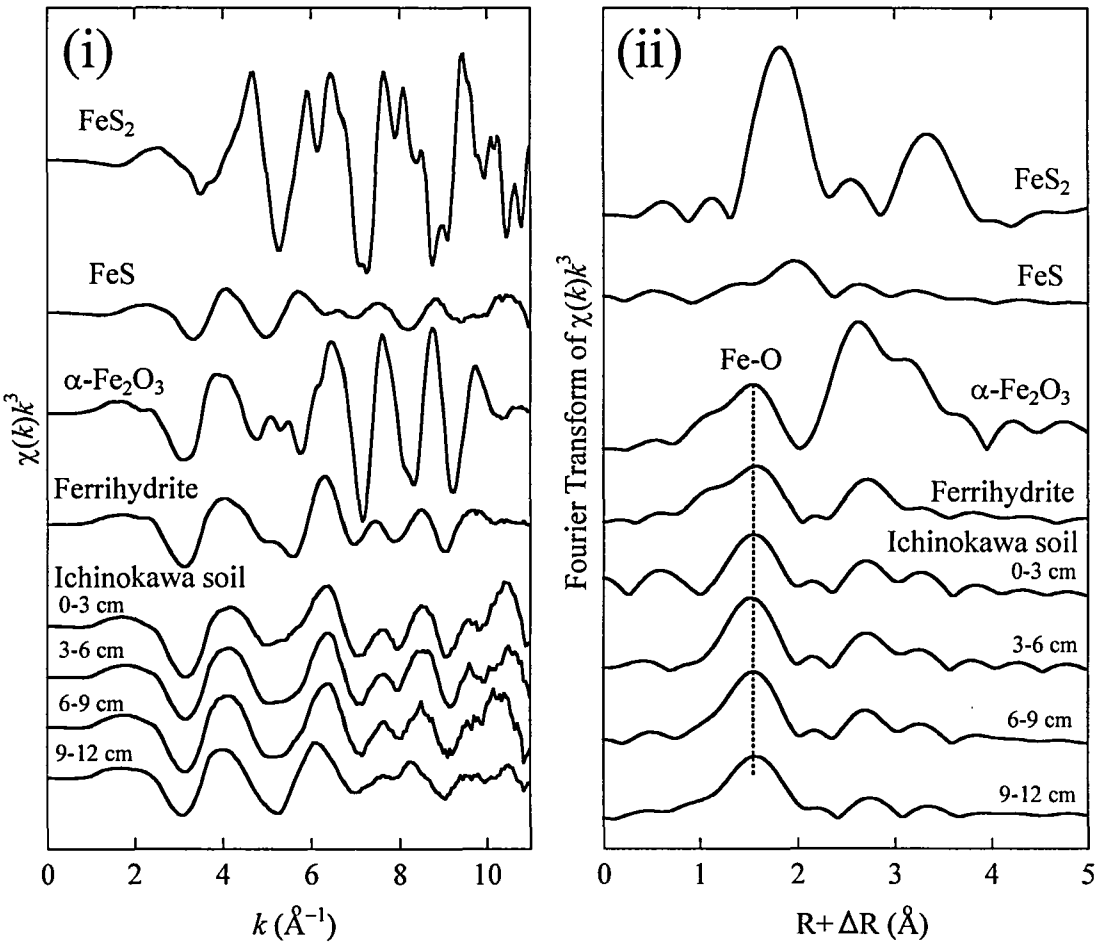

Figure 2-4. (i) Normalized k^3-weighted EXAFS spectra at the Fe K-edge and (ii) Fourier-transformed EXAFS spectra of Fe in the Ichinokawa soil samples and model compounds (FeS2, FeS, a-Fe2O3, and Ferrihydrite). Fourier transformation was conducted with k range of 3.0-11.0 Å. Radial distances are not corrected for the phase shift.

Schulze et al. (1995). As a result, the Mn(II) fraction increased drastically below a depth of 6-9 cm and Mn was mainly present as Mn(II) (> 90%) below 6 cm. These results indicate that the contribution of Mn(IV) oxide as adsorbent for Sb and As is not important, at least at depths below 6 cm in the Ichinokawa system. In the paddy field system, similar results were obtained by Fe and Mn XANES data (Takahashi et al., 2004), indicating that Fe is present as Fe(III) hydroxide whereas Mn is as Mn(II) under reducing condition.

Combining the Fe and Mn XANES results and the positive correlation of Sb and As concentrations with Fe (Table 2-1), we suggest that the host phases of Sb and As are Fe(III) hydroxide at all the depths in the soil profile, which will be confirmed by Sb and As K-edge XAFS.

XAFS analyses for Sb and As. Figure 2-3c shows the normalized Sb K-edge XANES spectra of reference materials, Ichinokawa samples, and laboratory experiment samples. It is obvious that the absorption edge shifts to higher energy at the higher oxidation state of Sb. This suggests that the position of the XANES peak can be used to distinguish Sb(III) and Sb(V). The absorption edges of Sb in Ichinokawa soil samples at all the depths were similar to that of $Sb(OH)_6^-$ solution. In the laboratory experiments, the dominance of Sb(V) was also shown in XANES spectra at various W_S (Figure 2-3c). These results, in both Ichinokawa and laboratory systems, suggest that Sb(V) is the stable oxidation state over a wide Eh range in soil.

On the other hand, in As K-edge XANES spectra, the absorption edges of As in soil samples shifted to lower energy at the depth of 9-12 cm in the Ichinokawa system and also at larger W_S in the laboratory experiments (Figure 2-3d). These results suggest that As(III) fraction in soil increased under reducing conditions. Simulation of XANES spectra was conducted for soil samples based on the spectra of the reference materials ($NaAs^{III}O_2$ and $NaH_2As^{V}O_4$) following Takahashi et al. (Langmuir, 1997) (Figures 2-5b,c). In Ichinokawa soil samples, more than 95% of As is present as As(V) at a depth of 0-3 cm (Eh = 360-65 mV, pH 7.6-8.1). However, the As(III)/As(V) ratio gradually increased and the As(III) ratio was almost 70% at the depth of 9-12 cm (Eh = −140 mV, pH 7.9), whereas Sb was completely in the oxidized

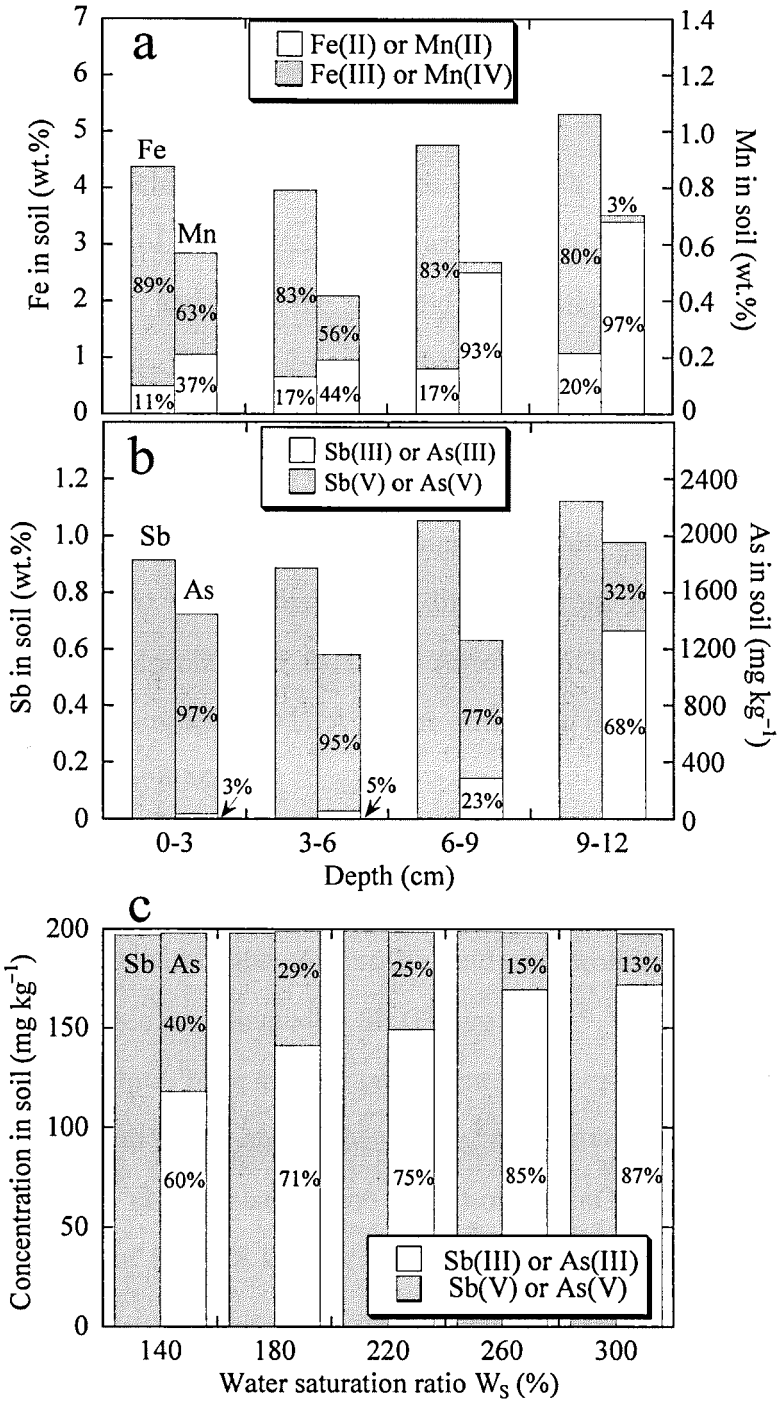

Figure 2-5. (a) Depth profile of Fe (Fe(II) and Fe(III)) and Mn (Mn(II) and Mn(IV)) concentrations in the soil profile of the Ichinokawa system by the simulation of Fe and Mn K-edge XANES, (b) depth profile of Sb and As (As(III) and As(V)) concentrations in the soil profile by the simulation of As K-edge XANES, and (c) concentrations of Sb and As (As(III) and As(V)) in soil in the laboratory experiments by the simulation of As K-edge XANES.

form, Sb(V). Therefore, it is suggested that As is reduced at more positive Eh than Sb. In the laboratory experiments, the As(III)/As(V) ratio also increases at lower Eh (at higher W_S) (Figure 2-5c). The sample with the highest water proportion, W_S = 300% (Eh = 41 mV, pH 6.8), had about 90% As(III) in the soil. This trend is consistent with the results found in the Ichinokawa soil samples with depth.

Local structures of Sb and As were examined by EXAFS to obtain information on the host phases of Sb and As in the soil, and to investigate the variation of the host phase in the soil profile. Figures 2-6a,b show k^3-weighted EXAFS spectra of Sb and their Fourier transformations (FTs) for Ichinokawa soil samples and model compounds. The amplitudes and oscillations of EXAFS spectra are similar among the samples at all the depths, suggesting that Sb species are similar within the soil profile. EXAFS spectra of Sb(V) sorbed on ferrihydride is different from those on δ-MnO_2 in the oscillation structures, especially at 8-11 $Å^{-1}$ (arrows in Figure 2-6a). The spectral features of all the soil samples at 8-11 $Å^{-1}$ were similar to that of Sb(V) on ferrihydrite, but different from that on δ-MnO_2.

Fourier transformation was conducted against the EXAFS spectra of the soils and model compounds within the k range of 3.0-11.0 $Å^{-1}$ to obtain the RSF. All RSFs were also quite similar within the soil profile, and one prominent peak was observed near 1.5 Å due to oxygen coordinated to Sb (Figure 2-6b). The RSFs of Sb(V) sorbed on ferrihydrite and δ-MnO_2 have another prominent peak near 2.85 Å and 2.75 Å (phase shift uncorrected) due to Sb-Fe and Sb-Mn shells, respectively. The features in RSFs of all soil samples are not consistent with Sb(V) on δ-MnO_2, but similar to Sb(V) on ferrihydrite. Results of EXAFS spectra and RSFs suggest that Sb in the soil is mainly associated with Fe(III) hydroxide at all depths, which is consistent with a correlation between Fe and Sb abundances in the soil (Table 2-1). This suggestion is also supported by the fact that Fe(III) hydroxide is a major component of Fe species in the soil, as suggested by Fe XANES analysis (Figure 2-3a). Therefore, we conclude that major Sb is present as Sb(V) co-precipitated or/and adsorbed on Fe(III) hydroxide like ferrihydrite within the soil profile. The result of the shell-by-shell fitting of filtered Sb k^3-weighted EXAFS spectra of soil samples and reference materials are summarized in

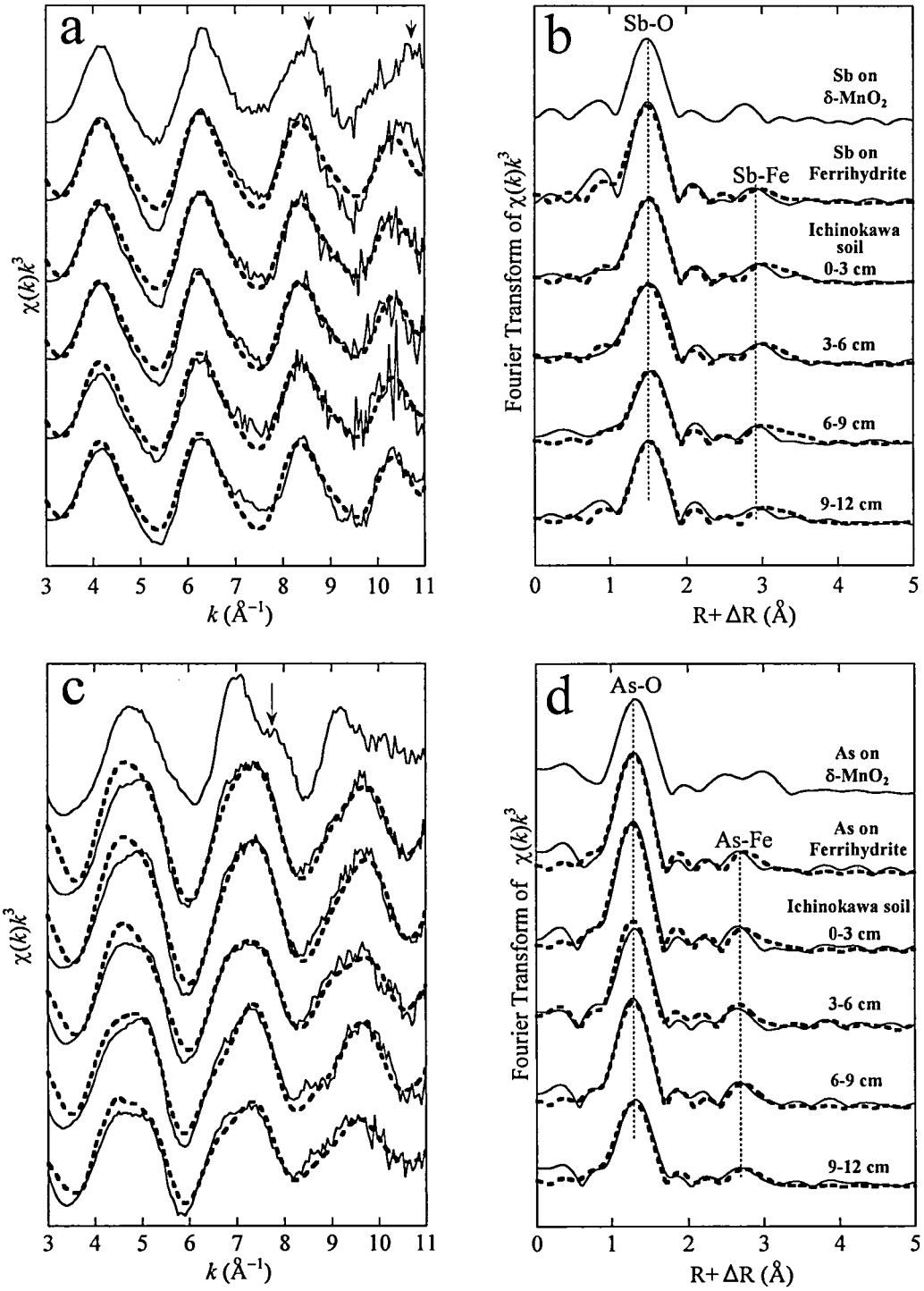

Figure 2-6. (a) Normalized k^3-weighted EXAFS spectra at the Sb K-edge and (b) Fourier-transformed EXAFS spectra of Sb in the Ichinokawa soil samples and model compounds (Fe sorbed on ferrihydrite andδ-MnO_2). Radial distances are not corrected for the phase shift. Arrows in (a) show the features in EXAFS spectra related to Sb(V) sorbed on δ-MnO_2. (c) Normalized k^3-weighted EXAFS spectra at the As K-edge and (d) Fourier-transformed EXAFS spectra of As in the Ichinokawa soil samples and model compounds. An arrow in (c) shows the feature in EXAFS spectrum related to As(V) sorbed on δ-MnO_2.

Table 2-3. Structual data on the local environment of Sb derived from the simulation of EXAFS data of natural soil samples and model compound[a]

Sample	shell	N	R (Å)	ΔE_0 (eV)	σ (Å)
Sb(V)-ferrihydrite	Sb-O	5.8	1.97	1.1	0.05
	Sb-Fe	2.2	3.59		0.12
0-3 cm	Sb-O	5.1	1.98	3.1	0.05
	Sb-Fe	2.1	3.59		0.08
3-6 cm	Sb-O	5.6	1.98	-0.8	0.06
	Sb-Fe	2.1	3.55		0.09
6-9 cm	Sb-O	5.1	1.98	4.1	0.05
	Sb-Fe	2.0	3.59		0.10
9-12 cm	Sb-O	5.1	1.98	4.7	0.03
	Sb-Fe	2.5	3.58		0.08

[a]R, interatomic distance; N, number of neighbors; σ, Debye-Waller factor; ΔE_0, energy offset.

Table 2-4. Structual data on the local environment of As derived from the simulation of EXAFS data of natural soil samples and model compound[a]

Sample	shell	N	R (Å)	ΔE_0 (eV)	σ (Å)
As(V)-ferrihydrite	As-O	4.3	1.69	5.6	0.06
	As-Fe	2.2	3.29		0.09
0-3 cm	As-O	4.5	1.68	2.7	0.06
	As-Fe	1.8	3.29		0.07
3-6 cm	As-O	5.0	1.70	5.6	0.08
	As-Fe	1.6	3.29		0.08
6-9 cm	As-O	4.2	1.70	4.4	0.06
	As-Fe	2.0	3.27		0.08
9-12 cm	As-O	4.2	1.73	6.9	0.07
	As-Fe	2.0	3.31		0.08

[a]R, interatomic distance; N, number of neighbors; σ, Debye-Waller factor; ΔE_0, energy offset.

Table 2-3. As a result, the Sb-Fe distances are 3.49±0.02 Å at all the depths. This distance was identical to that obtained for Sb in ferrihydrite (3.50 Å) prepared as a model compound. This result confirms that Sb(V) is in the Fe(III) hydroxide phase. Earlier researchers reported that the major host phases of Sb in sediments are Fe hydroxide, Mn oxide, and organic compounds, using adsorption and sequential extraction experiments (Lintschinger et al, 1998; Belzile et al., 2001; Chen et al., 2003). Our EXAFS study clearly showed that Fe(III) hydroxide is the host phase of Sb in the soil profile, which agrees with the earlier studies.

Arsenic k^3-weighted EXAFS spectra of the soil and model compounds are shown in Figure 2-6c. Manning et al. (2002) reported that the EXAFS spectrum of As(V) sorbed on Mn oxide has a dished spectral feature at 7–8 $Å^{-1}$, which was also observed in this study (arrow in Figure 2-6c). The features of EXAFS spectra of Ichinokawa soil samples agree with those of As(V) sorbed on ferrihydrite and differ from δ-MnO_2. From the EXAFS spectra, it is suggested that the major part of As was associated with the Fe(III) hydroxide phase in the soil and that the host phase of As does not depend on the depth, or redox condition. The k^3-weighted FT for all the samples and model compounds was conducted within the k range 3.0-11.0 $Å^{-1}$. All RSFs of the soil profile were similar and two prominent peaks were observed at 1.15 Å and 2.7 Å (phase shift uncorrected) due to As-O and As-Fe shells, respectively. The results of shell-by-shell fitting for As are summarized in Table 2-4. From the fitting, the distance of As-O at the 9-12 cm sample is 1.73 Å, longer than the other samples. This result is consistent with the XANES results showing that As(III) is dominant in soil (As(III): 68%), since the distance of As(III)-O is longer than that of As(V)-O (Farquhar et al., 2002). The As-Fe distance at 3.28±0.02 Å corresponds to As(V) bound to ferrihydrite by double corner sharing. Such an As complex has already been reported for synthetic samples of As(V) in amorphous Fe(III) hydroxide (Waychunus et al., 1993; Scherman and Randall, 2003) where the As-Fe distance was reproduced (Table 2-4) in the model compounds prepared in this study. Therefore, As EXAFS analysis also supports the idea that most of the As in the soil profile is incorporated into Fe(III) hydroxide.

Concentrations of Fe, Mn, Sb, and As in soil water. Under oxic conditions (above 3 cm depth) in the Ichinokawa system, dissolved Fe and Mn concentrations are low in the soil water (Figure 2-7a). In contrast, their concentrations increased with depth to 9 cm as reducing conditions develop. These results suggest that reductive dissolutions of Fe and Mn occur at the deeper part. In the laboratory system, a similar trend was observed, that dissolved Fe and Mn abundances increased under reducing condition (at higher W_S) was also obtained clearly (Figure 2-7c).

In the Ichinokawa soil samples, Sb abundance in soil water decreased with depth, whereas As abundance in the soil water increased (Figure 2-7b). This contrast in behavior of Sb and As is also shown in the soil water in the laboratory samples (Figure 2-7c). The good agreement of the results in both systems indicates that phenomena occurring in the Ichinokawa system were reproduced in the laboratory experiments and that the variation of redox condition influenced the partition of Sb and As in the soil-water system. The contrast in behavior between Sb and As concentrations in soil water are quite interesting considering that Sb belongs to the same group as As in the periodic table.

Based on the speciation by HPLC-ICP-MS, Sb in soil water was predominantly in the oxidized form, Sb(V), in both the Ichinokawa and laboratory systems (Figures 2-7b,c). In contrast, As is dissolved as the oxidized form, As(V), (As(V): 94%) at depth of 1 cm, whereas the reduced form, As(III), was the main component (As(III): 99%) at a depth of 9 cm (Figure 2-7b). It is strongly suggested that the contrast in behavior between Sb and As abundances in soil water is caused by the difference in their redox properties.

Under reducing conditions, the As concentration in soil water increased together with Fe and Mn in both the Ichinokawa and laboratory systems (Figure 2-7). It has been reported that the leaching of As under reducing condition depends on (1) the reductive dissolution of Fe(III) (hydr)oxide, host phase for As in soil (Smedley and Kinniburgh et al., 2002; Takahashi et al., 2004), and (2) the reduction of As(V) to As(III), since As(III) is liable to partition to the aqueous phase more readily than As(V)

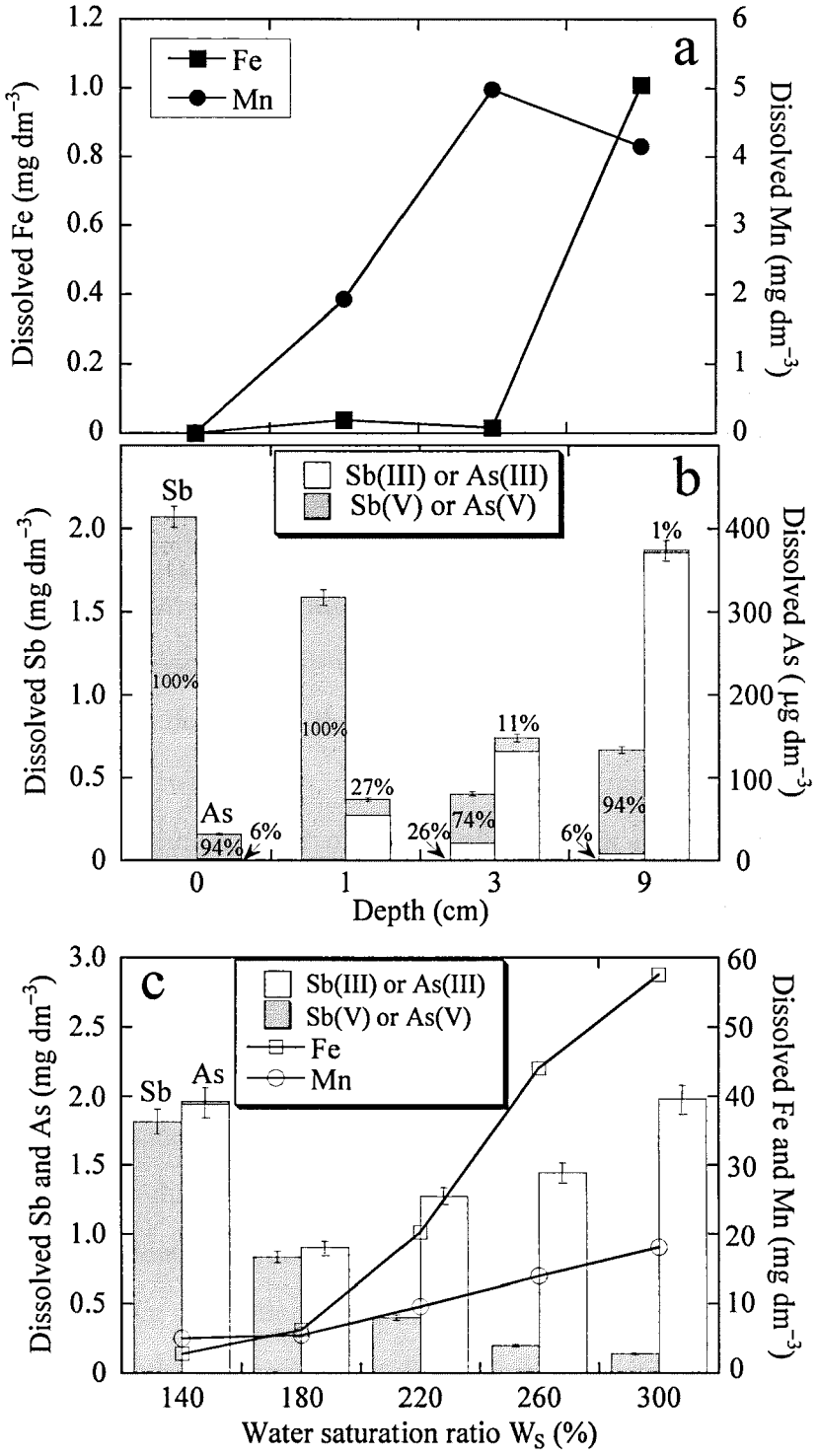

Figure 2-7. Depth profiles of (a) Fe, Mn, (b) Sb, and As concentrations in soil water in the natural system at Ichinokawa mine and (c) in soil water at different degrees of water saturation (W_S) in the laboratory experiments. For dissolved Sb and As, the ratios of trivalent and pentavalent forms are shown, respectively. The numerical values in each bar graph stand for the percentage of each form in soil water. Uncertainties of Fe and Mn in (a) and (c) are smaller than the sizes of the symbols.

(Pierce and Moore, 1982; Bowell, 1994; Smedley and Kinniburgh et al., 2002; Takahashi et al., 2004). In this study, Fe in soil is mainly present as Fe(III) hydroxide at all depths, based on the Fe XANES analysis (Figures 2-3a and 2-5a) and the Fe concentration in soil is still high at the deeper part. Therefore, it is suggested that the Fe(III) hydroxide phase keeps its potential as a host phase for As, and that the dissolution of Fe has little effect on the release of As to soil water. Thus, we conclude that As release from the soil strongly depends on the As redox property in the system.

On the other hand, Sb in Ichinokawa soil water showed the opposite trend to those of Fe and Mn (Figure 2-7a,b) with depth (redox condition), whereas Sb abundance in soil has a positive correlation with Fe and Mn abundances (Table 2-1). This result was also observed in the laboratory experiments, showing that the Sb concentration in soil water decreased with the increase of W_S, or lower Eh (Figure 2-7c). This result indicates that Sb behavior in soil-water system depends apparently on the redox condition and does not depend on the difference of the initial condition between the laboratory and Ichinokawa systems. As in the case of As, the host phase of Sb is Fe(III) hydroxide and the behavior of dissolved Sb is not directly influenced by the dissolution of Fe(III) hydroxide. Since Sb species (=Sb sorbed on Fe(III) hydroxide) did not change with redox condition in both soil and soil water phases, we considered that the decrease of dissolved Sb under more reducing condition in the Ichinokawa and laboratory systems is caused by the variation of adsorptive properties of the host phase of Sb (= Fe(III) hydroxide) as the redox potential changes. Under reducing conditions, (i) dissolution reaction due to the reduction of Fe(III) to Fe(II) and (ii) re-precipitation reaction due to the oxidation to Fe(III) hydroxide may be dynamically occurring in the system. In addition, Fe absorption edges of Ichinokawa soil samples shifted slightly to lower energy with depth (Figure 2-3a). These facts indicate that structural order of Fe(III) hydroxide may decrease with depth. Richmond et al. (2004) reported that when a structural order of ferrihydrite decreases, Fe(III) hydroxide precipitates have a larger surface area and stronger adsorptive potential. It is speculated that the larger surface area of disordered Fe(III) hydroxide at the depth leads to the larger partition ratio of Sb to soil under reducing condition.

Conclusions

In this study, speciations of Sb and As in a natural soil-water system were successfully conducted, both in the aqueous and soil phases, by HPLC-ICP-MS and XAFS. It was shown that Sb and As were similarly incorporated in Fe(III) hydroxide phase in the soil profile based on EXAFS analyses and the correlation among their abundances. However, the dependence of dissolved concentrations of Sb and As on depth, or Eh condition, is totally different between the two elements. Arsenic(V) can be reduced to As(III) as reducing conditions develop in the soil profile, which results in the increase of the dissolved As fraction in soil water. In contrast, Sb(V) is a stable oxidation state even under reducing condition (Eh = −180 mV, pH 8) and Sb is oxidized at lower Eh than As. As a result, dissolved Sb concentrations do not increase with decreasing redox potential. The different redox properties of Sb and As is of great importance to an understanding of the behavior of As and Sb and their fractionation in natural aquifers.

References

Bancroft, P. 1988. Famous mineral localities: the Ichinokawa mine. Mineral. Rec. 19, 229-238.

Bajt, S.; Sutton, S. R.; Delaney, J. S. 1994. X-ray microprobe analysis of iron oxidation-states in silicates and oxides using X-ray-absorption near-edge structure (XANES). Geochim. Cosmochim. Acta. 58, 5209-5214.

Belzile, N.; Chen, Y.W.; Wang, Z. 2001. Oxidation of antimony (III) by amorphous iron and manganese oxyhydroxides. Chem. Geol. 174, 379-387.

Berlepsch, P.; Armbruster, T.; Brugger, J.; Griddle, A. J.; Graeser, A. J. 2003. Tripuhyite, $FeSbO_4$, revised. Mineral. Mag. 67, 31-46.

Bowell, R. J. Sorption of arsenic by iron-oxides and oxyhydroxides in soil. 1994. Appl. Geochem. 9, 279-286.

Brannon, J. M.; Patrick, W. H., Jr. 1985. Fixation and mobilization of antimony in sediments. Environ. Pollut. 9B, 107-126.

Chen, Y.-W.; Deng, T.-L.; Filella, M.; Belzile, N. 2003. Distribution and early diagenesis of antimony species in sediments and pore water of freshwater lakes. Environ. Sci. Technol. 37, 1163-1168.

Council of the European Communities. Council Directive 76/ Substances Discharged into Aquatic Environment of the Community; Official Journal L 129, 1976; pp 23-29.

Crecelius, E. A.; Bothner, M. H.; Carpenter, R. 1975. Geochemistries of arsenic, antimony, mercury, and related elements in sediments of Puget Sound. Environ.Sci. Technol. 9, 325-333.

El Bilali, L.; Rasmussen, P. E.; Hall, G. E. M.; Fortin, 2002. D. Role of sediment composition in trace metal distribution in lake sediments. Appl. Geochem. 17, 1171-1181.

Farquhar, M. L., Charnock J. M., Livens F. R., Vaughan D. J. 2002. Mechanisms of arsenic uptake from aqueous solution by interaction with goethite, lepidocrocite, mackinawite, and pyrite: An X-ray absorption spectroscopy study. Environ. Sci. Technol. 36, 1757-1762.

Filella, M.; Belzile, N.; Chen, Y.–W. 2002. Antimony in the environment: a review focused on natural waters. II. Relevant solution chemistry. Earth-Sci. Rev. 57, 125-176.

Kanazawa, T.; Sager, W.W.; Escutia, C.; et al. Proc. ODP, Init, Repts. 2001, 191 [CD-ROM]. Available from Ocean Drilling Program, Texas A&M University, College Station, TX 77845-9547.

Kitahama, K.; Kiriyama, R.; Yoshida, B. 1975. Refinement of the crystal structure of scorodite. Acta Crystallogr., Sect. B B31, 322-324.

Krachler, M.; Emons, H. 2001. Urinary antimony speciation by HPLC-ICP-MS. J. Anal. At. Spectrom. 16, 20-25.

Langmuir, D. In Aqueous Environmental Geochemistry; Prentice–Hall: New Jersey, 1997.

Lintschinger, J.; Michalke, B.; Schulte-Hostede, S.; Schramel, P. 1998. Studies on speciation of antimony in soil contaminated by industrial activity. Int. J. Environ. Anal. Chem. 72, 11-25.

Manning, B. A.; Fendorf, S. E.; Bostick, B.; Suarez, D. L. 2002. Arsenic(III) oxidation and Arsenic(V) adsorption reactions on synthetic birnessite. Environ. Sci. Technol. 36, 976-981.

Mitsunobu, S.; Takahashi, Y.; Hirunuma, R., Haba, H.; Enomoto, S. 2005. Coupling of ICP-MS and multitracer technique as a new method to investigate dynamics of various elements in soil-water system. Chem. Lett. 34, 980-981.

Mitsunobu, S.; Harada, T.; Hoshino, K.; Takahashi, Y. 2005. X-ray absorption study on the dominance of Sb(V) as secondary antimony species in soil. Chem. Lett. 34, 1656-1657.

Murray, J. W. The surface chemistry of hydrous manganese dioxide. J Colloid Interface Sci. 1974, 46, 357-371.

Picard, C.; Bosco, M. 2003. Soil antimony pollution and plant growth stage affect the biodiversity of auxin-producing bacteria isolated from the rhizosphere of Achillea ageratum L. FEMS Microbial. Ecol. 46, 73-80.

Pierce, M. L.; Moore, C. B. 1982. Adsorption of arsenite and arsenate on amorphous iron

hydroxide. Water Res. 16, 1247-1253.

Richmond, W. R.; Loan, M.; Morton, J.; Parkinson, G. 2004. Arsenic removal from aqueous solution via ferrihydrite crystallization control. Environ. Sci. Technol. 38, 2368-2372.

Schulze, D. G.; Sutton, S. R.; Bajt, S. 1995. Determination manganese oxidation-state in soils using X-ray absorption near-edge structure (XANES) spectroscopy. Soil Sci. Soc. Am. J. 59, 1540-1548.

Schwertmann, U.; Cornell, R. M.; 1991, Iron Oxides in the Laboratory, 2nd ed.; Wiley–VCH: Weinheim; pp. 103–112.

Sherman, D. M.; Randall, S. R. 2003. Surface complexation of arsenic(V) to iron(III) (hydr)oxides: Structural mechanism from ab initio molecular geometries and EXAFS spectroscopy. Geochim. Cosmochim. Acta 67, 4223-4230.

Smedley, P. L.; Kinniburgh, D. G. 2002. A review of the source, behaviour and distribution of arsenic in natural waters. Appl. Geochem. 17, 517-568.

Takahashi, Y.; Minamikawa, R.; Hattori, H. K.; Kurishima, K.; Kihou, N.; Yuita, K. 2004. Arsenic behavior in paddy fields during the cycle of flooded and non-flooded periods. Environ. Sci. Technol. 38, 1038-1044.

Takahashi, Y.; Ohtaku, N.; Mitsunobu, S.; Yuita, K.; Nomura, M. 2003. Determination of the As(III)/As(V) ratio in soil by X-ray absorption near-edge structure (XANES) and its application to the arsenic distribution between soil and water. Anal. Sci. 19, 891-896.

United States Environmental Protection Agency. Water Related Fate of the 129 Priority Pollutants; Doc. 745-R-00-007; USEPA: Washington, DC, 1979; Vol. 1.

Waychunas, G. A.; Rea, B. A.; Fuller, C. C.; Davis, J. A. 1993. Surface-chemistry of ferrihydrite 1. EXAFS studies of the geometry of coprecipitated and adsorbed arsenate. Geochim. Cosmochim. Acta 57, 2251-2269.

Wedepohl, K. H. 1995. The composition of the continental-crust. Geochim. Cosmochim. Acta. 59, 1217-1232.

Wilke, M.; Farges, F.; Petit, P.; Brown, G. E., Jr.; Martin, F. 2001. Oxidation state and coordination of Fe in minerals: An Fe K-XANES spectroscopic study. Am. Min.

86, 714-730.

Zabinsky, S. I.; Rehr, J. J.; Ankudinov, A.; Albers, R. C.; Eller, M. J. 1995. Multiple-scattering calculations of X-ray-absorption spectra. Phys. Rev. B 52, 2995-3009.

CHAPTER 3

Characterization of Fe in the soil collected from Ichinokawa mine tailing

Introduction

Fe(III) hydroxides are ubiquitous components of soils and sediments, where they occur in a variety of phases ranging from poorly crystalline ferrihydrite to well-crystallized minerals such as goethite and hematite (Cornell and Schwertmann, 2003). Fe(III) hydroxides play an important role in the natural environment, since they can be a sorbent of various trace elements due to their high oxidative capability, high adsorptive capacity, and large abundance in the environment. For example, it is reported that Fe(III) hydroxides being host-phase of As play an important role for As behavior in the Ganges delta plain (Bangladesh and West Bengal in India), where As concentration in groundwater is highly contaminated (Nickson et al., 1998; 2000; McArthur et al., 2001; Dowling et al., 2002). For a particular Fe(III) hydroxides phase, a range of crystallinity can exist, which correlates with the particle size, surface area, and solubility of the mineral. Such variations lead to various reactivities of Fe(III) hydroxides toward chemical dissolution for diverse assemblages of Fe(III) oxides present in environmental samples (Postma, 1993). There are many examples for the dynamic change of Fe oxides and their influence on the behaviors of trace elements in the environment. In relation to this, it is reported that when a structural order of ferrihydrite decreases, Fe(III) hydroxides have a larger surface area and a greater potential for As removal (Riveros et al., 2001; Richmond et al., 2004).

Our recent study showed that host-phase of As is Fe hydroxides in a soil-water system in a mine tailing (Ichinokawa mine) in Japan and that As concentration in soil water increases together with Fe under reducing condition at deeper part (Fig. 3-1; Mitsunobu et al., 2006). This finding suggests that the dissolution of As can be controlled by (1) the reductive dissolution of Fe hydroxides and/or (2) the reduction of As to As(III) which is regarded to be more mobile than As(V) in the system. Similar examinations for the As release under reducing condition have been done in soil-water system previously (Nickson et al., 1998; 2000; Takahashi et al., 2004; Kocar et al., 2006).

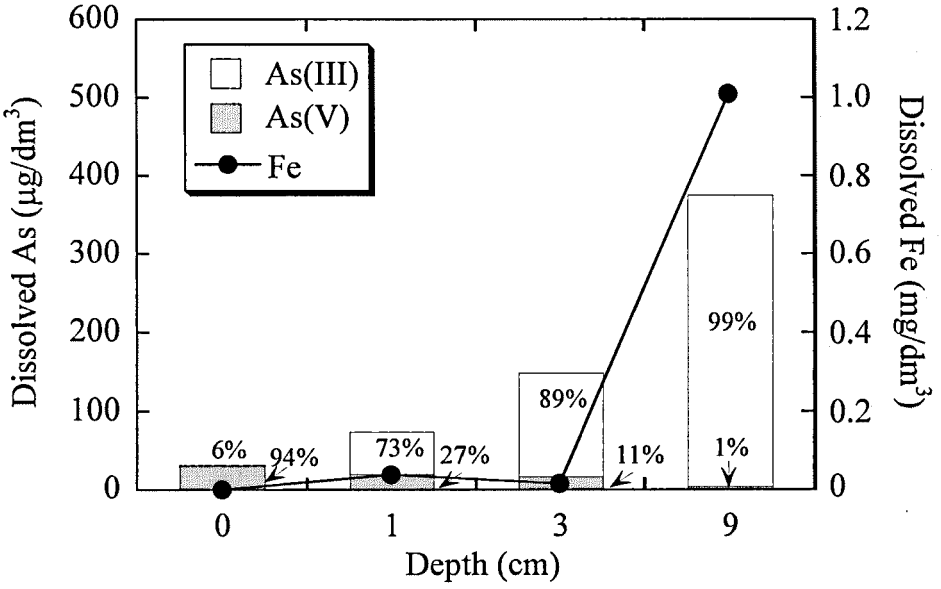

Fig. 3-1. Depth profile of As and Fe concentrations in soil water in the natural system near Ichinokawa mine. For dissolved As, the ratios of trivalent and pantavalent forms are shown, respectively.

However, distinction of these two factors regarding to their importance on As migration is still not clear, since the sorptive potential of Fe hydroxides such as particle size and crystallinity has not been evaluated with the speciation of As in many cases.

Mitsunobu et al. (2006) also reported a possibility that the absorptive capacity of amorphous Fe(III) hydroxide changes at redox boundary in soil. In the study, it was suggested that Sb(V) was more strongly adsorbed to Fe(III) hydroxide at relatively reducing condition than at oxic condition (Mitsunobu et al.,2006). Fe(III) hydroxide in such environment can partially remain, where the adsorptive potential of the remaining Fe(III) hydroxide could be larger than that of the Fe(III) hydroxide formed under oxic condition. Thus, we can hypothesize that the partial reduction of Fe(III) in the Fe(III) hydroxide influences its adsorptive property as sorbent in soil under reducing condition.

In addition, since Fe(III) hydroxides can be the host phase in soils and sediments of many toxic elements, it is important to characterize Fe species and its crystallinity to understand the fate and distribution of trace elements in soil/sediment-water system under various redox conditions. However, few studies have examined the effect of the change of redox condition on the morphology of Fe(III) hydroxides such as particle size, crystallinity, and surface area.

The objective of this research is to characterize Fe species in the soil profile in the mine tailing (Fig. 3-1) related to the As release in the system. In particular, structural order of Fe(III) hydroxides such as morphology and particle size under various redox condition will be discussed, which may affect As release in the system. In the analyses of the Fe(III) hydroxides, we employed X-ray absorption fine structure (XAFS) and Mössbauer spectroscopic analyses to directly obtain information on the Fe species, the mineral, oxidation state, and structural order. Both methods are *in-situ* analyses, sensitive only to Fe without the interruption of any matrix elements, and are thus powerful in determining the Fe forms. For the basis of the discussion, we also examined Fe(III) hydroxides prepared at various degrees of supersaturation, which allows us to study the dependence of the characteristics in XAFS and Mössbauer spectra on the crystallinity, or particle size, of Fe(III) hydroxides.

Materials and methods

Natural samples

Natural soil samples were collected in October 2005 around the Ichinokawa mine pithead (33.53N, 133.12E) in Ehime, Japan, which was formerly one of the largest Sb (stibnite: Sb_2S_3) mines (Bancroft, 1988). The soil is heavily contaminated with As and Sb (As: 1200-2000 mg/kg; Sb: 0.9-1.1 wt%), details of which were already reported in our previous paper (Mitsunobu et al., 2006). The sampling site was flooded soil located at about 5 m downward from the mine pithead. To allow us to observe the variation of the Fe(III) structure under various redox conditions, the soil samples were collected at four depth ranges (0-3, 3-6, 6-9, and 9-12 cm) using a plastic spatula in the wetland-tailing site. The Eh and pH were measured by a Pt electrode (Fujiwara Sci., EHS-120) and a glass electrode (Horiba, D-51), respectively, at the sampling site. The Eh values decreased monotonically from 360 to –140 mV with depth in the Ichinokawa soil samples (Fig. 3-2). This result shows that the redox condition became reductive in the soil with depth, presumably because oxygen supply diminishes with depth for the bacterial activity (Mitsunobu et al., 2005; Takahashi et al., 2004). The pH values of soil water were relatively uniform with depth.

The collected soil samples were immediately sealed in polystyrene bottles and were kept at 4°C during transportation to our laboratory. In the laboratory, the soil samples were passed through a 500 μm stainless steel sieve to remove large organic particles and gravel fractions, and then were homogenized. Aliquots of the homogenized soil were packed into polyethylene bags for XAFS and Mössbauer analyses, and were stored at −20°C to avoid unexpected oxidation before analyses. The concentrations of major elements in soil samples were measured by X-ray fluorescence spectrometry (XRF; Rigaku ZSX-101e) as reported in the work of Mitsunobu et al. (2006). Mineral compositions were analyzed using an X-ray diffractometer (XRD; MAC Sci., M18XHF), with the Cu Kα radiation set at 20 kV and 10 mA. The major minerals in all the soil samples were kaolinite, quartz, and mica. The minerals containing low spin Fe(II) such as ilmenite and pyrite were not observed in the XRD

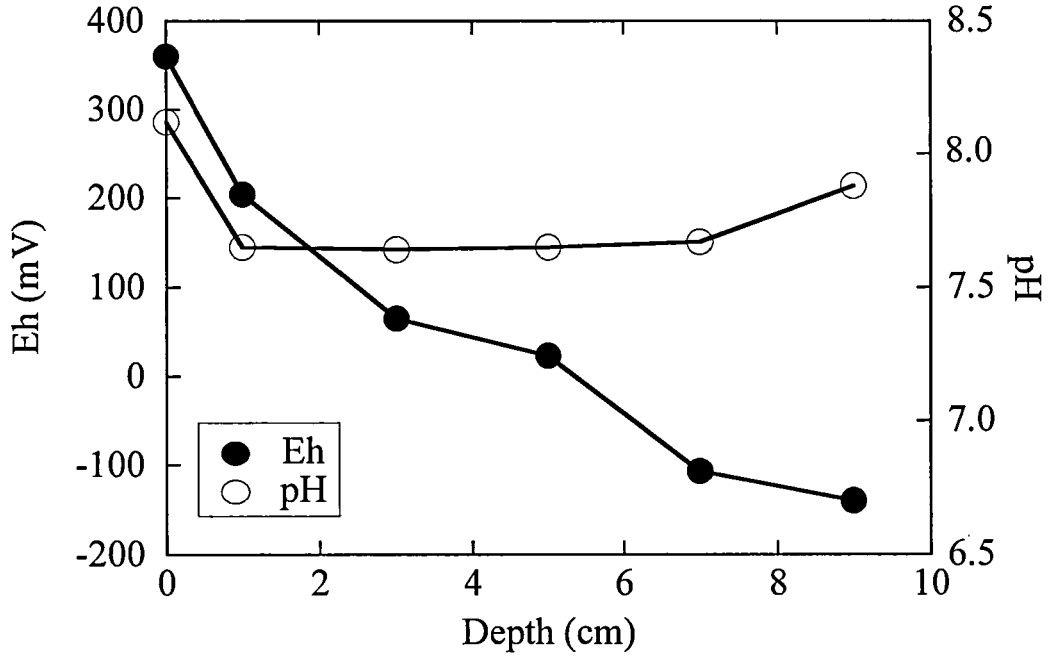

Fig. 3-2. Eh and pH variations with depth in the Ichinokawa soil-water system.

patterns of all soil samples.

Synthesis of Fe hydroxide (ferrihydrite) with crystallization control

Ferrihydrite with different crystallinity was prepared by hydrolysis of ferric sulfate at 85°C as a standard material in this study according to Richmond et al. (2004). The solution was then neutralized to pH 7 by a single addition of NaOH (10 and 1 M, in the appropriate volumes). The solids were collected by vacuum filtration with a 0.2 μm filter membrane, and then were washed twice with Milli-Q water. After which, the solids were dried in air for 24 h at 50°C. The synthesis was designed in such a way as to vary the ferrihydrite supersaturation by altering the initial Fe(III) ion concentration. Supersaturation is generally expressed as the ratio $S = c/c^*$, where c is the concentration of the solute and c^* is the equilibrium solubility of the solute. We have estimated the supersaturation ratios using the value 1.07×10^{-6} M for the concentration of Fe^{3+} in equilibrium with 6-line ferrihydrite at pH 7, as reported by Cornell and Schwertmann (2003). The estimated supersaturation ratios (S_E) for ferrihydrite syntheses at pH 7 are given in Table 3-1. The dried samples were characterized by XRD and surface area measurements using the BET method after levigation by a mortar. The samples were evacuated for 6 hours at 117°C to remove physically adsorbed water before BET analyses (Cornell and Schwertmann, 2003).

XAFS measurements and data analysis

Iron K-edge XAFS spectra were measured at the beamline BL01B1 at SPring-8 (Hyogo, Japan). Energy calibration was made by defining the pre-edge peak maximum of hematite fixed at 7.113 keV. All spectra of the soil samples were collected in the fluorescence mode with a Lytle detector. The spectra of Fe model compounds including the synthesized ferrihydrite were collected in the transmission mode with an ion chamber. The measurements were carried out at room temperature under ambient air condition. Several XAFS spectra were also recorded at the beamline BL12C in the Photon Factory (PF), KEK (Tsukuba, Japan), which gave identical results as what were observed at SPring-8. The set-up of the BL12C at PF is similar to that of BL01B1 at SPring-8.

Table 3-1. Estimated supersaturation ratios (S_E) of ferrihydrite solids for syntheses at pH 7.

Sample name	Initial [Fe^{3+}] (M)	S_E/1000	Surface area[a] (m^2/g)
S_E^{13}	0.014	13	117.4
S_E^{26}	0.028	26	142.6
S_E^{220}	0.236	220	224.4

[a] Surface area of solid was measured by BET method.

Extended X-ray absorption fine structure (EXAFS) data were analyzed by REX2000 (Rigaku Co. Ltd.). The oscillation was extracted from the original spectrum by a spline smoothing method. E_0 was initially set to the edge inflection point for all the samples studied. The Fourier transformation of the $k^3\chi(k)$ EXAFS oscillation from k space to r space was performed in the range 3.5 – 9.5 $Å^{-1}$ to obtain a radial structure function (RSF) for Fe.

Mössbauer spectrometry

The ^{57}Fe Mössbauer spectra were measured at 78 K and at room temperature (RT, 20°C) in transmission mode using Topologic Systems MD-222B Mössbauer spectrometers against 370-MBq or 925-MBq ^{57}Co in Rh foil. The cryogenic measurements were performed at 78 K using a liquid nitrogen cryostat DN1726 fabricated by Oxford Instruments. All synthesized ferrihydrites were diluted by BN to ca. 13 wt%. Each sample was mounted to an Al holder with a 1.0 cm diameter window to measure the Mössbauer spectra. Natural soil was packed in a polyethylene bag to protect the sample from oxidation during analysis, that is, the Mössbauer measurements were conducted without dilution for the natural soil samples. The measurement time to record a spectrum was 10 to 20 h. The spectra were not corrected for thickness effects (Rancourt et al., 1993). The Mössbauer spectra were analyzed by MossWinn 3.0i (Sakai et al., 2002), and the curve fitting of spectra was performed by a nonlinear least-squares method assuming that all spectra were composed of Lorentzian-shaped peaks. The Mössbauer parameters of isomer shift (IS) and quadrupole splitting (QS) were calibrated with respect to the centroid of the sextet of α-iron at room temperature. Each relative peak area of the Fe components was calculated using peak intensity, and the line-width (LW) of the peak as fitting parameters in Mössbauer spectrum. All errors in the Mössbauer fitting parameters are one-SD (1σ) errors, as calculated by MossWinn 3.0i.

Results and discussion

Structural order and surface area of synthesized ferrihydrite

To estimate the effects of the level of supersaturation on the ferrihydrite structure, powder XRD analysis of the synthesized sample was conducted. In the XRD patterns presented in Fig. 3-3, it can be seen that as the degree of supersaturation is lower (S_E = 1.3×10^4; sample name: S_E^{13}), the peak of ferrihydrite in the XRD pattern is sharper, similar to 6-line ferrihydrite. Conversely, as the degree of supersaturation is high (S_E^{220}), the pattern shows two broad peaks, which indicates an amorphous structure like a 2-line ferrihydrite. These results indicate that the decrease in supersaturation results in the increase of structural order of the ferrihydrite precipitates. The change in the degree of crystallinity in these synthesized ferrihydrites is therefore due to the change in the driving force for precipitation at a higher supersaturation ratio, that is, the higher the precipitation rate, the lower the crystallinity of the product (Schwertmann et al., 1999).

The order of the surface area of synthetic solids was $S_E^{220} > S_E^{26} > S_E^{13}$ (Table 3-1), showing that the surface area of ferrihydrite increased with the increase in the supersaturation degree during precipitation. This result indicates that as the precipitation rate increases during the synthesis, the particle size becomes smaller. This finding was consistent with the results of the XRD analysis, suggesting that the crystallinity of ferrihydrite decreases as the surface area increases and the particle size decreases.

As shown above, XRD analysis and surface area measurement are effective in discussing the crystallinity and particle size of Fe(III) hydroxides. In the next step, we tried to estimate the crystallinity and particle size of ferrihydrite in our natural soil samples to discuss the reactivity of the ferryhydrite. However, XRD and surface area analyses cannot be applied to natural soil samples, since these methods are not elemental selective method, which are seriously interfered by other materials. Therefore, XAFS and Mössbauer spectroscopies are essential to characterize the Fe species in the natural soil samples.

XAFS analysis of the natural and synthesized samples for Fe

(1) XANES analysis

Figure 3-4 shows the normalized Fe K-edge X-ray absorption near-edge-structure

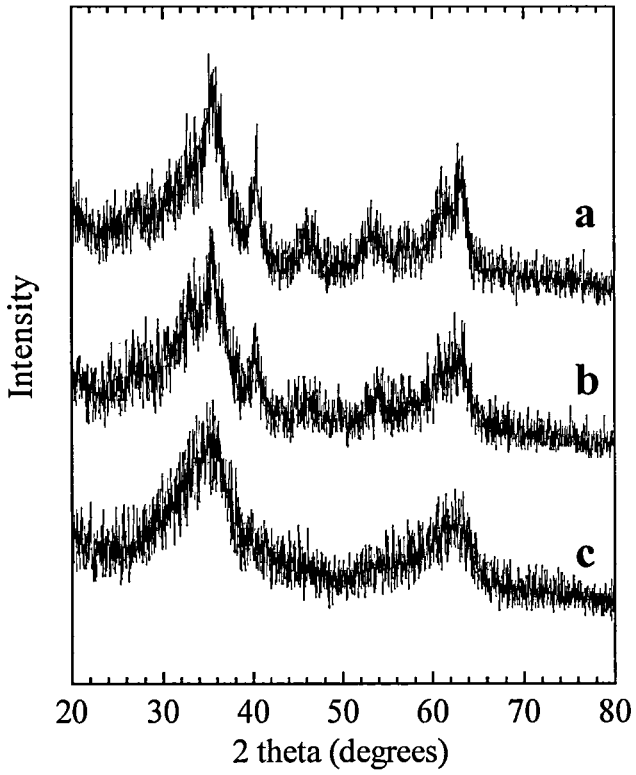

Fig. 3-3. Powder XRD patterns of ferrihydrite precipitated from an Fe^{3+} solution at pH 7 at various supersaturation ratios (S_E). (a) S_E^{13}: S_E = 1.3×10^4, (b) S_E^{26}: $S_E = 2.6 \times 10^4$, and (c) S_E^{220}: $S_E = 2.2 \times 10^5$.

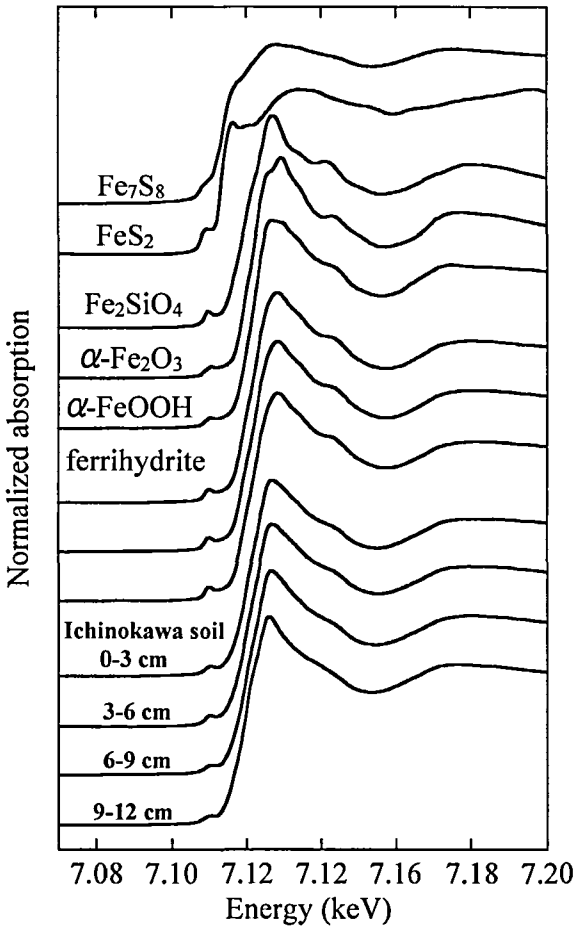

Fig. 3-4. Normalized Fe K-edge XANES spectra of the reference materials (Fe_7S_8 (pyrrhotite), FeS_2 (pyrite), Fe_2SiO_4 (fayalite), α-Fe_2O_3 (hematite), α-FeOOH (goethite), and ferrihydrite) and Fe in the natural soil samples from the Ichinokawa mine tailing. In the ferrihydrite, the Fe K-edge XANES spectra for solid samples precipitated at various supersaturation ratios (S_E^{13}, S_E^{26}, and S_E^{220}) are shown.

(XANES) spectra of the model compounds and the Ichinokawa soil samples. The features around the absorption edge of all the soil samples showed little variation, and they were mostly similar to those of ferrihydrite within the depth profile. This result suggests that Fe is mainly present as Fe(III) hydroxide, like ferrihydrite, at all the depths.

(2) EXAFS analysis

EXAFS analysis was conducted to obtain the local structure of Fe in soil under various redox conditions, which may give information about the structural order of Fe(III) oxide. Figures 3-5(a) and (b) show the k^3-weighted EXAFS spectra of Fe and their Fourier transformations (FTs) for the Ichinokawa soil samples and the model compounds, respectively. The amplitudes and oscillations of the EXAFS spectra for ferrihydrite are very similar within all synthetic ferrihydrites (Fig. 3-5a), implying that we cannot discuss the crystallinity of ferrihydrite using the EXAFS spectrum only. The spectral features of all the soil samples at the k range of 6-8 $Å^{-1}$ were similar to those of ferrihydrite but were not to other Fe(III) oxides such as hematite and goethite.

Fourier transformation was conducted to the EXAFS spectra of the soils and model compounds within the k range of 3.5-9.5 $Å^{-1}$ to obtain the RSF. All RSFs of the soil samples were also quite similar within the soil profile, and one prominent peak was observed near 1.5 Å due to the oxygen both in all the soil samples and ferrihydrite (Fig. 3-5b; phase shift uncorrected). The RSFs of all the soil samples and ferrihydrite have another peak near 2.7 Å (phase shift uncorrected) due to the Fe-Fe shell. The features in the RSFs of the soil samples are similar to those of ferrihydrite, but not to other model compounds. The results of the EXAFS spectra and RSFs suggest that Fe in the soil is mainly present as ferrihydrite at all the depths. This suggestion is also supported by the fact that Fe(III) is a major component of Fe species in the soil, as seen in the Fe XANES analysis (Fig. 3-4).

The EXAFS spectra and RSFs of synthesized ferrihydrite do not change significantly among three samples, namely, S_E^{220}, S_E^{26}, and S_E^{13}, which implies that a detailed examination of the crystallinity of Fe(III) oxide by XAFS analysis could not be

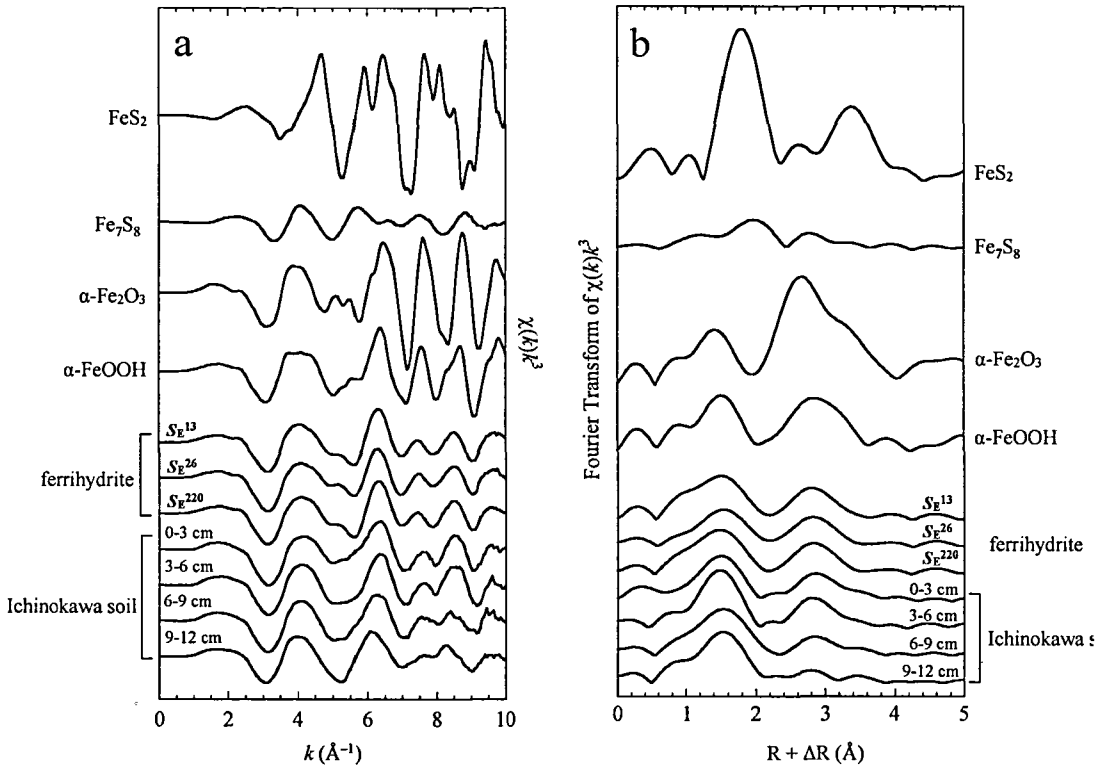

Fig. 3-5. (a) Normalized k^3-weighted EXAFS spectra at Fe K-edge and (b) their Fourier-transformed EXAFS spectra in the Ichinokawa soil samples and model compounds (FeS_2 (pyrite), Fe_7S_8 (pyrrhotite), a-Fe_2O_3 (hematite), a-FeOOH (goethite), and ferrihydrite). In ferrihydrite, both the EXAFS and Fourier-transformed EXAFS spectra of Fe are shown for various crystallinity degrees (S_E^{13}, S_E^{26}, and S_E^{220}). Fourier transformation was conducted with a k range of 3.5-9.5 Å. Radial distances are not corrected for the phase shift.

made for the synthetic solids and the soil samples.

^{57}Fe Mössbauer characterization

Mössbauer spectrometry was employed to obtain some information on the structural order of Fe(III) hydroxides in Ichinokawa soil and to investigate whether or not the crystallinity of Fe(III) hydroxide varies in the soil profile. In Mössbauer spectroscopy, each spectral component corresponds to one Fe-bearing solid phase (or mineral, if crystalline) or to a group of unresolved Fe-bearing solid phases. In addition, assuming equal Mössbauer recoilness fractions (Rancourt, 1998), the total spectral area of a given component is proportional to the amount of Fe in the corresponding solid phase(s).

Figure 3-6 shows the Mössbauer spectra of Fe for synthesized ferrihydrites and the Ichinokawa soil at RT and 78 K. In the RT Mössbauer spectra, two spectral components can be extracted: (1) a high-spin Fe(III) quadrupole doublet corresponding to Fe(III) hydroxides that are paramagnetic at RT, and (2) a high-spin Fe(II) quadrupole doublet (Thompson et al., 2006). The Mössbauer parameters obtained by fitting are summarized in Table 3-2 at RT. Since relatively small changes in bulk Fe oxide composition occur in both synthesized ferrihydrite and Ichinokawa soil, it is important to examine the possible systematic errors that can occur in the fitting of the Mössbauer spectra. In Fig. 3-6a, the Mössbauer spectra of synthesized ferrihydrite do not change significantly with the structural order at RT. The IS and QS values obtained for the Ichinokawa soil samples indicate that both Fe(III) and Fe(II) are high-spin Fe (Fig. 3-6b). In relation to this, Menil (1985) reported that when the nearest coordination atom of Fe is oxygen, the IS value in the case of octahedral structure (O_h) is significantly different from that in tetrahedral structure (T_h) (Fe(III)-O_h: 0.3-0.5 mm/s, Fe(III)-T_h: 0.1-0.3 mm/s, Fe(II)-O_h: 0.1-0.3 mm/s, Fe(II)-T_h: < 0.95 mm/s). The IS values obtained in this study for all the soil samples are 0.37-0.38 mm/s for Fe(III) and 1.1-1.3 mm/s for Fe(II), which suggests that both Fe(II) and Fe(III) in soil coordinate to oxygen in octahedral structure. This finding is consistent with the Fe XAFS results that Fe species in the soil is mainly Fe(III) hydroxides, like ferrihydrite, at all depths, since ferrihydrite is Fe(III) hydroxide

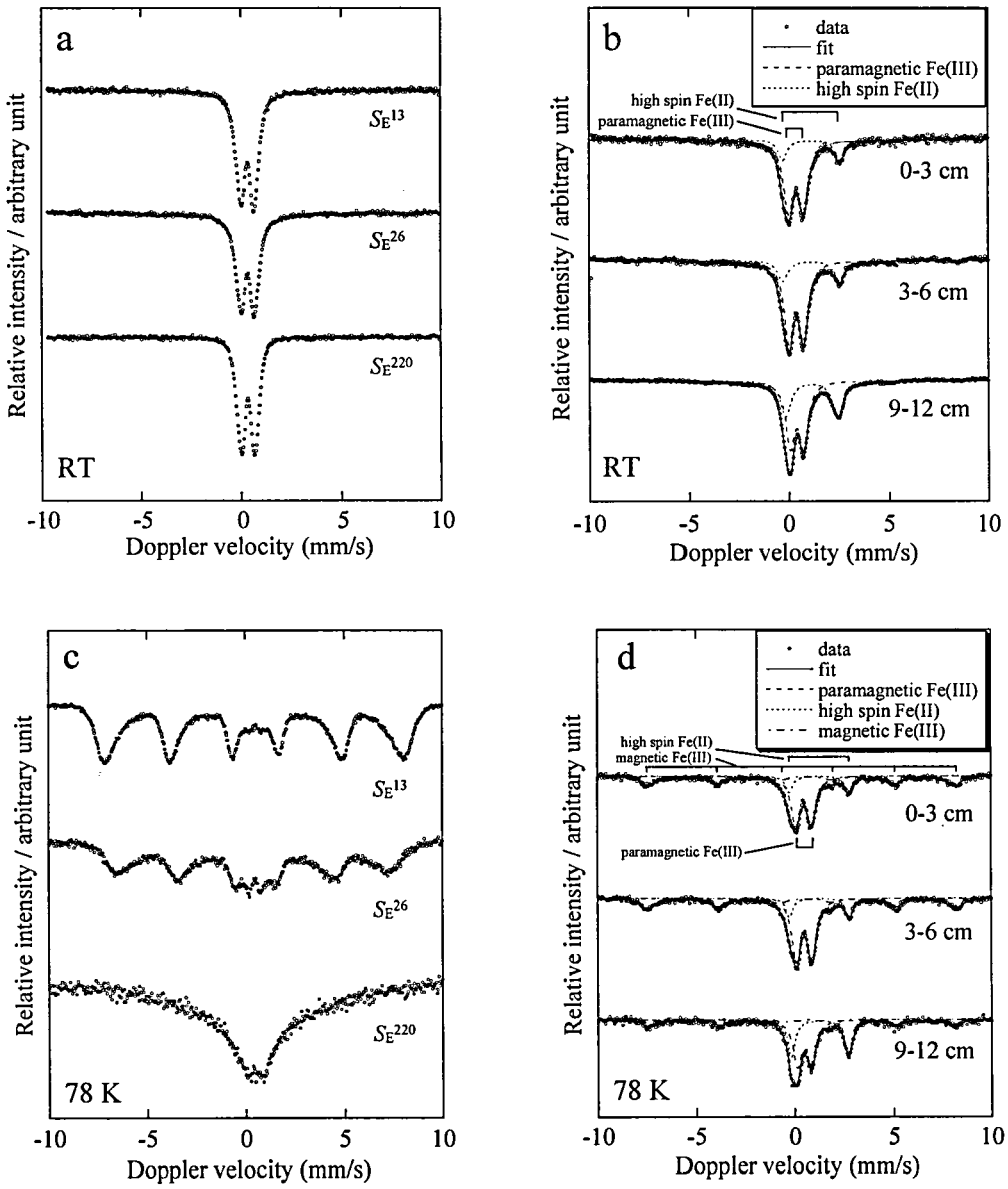

Fig. 3-6. Room temperature (RT) Mössbauer spectra of (a) synthetic ferrihydrite and (b) the Ichinokawa soil samples (0-3 cm, 3-6 cm, and 9-12 cm). 78 K Mössbauer spectra of (c) synthetic ferrihydrite and (d) the Ichinokawa soil samples (0-3 cm, 3-6 cm, and 9-12 cm). In (a) and (c), the Mössbauer spectra for synthetic ferrihydrite precipitated at various supersaturation ratios (S_E^{13}, S_E^{26}, and S_E^{220}) are shown.

Table 3-2. Fitting and calculated Mössbauer parameters for the RT spectra.

sample			IS[a] (mm/s)	QS[b] (mm/s)	LW[c] (mm/s)	*RA*[d] (%)
synthesized ferrihydrite	$S_E = 1.3\times10^4$		0.330 (1)[e]	0.681 (2)	0.527 (3)	100
	$S_E = 2.6\times10^4$		0.328 (1)	0.702 (2)	0.543 (3)	100
	$S_E = 2.2\times10^5$		0.325 (1)	0.693 (1)	0.468 (2)	100
Ichinokawa soil	0-3 cm	Fe(III)	0.376 (3)	0.742 (5)	0.594 (8)	78.3
		Fe(II)	1.128 (8)	2.820 (2)	0.520 (2)	21.7
	3-6 cm	Fe(III)	0.370 (2)	0.734 (3)	0.556 (5)	76.6
		Fe(II)	1.128 (6)	2.800 (1)	0.600 (2)	23.4
	9-12 cm	Fe(III)	0.380 (1)	0.663 (2)	0.527 (3)	60.1
		Fe(II)	1.124 (2)	2.582 (4)	0.618 (6)	39.9

[a] Isomer shift with respect to that of α-Fe foil.

[b] Quadrupole splitting.

[c] Full width at half maximum.

[d] Relative area of each component.

[e] Errors (in parentheses) are in scientific notation (e. g., 1.24 (5) = 1.24 ± 0.05).

where Fe(III) coordinates to oxygen with octahedral structure. In the Ichinokawa soil, the relative area analysis in the fitting indicates that almost 80% of Fe is present as Fe(III) at a depth of 0-3 cm (Eh = 360-65 mV, pH 7.6-8.1). However, the Fe(II)/Fe(III) ratio gradually increased, and the Fe(II) contribution to total Fe was ca. 40% at the depth of 9-12 cm (Eh = −140 mV, pH 7.9). This finding was consistent with the progress of reducing condition at deeper part (Fig. 3-2). It is reported that ferrihydrite, like natural and synthetic Fe(III) hydroxides, are often superparamagnetic (SP) at RT (Van Der Zee et al., 2003), which agrees with our findings that magnetic component is absent at RT.

Figures 6c and 6d show the Mössbauer spectra of the synthetic ferrihydrite and Ichinokawa soil samples, respectively, at 78 K. In synthesized solids, a sextet of ferrihydrite is shown in the spectra of S_E^{13} and S_E^{26} (Fig. 3-6c), indicating that the samples have magnetism. The magnetism obtained at 78 K indicates SP effect in synthetic ferrihydrite, which is often observed in nanosize Fe(III) oxides. Thus, this finding suggests that the synthetic solids are fine-grained Fe(III) hydroxides. The contribution of the magnetic component observed at 78 K depends on the particle size, since Fe species in all the synthetic solids are uniformly ferrihydrite as shown from the XRD and XAFS analyses. In Fig. 3-6c, a systematic trend was observed between the structural order and the magnitude of sextet due to the magnetism of ferrihydrite; the higher the crystallinity of ferrihydrite, the larger magnitude of the sextet. Thus, this result confirms that the order of particle size of ferrihydrite is $S_E^{13} > S_E^{26} > S_E^{220}$ or the order of surface area is $S_E^{13} < S_E^{26} < S_E^{220}$, as shown in Section 3.1. These results for synthetic ferrihydrite suggest that a larger magnetic fraction at 78 K in ferrihydrite is related to a high structural order and large particle size. Using this observed trend between magnetism and the structural order of synthetic ferrihydrite at 78 K, it may be possible to discuss the crystallinity of Fe(III) hydroxides in the Ichinokawa soil samples, since the major component of Fe species is amorphous Fe(III) hydroxide (ferrihydrite) at all depths from the XAFS and RT Mössbauer analyses.

In natural soil samples, the spectra at 78 K were fitted using a model composed of two doublets and a sextet (Fig. 3-6d). The doublets are due to paramagnetic Fe(III) and Fe(II) species both with a high-spin state. Unfortunately, the dynamic variation as

observed in synthetic ferrihydrite was not clear in the soil samples at different depths. However, a change in the contribution of the sextet fraction was slightly observed with depth (Fig. 3-6d). A sextet due to the magnetic component of Fe(III) at 78 K was shown to be at higher degree in the Mössbauer spectra as compared to the spectra at RT for all the soil samples. This finding indicates that ferrihydrites in the soil samples also consist of nanosize particles. Since the reported Néel temperature of $Fe(OH)_2$ (= possible solids Fe(II) species in the soil samples) is near 34 K (Cornell and Schwertmann, 2003), the SP and the magnetism should not be observed in the spectra at 78 K, suggesting that the observed sextets in the spectra of the soil samples are due to Fe(III) hydroxides. Hence, the Mössbauer spectra at 78 K consist of the paramagnetic and the magnetic fractions originating from the Fe(III) components in the soil samples. This indicates that Fe(III) hydroxides in the soil sample is approximately the mixture of the nanosize and the relatively larger size solid at all the depths, and the proportion slightly changes with depth. To examine quantitatively the contribution of the nanosize Fe(III) hydroxides in soil and to compensate for small variations in hyperfine parameter, we defined magnetic/paramagnetic components ratio $P = M/PM$ (dimensionless), where M is the relative area of the magnetic fraction (%), and PM is that of the paramagnetic fraction (%) for Fe(III) in the Mössbauer spectrum of the soil samples based on the fitting of the spectra. The order of P value at 78 K is 0-3 cm ($P = 0.63$) > 3-6 cm ($P = 0.60$) > 9-12 cm ($P = 0.50$) (Table 3-3); thus, the magnetic component in soil slightly increased under reducing condition (at deeper part). These results indicate that the contribution of the nanosize Fe(III) hydroxides fraction to the total Fe(III) hydroxides increased with depth. Therefore, it is suggested that the structural order of Fe(III) hydroxides in the soil decreases under reducing condition (at deeper part), where the concentration of Fe in the soil slightly increases and the Fe concentration dissolved in the soil water also increases in the system (Mitsunobu et al., 2006). These facts imply that (i) the dissolution reaction due to the reduction of Fe(III) to Fe(II), and (ii) the reprecipitation reaction due to the oxidation to Fe(III) hydroxides may be dynamically occurring in the soil-water system under reducing condition. This may lead to the formation of a lower-ordered Fe(III) oxide. Thompson et al. (2006) reported using the wet chemistry method that the

Table 3-3. Quantitative Fe composition and magnetic/paramagnetic ratio in Ichinokawa soil samples from Mössbauer analysis at 78 K.

	sample	component	*RA* [a] (%)	*P* [b]
Ichinokawa soil	0-3 cm	Fe(III) paramagnetic	52.0	0.63 (3)[c]
		Fe(III) magnetic	33.0	
		Fe(II)	15.0	
	3-6 cm	Fe(III) paramagnetic	54.0	0.60 (2)
		Fe(III) magnetic	32.2	
		Fe(II)	13.8	
	9-12 cm	Fe(III) paramagnetic	45.0	0.50 (3)
		Fe(III) magnetic	22.5	
		Fe(II)	32.5	

[a] Relative area of each component.

[b] Ratio of magnetic/paramagnetic components for Fe(III).

[c] Errors (in parentheses) are in scientific notation (e. g., 1.24 (5) = 1.24 ± 0.05).

composition of short-range ordered Fe hydroxides such as ferrihydrite increases under reducing condition, following the reoxidation of released Fe^{2+} in soil water. These facts and reports are consistent with the Mössbauer spectrometric evidence in this study in which the structural order of Fe(III) hydroxides decreases under reducing condition (at deeper part).

It has often been shown that Fe(III) hydroxides can be the host phase in soil and sediment of As and other trace elements due to its large surface area, high adsorptive capacities, and large abundance in soil and sediment (Cornell and Schwertmann, 2003). When the trace element distribution is governed by Fe(III) hydroxides, the change in crystallinity of Fe(III) hydroxides with redox variation has a direct influence on the behavior of the trace element in the soil-water system. Actually, in the Ichinokawa soil samples employed in this study, it was shown that the As concentration and the As(III)/As(V) ratio in soil water increase with depth under more reducing condition (Fig. 3-1). Arsenic K-edge XAFS analyses in Mitsunobu et al. (2006) also showed that the host mineral of As is Fe(III) hydroxide at any depths and As(III) fraction in soil gradually increases with depth. It has been reported that the leaching of As under reducing condition depends on (1) the reductive dissolution of Fe(III) (hydr)-oxide, host phase for As in soil and (2) the reduction of As(V) to As(III), since As(III) is more labile to partition to the aqueous phase than As(V) (Bowell, 1994; Smedley and Kinniburgh, 2002; Takahashi et al., 2004; Herbel and Fendorf, 2006; Kocar et al., 2006). In this study, Fe is mainly present as amorphous Fe(III) hydroxides like ferrihydrite at all depths, and the crystallinity of Fe hydroxides in soil slightly decreased at deeper part, indicating that the potential as sorbent of Fe hydroxides slightly increases under reducing condition. When a crystallinity of ferrihydrite decreases, the adsorption amount of As on the ferrihydrite can increase due to a larger potential for As removal (Richmond et al., 2004). Thus, the present results in this study suggests that the Fe(III) hydroxides phase would promote adsorption of As or at least keep its potential as an adsorbent of As under reducing condition in the system, whereas As leaching to the aqueous phase increases under reducing condition. Therefore, we can conclude that As release from the soil largely depends on the As redox property in the system rather than the reductive dissolution of

Fe(III) hydroxides as was suggested in Kocar et al. (2006).

In addition, in the Ichinokawa soil samples, it was already reported that the adsorption of Sb(V) to the soil is more enhanced at deeper soil under a more reducing condition (Mitsunobu et al., 2006). Antimony K-edge EXAFS analyses also showed that the host mineral of Sb(V) is Fe(III) hydroxides at all depths (Mitsunobu et al., 2006). Therefore, it is suggested that ferrihydrite at a deeper zone is more likely to adsorb Sb(V), to a larger degree than at the surface zone, possibly due to the lager surface area and high adsorptive capacities as suggested in this study.

Conclusions

In this study, characterization of Fe(III) hydroxides in natural soil was successfully conducted by XAFS and Mössbauer spectroscopic methods. It was shown that Fe is mainly present as Fe(III) hydroxides, like ferrihydrite, at all depths based on XANES and EXAFS analyses. Moreover, the morphologic examination of Fe(III) hydroxides was conducted using Mössbauer spectrometry, since XAFS analysis is limited to discussing the structural order of Fe(III) hydroxides. Under reducing condition, or deeper part in the soil profile, the crystallinity of ferrihydrite slightly decreased. It was revealed that in the redox range of this study, the Fe species remains as ferrihydrite, but the morphology of amorphous Fe(III) hydroxides, such as the particle size and the crystallinity, can change with the progress of the reducing condition. This finding is important in understanding the behaviors of As and other elements in soil- and sediment-water systems, since the distribution of trace element in such environments is often governed by Fe(III) hydroxides. In the soil-water system examined here, As concentration and As(III)/As(V) ratio in soil water increased with the depth. Since Fe(III) hydroxide phase keeps its potential at any depths in the soil profile, it was suggested that As release from the soil is mainly due to the larger mobility of As(III) than As(V), while the contribution of reductive dissolution of Fe(III) hydroxides is not primarily important. Since the crystallinity of Fe(III) hydroxides partly decreases at deeper part, the change may explain the decline of Sb concentration in soil water in Ichinokawa soil-water system.

References

Bancroft, P., 1988. Famous mineral localities: the Ichinokawa mine. Mineral. Rec. 19, 229-238.

Brannon, J. M., Patrick, W. H., Jr., 1985. Fixation and mobilization of antimony in sediments. Environ. Pollut. 9B, 107-126.

Cornell, R. M., Schwertmann, U., 2003. The iron oxides. In: Cornell, R. M., Schwertmann, U. (Eds.), The iron oxides. 2nd ed., VCH.

Dowling, C. B., Poreda, R. J., Basu, A. R., Peters, S. L., Aggarwal, P. K., 2002. Geochemical study of arsenic release mechanisms in the Bengal Basin groundwater. Water Resour. Res. 38, 1173.

Herbel, M., Fendorf, S., 2006. Biogeochemical processes controlling the speciation and transport of arsenic within iron coated sands. Chem. Geol. 54, 16-32.

Kocar, B. D., Herbel, M. J., Tufano, K. J., Fendorf, S., 2006. Contrasting effects of dissimilatory iron(III) and arsenic(V) reduction on arsenic retention and transport. Environ. Sci. Technol. 40, 6715-6721.

Langmuir, D., 1997. In Aqueous Environmental Geochemistry; Prentice–Hall: New Jersey.

MacArthur, J. M., Ravenscroft, P., Safiulla, S., Thirlwall, M. F., 2001. Arsenic in groundwater: testing pollution mechanisms for sedimentary aquifers in Bangradesh. Water Resour. Res. 37, 109-117.

Menil, F., 1985. Systematic trends of the ^{57}Fe Mössbauer isomer shifts in (FeO_n) and (FeF_n) polyhedra. Evidence of a new correlation between the isomer shift and the inductive effect of the competing bond *T-X* (→ Fe) (where X is O or F and T any element with a formal positive charge). J. Phys. Chem. Solids, 46, 763-789.

Mitsunobu, S., Takahashi, Y., Hirunuma, R., Haba, H., Enomoto, S., 2005. Coupling of ICP-MS and multitracer technique as a new method to investigate dynamics of various elements in soil-water system. Chem. Lett. 34, 980-981.

Mitsunobu, S., Harada, T., Takahashi, Y., 2006. Comparison of antimony behavior with that of arsenic under various soil redox conditions. Environ. Sci. Technol., 40, 7270-7276 .

Nealson K. H., Saffarini D., 1994. Iron and manganese in anaerobic respiration: Environmental significance, physiology, and regulation. Annu. Rev. Microbiol. 48, 311-343.

Nickson, R. T., McArthur, J. M., Burgess, W. G., Ahmed, K. M., Ravenscroft, P., Rahman, M., 1998. Arsenic poisoning of Bangladesh groundwater. Nature 395, 338.

Nickson, R. T., McArthur, J., Ravenscroft, P., Burgess, W. G., Ahmed, K. M., 2000. Mechanism of arsenic release to groundwater, Bangladesh and West Bengal. Appl. Geochem. 15, 403-413.

Postma, D., 1993. The reactivity of iron-oxides in sediments–a kinetic approach. Geochim. Cosmochim. Acta 57, 5027-5034.

Rancourt, D. G., Mcdonald, A. M., Lalonde, A. E., Ping, J. Y., 1993. Mössbauer absorber thickness for accurate site population in Fe bearing minerals. Am. Mineral. 78, 1-7.

Rancourt, D. G., 1998. Mössbauer spectroscopy in clay science. Hyperfine Interact. 117, 3-38.

Riveros, P. A., Dutrizac, J. E. Spencer, P, 2001. Arsenic disposal practices in the metallurgical industry. Can. Metall. Q. 40, 395-420.

Richmond, W. R., Loan, M., Morton, J., Parkinson, G., 2004. Arsenic removal from aqueous solution via ferrihydrite crystallization control. Environ. Sci. Technol. 38, 2368-2372.

Sakai, Y., Ariyoshi, K., Ozuku, T., 2002. In situ ^{57}Fe Mössbauer investigation of solid-state redox reactions of lithium insertion electrodes for advanced batteries. Hyperfine Interact. 139/140, 67-76.

Schwertmann, U., Friedl, J., Stanjek, H., 1999. From Fe(III) ions to ferrihydrite and then to hematite. J. Colloid Interface Sci. 209, 215-223.

Smedley, P. L., Kinniburgh, D. G., 2002. A review of the source, behaviour and distribution of arsenic in natural waters. Appl. Geochem. 17, 517-568.

Takahashi, Y., Ohtaku, N., Mitsunobu, S.; Yuita, K., Nomura, M., 2003. Determination of the As(III)/As(V) ratio in soil by X-ray absorption near-edge structure (XANES) and its application to the arsenic distribution between soil and water. Anal. Sci. 19, 891-896.

Takahashi, Y., Minamikawa, R., Hattori, H. K., Kurishima, K., Kihou, N., Yuita, K., 2004. Arsenic behavior in paddy fields during the cycle of flooded and non-flooded periods. Environ. Sci. Technol. 38, 1038-1044.

Thompson, A., Chadwick, O. A., Rancourt, D. G., Chorover, J., 2006. Iron-oxide crystallinity increases during soil redox oscillations. Geochim. Cosmochim. Acta 70, 1710-1727.

Zabinsky, S. I., Rehr, J. J., Ankudinov, A., Albers, R. C., Eller, M. J., 1995. Multiple-scattering calculations of X-ray-absorption spectra. Phys. Rev. B 52, 2995-3009.

Van Der Zee, C., Roberts, D. R., Rancourt, D. G., Slomp, C. P., 2003. Nanogoethite is the dominant reactive oxyhydroxide phase in lake and marine sediments. Geology 31, 993-996.

CHAPTER 4

Microscopic speciation of antimony and iron in Ichinokawa soil grain

Materials and Methods

Samples. Natural soil samples were collected in October 2005 around the Ichinokawa mine pithead (33.53N, 133.12E) in Ehime, Japan, which was formerly one of the largest Sb (stibnite: Sb_2S_3) mines (Bancroft, 1988). The soil is heavily contaminated with As and Sb (As: 1200-2000 mg/kg; Sb: 0.9-1.1 wt%), details of which were already reported in our previous paper (Mitsunobu et al., 2006). The sampling site was flooded soil located at about 5 m downward from the mine pithead. To allow us to observe the variation of the Sb behavior under various redox conditions, the soil samples were collected at four depth ranges (0-3, 3-6, 6-9, and 9-12 cm) using a plastic spatula in the wetland-tailing site. The Eh and pH were measured by a Pt electrode (Fujiwara Sci., EHS-120) and a glass electrode (Horiba, D-51), respectively, at the sampling site. The Eh values decreased monotonically from 360 to –140 mV with depth in the Ichinokawa soil samples (Mitsunobu et al., 2006). The collected soil samples were immediately sealed in polystyrene bottles and were kept at 4°C during transportation to our laboratory. In the laboratory, the soil samples were passed through a 500 μm stainless steel sieve to remove large organic particles and gravel fractions and stored at –20°C prior to analyses.

To understand the unclear Sb behavior under reducing condition in detail, thin section for microscopic analyses was prepared for a soil sample collected at deepest range (9-12 cm), the most reductive soil, in this study (Figure 4-1). To prepare the thin section, the soil sample was air-dried in N_2 purged glovebox to prevent solid phase to further reaction. Polished thin section was prepared as intact specimens without the fragmentation of grain and the soil grain was mounted on a glass slide using room-temperature-set epoxy. The thin section was polished to a final thickness of approximately 40 μm.

Characterization.

The soil sample was characterized by an electron probe microanalyzer (EPMA,

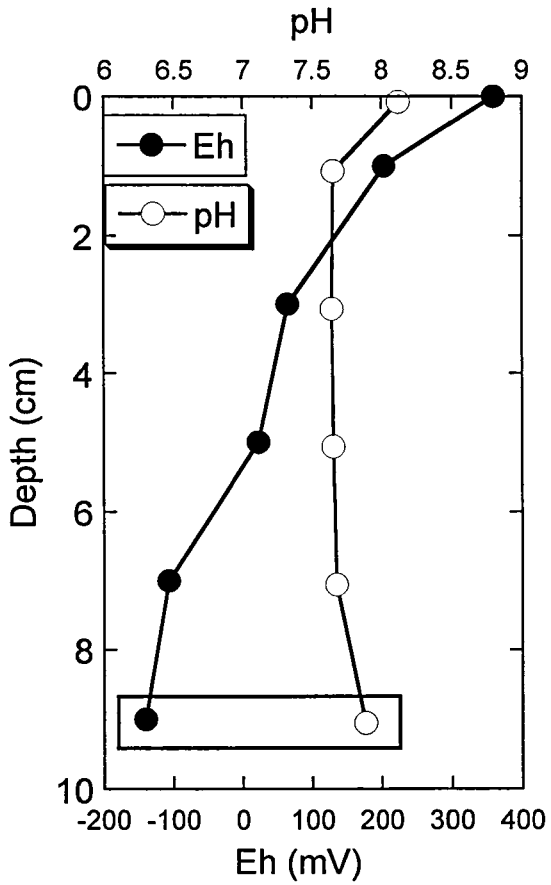

Figure 4-1. Eh and pH variations with depth in Ichinokawa soil-water system around Ichinokawa mine adit. The soil sample in enclosed area in the figure was used for microscopic analyses in this study.

JXA-8200, JEOL) and powder X-ray diffraction techniques (XRD). The quantitative EPMA analyses were performed by wavelength dispersion spectrometry (WDS) operated at 15 kV with a beam current of 15 nA. The beam size was set to 2 μm × 2 μm. The counting times were 20 s for each element except Sb (30 s) and S (10 s), and raw data corrections were applied for ZAF (i.e., correction for atomic number, absorption, and fluorescence effects in X-ray microanalysis). The following X-ray lines and standards were used: Si Kα (Jadeite), Al Kα (synthetic Al_2O_3), Fe Kα (synthetic Fe_2O_3), Mn Kα (synthetic MnO), S Kα (chalcopyrite), P Kα (synthetic InP), Ca Kα (wollastonite), Sb Lα (stibnite), and As Lα (synthetic As metal). Elemental distribution map in each soil grain was identified by the backscattered electron micrograph and X-ray map of each element in EPMA analysis operated at 15 kV, beam current 30 nA, counting time 0.4 s/point, and beam size 1 μm × 1 μm.

The samples were also characterized by XRD (Rigaku Multiflex) with a Cu Kα radiation source (λ = 1.54056 Å) at 40 kV, 40 mA current, and scan rate 4°/min in 2θ.

X-ray Absorption Fine Structure (XAFS) spectroscopy.

Antimony μ-XANES experiments were carried out at BL37XU of SPring-8 (Hyogo, Japan). The X-rays from the undulator were monochromatized by the Si(111) double-crystal monochromator and were focused to 1 × 1 μm^2 by the Kirkpatrick-Baez (K-B) mirror optics which consists of a pair aspheric total reflection mirrors fabricated by the bent-polishing method (Takeuchi et al., 2005). The thin section sample was kept the frozen condition by a cold flow from a cryojet system to minimize unexpected alteration due to the X-ray radiation effect. All the Sb μ-XANES experiments were made by scanning through the Sb K-edge in fluorescence mode with a Si(Li) detector.

Iron μ-XANES spectra were collected at the beamline BL-4A of KEK-PF (Tsukuba, Japan) with Si(111) double-crystal monochromator (Iida and Noma, 1993). The beam was focused by K-B optics, and the size was 5 × 5 μm^2. The spectra of the samples and standards were collected in the fluorescence mode using a Si(Li) solid-state detector and in the transmission mode using an ionization chamber, respectively. For both Sb and Fe XANES measurements, the thin section and standards are attached to

plastic holder with a hole, and fixed to an XY stage controlled by X-Y pulse motor, oriented 45° to the beam.

All the XAFS analyses were conducted prior to EPMA analysis to prevent from alteration of the species in soil by the heating during electron radiation. The energy calibration was made by the white-line peak maximum of Sb_2O_3 at 30.486 keV for Sb and pre-edge peak maximum of hematite fixed at 7.113 keV for Fe. The XAFS data were normalized and background subtracted using standard procedures in a REX2000 program, ver. 2.5.7. (Rigaku Co., Japan). The μ-XANES spectra for Sb and Fe were measured with a step size of 0.86 and 0.86 eV for the edge region, respectively.

To provide quantitative information about the oxidation states of Sb, linear least-squares combination fitting of the XANES data was done using REX2000. The experimental spectra were fitted with linear combination of Sb standard ($KSb^{V}(OH)_6$ and $Sb^{III}{}_2O_3$) (Mitsunobu et al., 2006). The data were fitted in the energy range ±20 eV from Sb_2O_3.

To test the effect of possible radiation-induced alteration on soil samples during Sb μ-XANES scan, we collected several successive scans for same point in soil grain (grain C) on the thin section of Ichinokawa soil. From three to five scans of the point were collected with each scan taking 7 min. From comparison of each spectrum and the quantitative fitting analyses of the spectra, the alteration was not observed in all the spectra obtained, suggesting that the alteration would not occur during the scan period. Therefore, to secure no-alteration in measured spectra for Sb XANES, all the Sb XANES were measured within this scan period.

Results and Discussion

Elemental distribution in Sb hot spot.

Figure 4-2 shows the backscattered electron photomicrographs and X-ray maps of 3 grains that Sb are heavily concentrated (grains A-C) in Ichinokawa soil based on EPMA analyses. In elemental distributions, Sb abundances correlates with Fe in grains A-C, which suggests that Sb in those grains are incorporated in the phases bearing Fe. This finding is agreeable with the bulk analyses for Sb in Ichinokawa soil that host phase of Sb

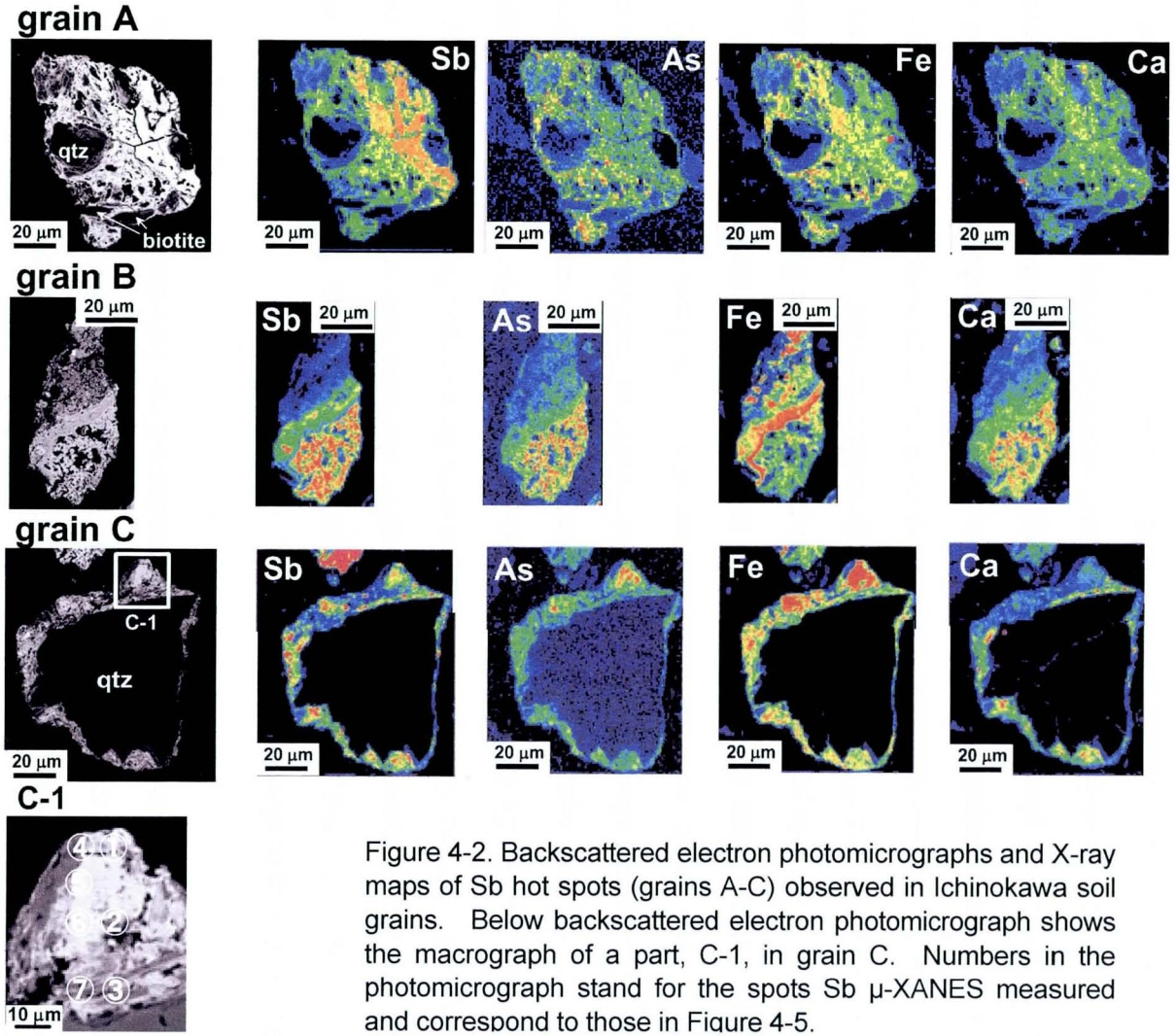

Figure 4-2. Backscattered electron photomicrographs and X-ray maps of Sb hot spots (grains A-C) observed in Ichinokawa soil grains. Below backscattered electron photomicrograph shows the macrograph of a part, C-1, in grain C. Numbers in the photomicrograph stand for the spots Sb μ-XANES measured and correspond to those in Figure 4-5.

in soil is amorphous Fe(III) hydroxides. In all the grains, Fe phases consist of the discrete particles displaying colloform texture, which is often observed in Fe hydroxides secondary deposited (Paktunc et al., 2003; 2004).

In grain A and C, detrital particles such as quartz and biotite are covered with Fe phases and Sb in the grains are concentrated in the parts. These findings indicate that the Fe phases in grains A and C is authigenic products secondary deposited from the aqueous phase and not the replacement products. Here, the replacement is defined as the dissolution of one mineral and simultaneous deposition of another mineral in its place.

Chemical composition.

Antimony hot spots in all the grains A-C have high Fe concentrations, while contain trace to minor concentrations of other elements such as Mn, Ca, Si, Al, and S (Table 4-1). These findings are consistent with the findings observed in X-ray maps and thus suggest that Fe bearing phase is the host phase for Sb. In addition, Si and S concentrations are significantly low compared with Sb and Fe concentration in all Sb hot spot of the grains, silicate and sulfide are eliminated as candidate of Fe and Sb species in Sb hot spot based on stoichiometry of the phases. Relationship between Sb_2O_3 and Fe_2O_3 concentrations in each Sb hot spot in grains A-C was shown in Figure 4-3. It is remarkable that data points of grain A were plotted around the line of Sb/Fe molar ratio = 1 similar to Fe and Sb hosting mineral, tripuhyite ($FeSbO_4$). This finding suggests that the Sb hot spot has a chemical composition similar to tripuhyite and that the Sb hot spot mainly contains tripuhyite, if we can assume that Sb abundance in the Sb hot spot depends on the Fe phases. Main clustering of the data points in grains B and C were are confined to Sb/Fe molar ratio of 3 and greater, which suggesting that Sb in grain B and C are adsorbed or co-precipitated with Fe(III) hydroxide. This finding is consistent with bulk Sb EXAFS analyses of Ichinokawa soil.

μ-XANES analysis for Fe.

To determine the Fe species in Sb hot spots, Fe μ-XANES in each grain was measured. Figure 4-4a shows the Fe K-edge μ-XANES of standard materials (pyrite,

Table 4-1. Representive electron microprobe analysis (wt%) of each grain Sb concentrated in Ichinokawa soil.

Fe_2O_3	Sb_2O_5	As_2O_5	SiO_2	MnO	CaO	Al_2O_3	SO_3	P_2O_5	Total
grain A									
23.65	60.53	0.94	0.90	2.83	1.44	2.78	0.51	0.20	93.76
24.48	59.05	0.98	0.97	2.85	1.09	3.35	0.61	0.24	93.62
23.56	59.11	0.79	1.53	2.94	1.57	3.97	0.47	0.14	94.06
24.21	60.25	0.96	1.16	2.48	1.68	3.29	0.30	0.19	94.51
20.29	49.71	0.78	9.10	2.38	1.50	8.30	0.34	0.21	92.60
24.03	57.86	0.84	1.22	3.04	1.32	3.70	0.33	0.20	92.54
22.47	51.94	0.81	1.59	2.79	1.39	3.55	0.36	0.13	85.02
26.95	47.28	1.19	5.86	2.07	1.56	6.61	0.32	0.15	91.98
23.76	48.45	1.22	5.91	2.14	1.66	5.35	0.18	0.16	88.82
27.72	51.26	1.29	5.31	2.13	1.52	5.51	0.15	0.17	95.06
20.42	39.39	0.54	3.75	1.69	1.83	2.23	0.16	0.15	70.17
27.30	52.05	1.20	5.49	1.80	1.62	5.44	0.22	0.20	95.31
24.12	43.16	1.30	1.33	2.01	0.95	1.24	0.37	0.12	74.58
20.38	40.47	0.85	10.08	1.50	1.33	9.34	0.26	0.19	84.41
25.90	49.17	1.22	1.67	1.64	1.32	1.82	0.14	0.19	83.07
grain B									
70.89	11.44	0.76	1.28	1.81	0.66	0.55	0.63	1.53	89.55
71.62	9.62	0.70	1.35	1.65	0.69	0.35	0.63	1.59	88.18
66.94	12.92	0.92	2.53	1.28	0.76	1.60	0.72	1.56	89.23
71.19	10.77	0.77	1.38	1.57	0.83	0.46	0.60	1.28	88.85
70.61	12.54	1.06	1.16	2.30	0.59	0.50	0.59	1.32	90.67
50.97	30.00	1.39	2.97	1.94	1.21	2.47	0.53	1.69	93.19
48.82	32.62	1.39	2.72	1.78	1.28	2.63	0.31	1.55	93.09
60.13	17.72	1.06	5.34	2.47	0.90	3.93	0.40	1.36	93.31
42.84	33.73	1.38	1.79	1.68	1.26	1.77	0.44	1.37	86.27
53.94	22.64	1.27	5.75	2.24	1.26	4.75	0.62	1.57	94.02
51.33	27.00	1.36	2.62	1.94	1.41	2.78	0.42	1.40	90.25
44.55	30.29	1.49	4.21	1.82	1.30	3.37	0.59	1.36	88.97
48.19	31.14	1.47	2.00	2.27	1.49	2.16	0.46	2.00	91.18
51.42	26.90	1.90	3.06	2.30	1.15	2.76	0.44	1.63	91.58
45.67	32.98	1.48	2.62	1.87	1.49	2.34	0.65	1.59	90.67
40.55	32.86	1.39	4.61	1.69	1.16	3.93	0.48	1.27	87.93
43.93	35.78	1.43	2.84	2.11	1.27	2.63	0.29	1.28	91.55
grain C									
64.95	13.41	2.57	1.55	2.64	0.84	0.97	0.33	0.57	87.82
64.97	13.41	2.84	2.89	2.61	0.85	0.99	0.34	0.57	89.48
66.38	13.37	2.80	1.08	2.86	1.02	1.03	0.42	0.63	89.57
60.14	7.56	1.91	10.64	2.52	0.71	7.58	0.40	0.35	91.83
67.52	11.92	2.51	3.51	2.94	0.84	0.93	0.33	0.43	90.93
64.20	6.39	1.57	7.10	2.66	0.76	4.37	0.47	0.35	87.85
59.47	3.91	1.43	10.19	2.29	0.63	8.37	0.47	0.27	87.02
64.18	12.95	2.46	2.14	1.98	0.94	1.37	0.61	0.19	86.82
69.31	14.82	1.65	1.34	1.98	0.57	0.42	0.60	0.18	90.86

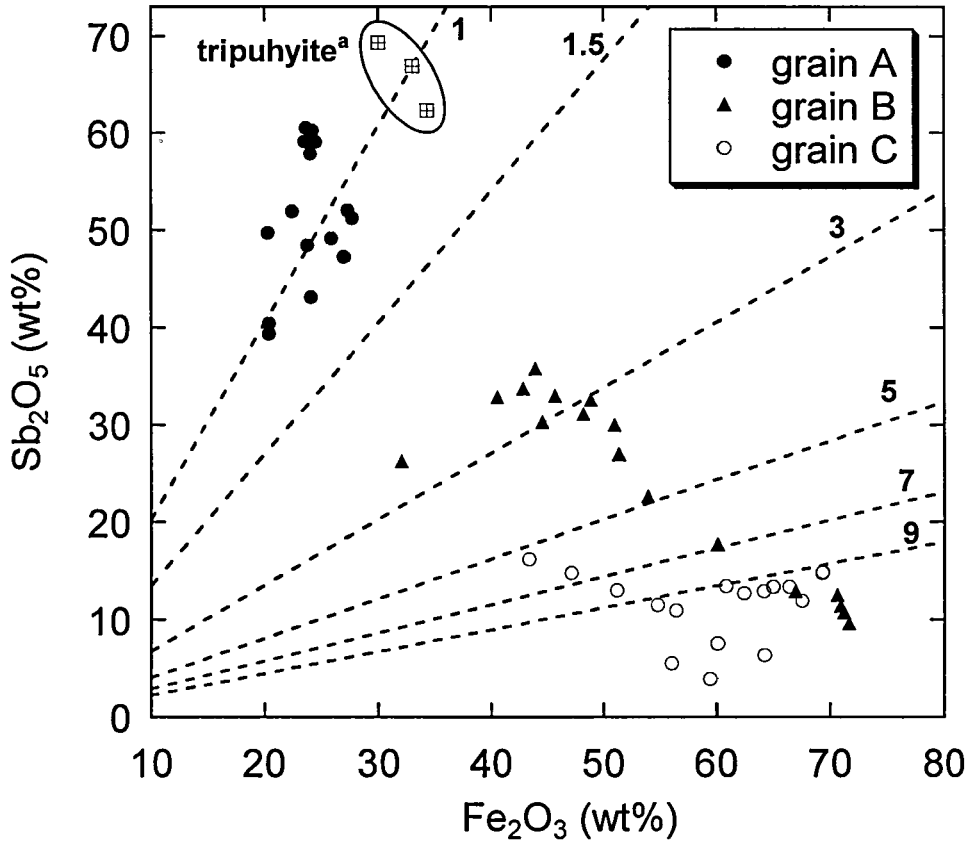

(a) Chemical components of tripuhyite are the data reported by Berlepsch et al. (2003).

Figure 4-3. Variation of Sb_2O_5 as a function of Fe_2O_3 in Sb hot spots in the Ichinokawa soil grains. Dotted lines are Fe/Sb molar ratios.

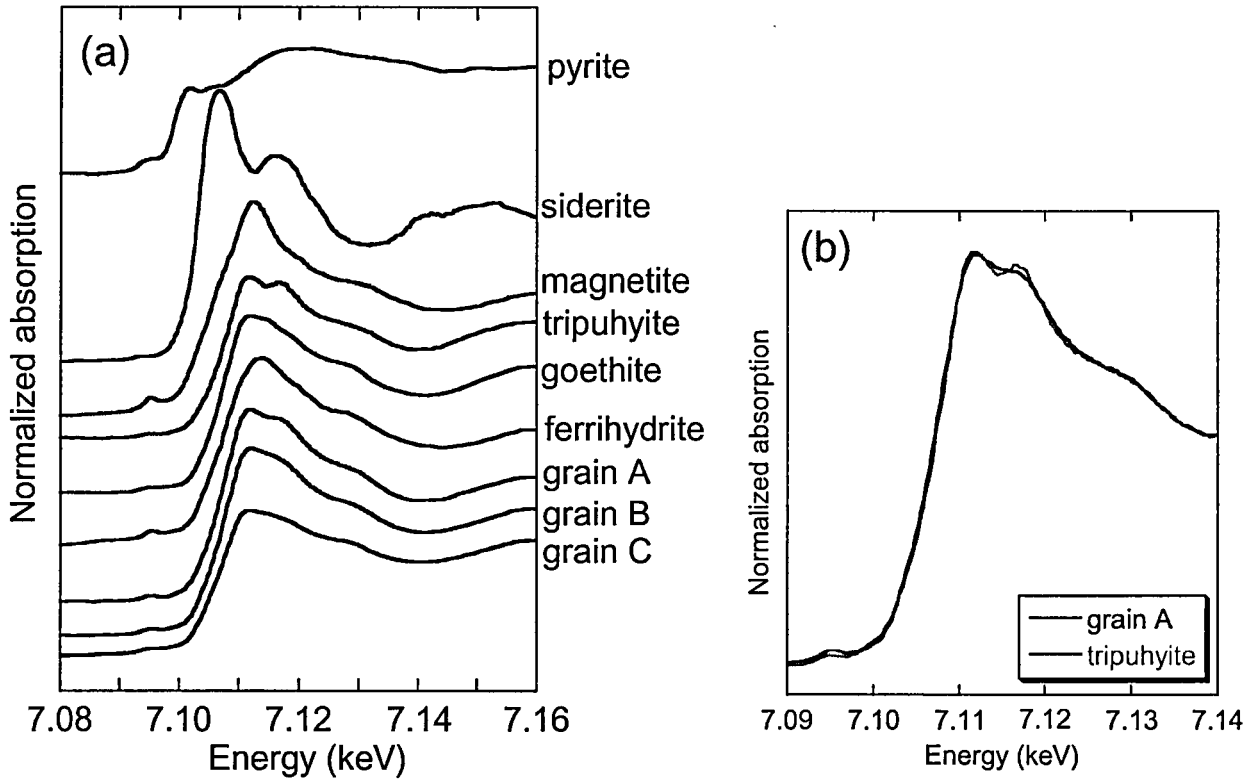

Figure 4-4. (a) K-edge Fe μ-XANES spectra of standard materials and Sb hot spots in Ichinokawa soil. (b) Comparison of the Fe XANES spectrum of grain A with that of tripuhyite.

siderite, magnetite, tripuhyite, and goethite) and Sb hot spots in grains A-C contained in Ichinokawa soil. The features observed at white-line and peak top of grains A-C spectra are similar to those of Fe(III) hydroxides and not similar to other phases such as pyrite and siderite, significantly. This suggests that Fe species in all the Sb hot spots are Fe(III) hydroxides. Thus, Sb in soil exists as incorporated form with Fe(III) hydroxide based on Fe XANES and EPMA analyses. In grain A, two peaks at peak top were observed in Fe XANES spectrum of Sb hot spot. Moreover, similar peaks were observed at peak top of tripuhyite spectrum (Figure 4-4a) and the feature and position were much similar shown in Figure 4-4b, which suggests that grain A dominantly contains the tripuhyite. Therefore, the Fe XANES and the Fe_2O_3 vs. Sb_2O_3 plot strongly suggest the existence of Fe and Sb hosting mineral, tripuhyite in grain A and that the tripuhyite were authigenically deposited from aqueous phase during sedimentation. This is the first report of authigenic tripuhyite in soil.

μ-XANES analysis for Sb.

To observe the species of Sb incorporated under various reducing conditions, Sb μ-XANES were measured from the edge part to center in C-1 part of grain C (Figure 4-2). The energy at absorption edge of samples are similar to that of $KSb(OH)_6$ (Figure 4-5a), suggesting that major Sb species in Sb in C-1 part is Sb(V). Simulation of XANES spectra was conducted for spectra of all spots in C-1 part based on the spectra of the reference materials (Sb_2O_3 and $KSb(OH)_6$) following Mitsunobu et al., (2006). In all the spots in C-1, significant Sb(III) (Sb(III): 15-22%) were observed particularly in the edge part, whereas the oxidation states of Sb in the center were exclusively Sb(V). Actually, these findings indicate that some Sb are reduced to Sb(III) on the surface of Fe hydroxides under reducing condition, since the Fe hydroxide on the edge part should be reacted under reducing condition and Sb on the part are also exposed to the reducing condition compared with inner part of the mineral. It is reported that the solubility of Sb(III) is much lower than that of Sb(V) (Filella et al., 2002 and Figure 4-6), and the Sb(III) was also slightly observed in both soil and soil water phases under reducing condition in bulk analysis (Chapter 2). The concentration of Sb was over the solubility of Sb(III) and

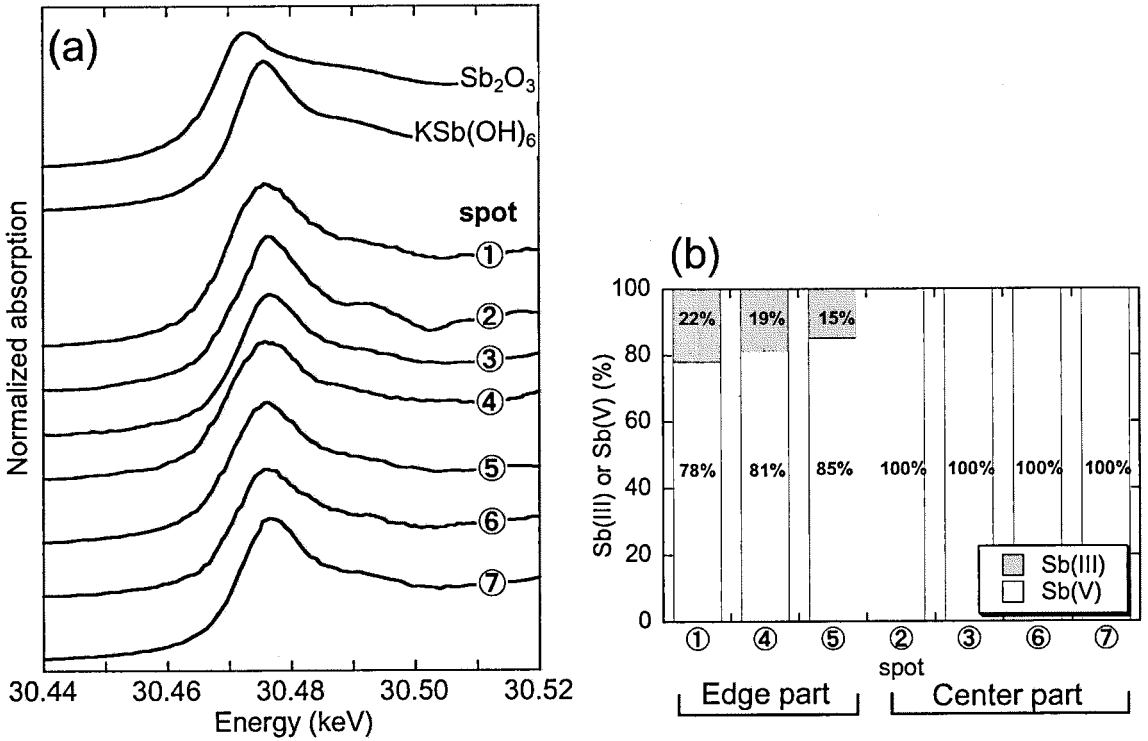

Figure 4-5. (a) K-edge Sb μ-XANES spectra of standard materials and each spot of C-1 part in grain C in Ichinokawa soil. (b) Sb(III) or Sb(V) ratio in each spot in grain C determined by the simulation of Sb K-edge XANES.

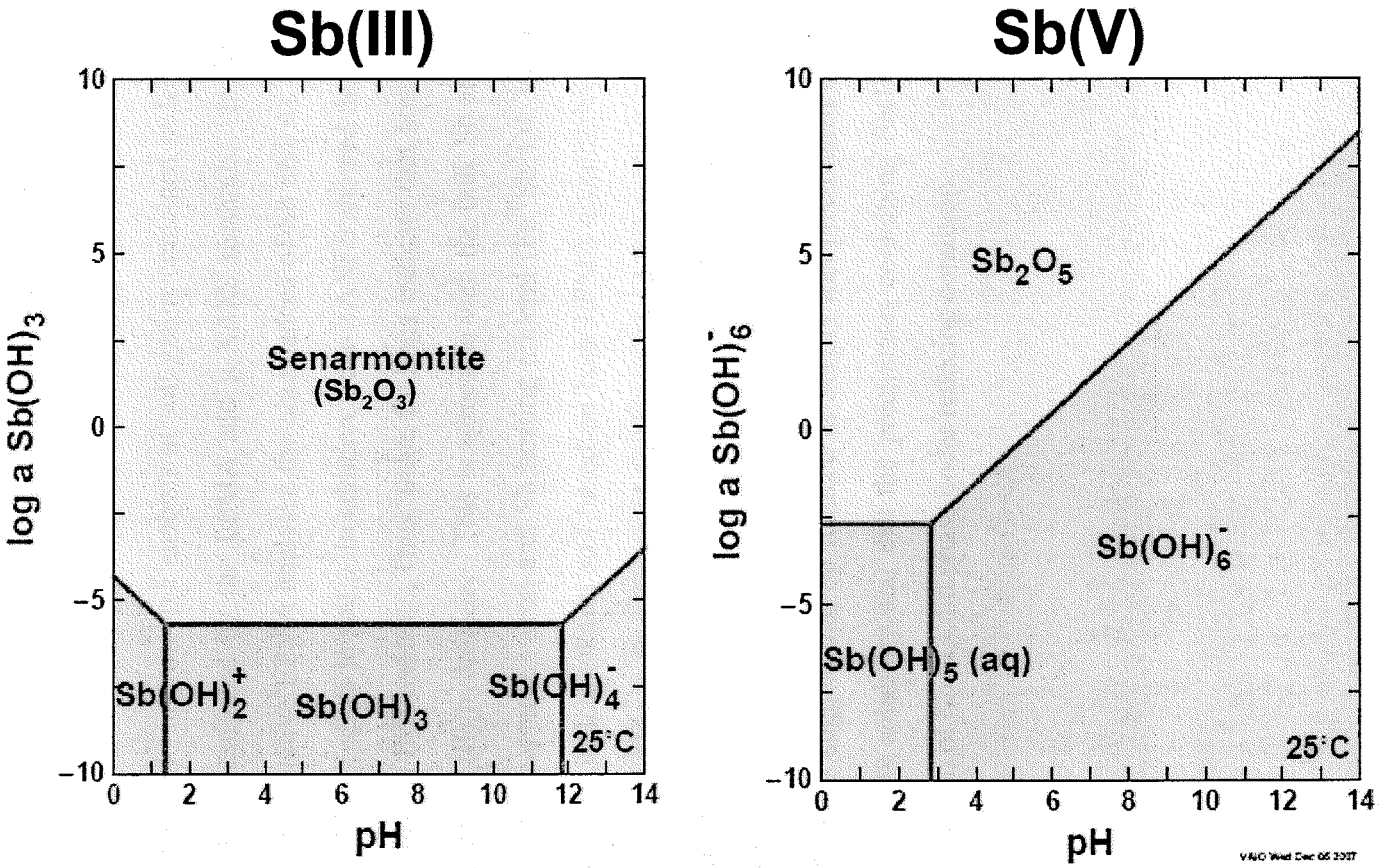

Figure 4-6. Solubilities of Sb(III) and Sb(V) calculated using MINTEQ database.

saturated to the Sb(III) hosting mineral ($Sb^{III}_2O_3$), senarmontite. Therefore, the findings obtained by the microscopic analysis suggest that Sb reduced to Sb(III) was precipitated on the mineral surface due to its low solubility and that the precipitates containing Sb(III) like Sb_2O_3 may cause the fixation of Sb to solid phase under reducing condition.

Conclusions

In present work, microscopic analysis of soil grains contained in Ichinokawa soil was successively investigated by the EPMA and μ-XAFS methods. In Sb hot spots assigned using quantitative EPMA analysis, the abundances of Sb and As correlate with that of Fe in all Sb hot-spots in soil. In addition, Fe μ-XANES showed the Fe species in Sb hot-spot is Fe(III) hydroxides. Thus, these findings indicate that host phases of Sb and As in soil are Fe(III) hydroxide. This is agreeable with the bulk Sb and As EXAFS analyses shown in Chapter 2. Iron and Sb hosting mineral ($Fe^{III}Sb^{V}O4$, tripuhyite) was found in a soil grain in Ichinokawa soil based on both EPMA quantitative analysis and μ-XANES analysis. This is first report of authigenic tripuhyite mineral in the soil. In addition, significant Sb(III) was observed in the rim part of the grain Sb concentrated based on the Sb μ-XANES, whereas Sb(III) was exclusively not observed in the center part. These findings suggest that Sb reduced to Sb(III) was precipitated on the mineral surface due to its low solubility and that the precipitates containing Sb(III) like Sb_2O_3 may cause the fixation of Sb to solid phase under reducing condition.

References

Berlepsch, P.; Armbruster, T.; Brugger, J.; Criddle, A.j.; Graeser, S. 2003. Tripuhyite, $FeSbO_4$, revised. Mineral. Mag. 67, 31-46.

Filella, M.; Belzile, N.; Chen, Y.-W. 2002b. Antimony in the environment: a review focused on natural waters. II. Relevalent solution chemistry. Earth-Sci. Rev. 57, 125-176.

Iida, A.; Noma, T.; Nucl. 1993. Synchrotron X-ray microprobe and its application to human hair analysis. Instrum. Mthods Phys. Res., Sect. B, 82, 129.

Takeuchi, A.; Suzuki, Y.; Takano, H.; Terada, Y. 2005. Kirkpatrick-Baez type X-ray focusing mirror fabricated by the bent-polishing method. Rev. Sci. Instrum., 76, 093708.

Mitsunobu, S., Harada, T., Takahashi, Y., 2006. Comparison of antimony behavior with that of arsenic under various soil redox conditions. Environ. Sci. Technol., 40, 7270-7276.

Pactunc, D.; Foster, A.; Laflamme, G. 2003. Speciation and characterization of arsenic in Ketza River mine tailings using X-ray absorption spectroscopy. Environ. Sci. Technol., 37, 2067-2074.

Pactunc, D.; Foster, A.; Heald, S.; Laflamme, G. 2004. Speciation and characterization of arsenic in gold ores and cyanidation tailings using X-ray absorption spectroscopy. Geochim. Cosmoshim. Acta, 68, 969-983.

CHAPTER 5

Interaction of Sb(V) with Fe(II)/Fe(III) hydroxide, green rust

Introduction

Antimony is the ninth most exploited metal worldwide being mined each year. It is heavily used (> 100 000 tons annually worldwide) in non metal products such as antimony trioxide (Sb_2O_3), primarily in flame retardants, but it is also used as a catalyst in plastics, for the fining of glassware, and as pigment in paints and lacquers (Krachler et al., 2001). In general, the natural abundance of Sb in soil is low (< 1 mg/kg) and in freshwater ranges from 10^{-6} to 10^{-9} g/dm^3 (Filella et al., 2002b). However, Sb concentrations up to several thousand mg/kg have been reported for soils influenced by mining activities (Filella et al., 2002a). Although Sb belongs to group 15 of the periodic table below As and can exist in four oxidation states (–III, 0, III, and V), Sb(III) and Sb(V) are the most frequently observed species in the environment. To a great extent, the behavior of Sb in the environment depends on its oxidation state. The toxicity of Sb also depends on the oxidation state; Sb(III) compounds have 10 times higher acute toxicity than Sb(V) species (Krachler et al., 2001). Antimony compounds are considered to be pollutants of priority interest by the United States Environmental Protection Agency (1979) and the European Union (1976). However, the geochemical behavior of Sb in natural soil and sediment is still largely unknown. Although very few studies of Sb on natural sorbents have been reported to date, the major host phase of Sb in natural soil and sediment can be Fe hydroxide (Chen et al., 2003; Scheinost et al., 2006; Mitsunobu et al., 2006).

Fe(II)-Fe(III) layered double hydroxides, usually called green rusts (GR), have a structure in which brucite-like $[Fe(II)^{(1-x)}Fe(III)^{x}(OH)_2]^{x+}$ alternates with interlayer anions (SO_4^{2-}, CO_3^{2-}, Cl^-, etc.) and water molecules (Bringley and Bish, 1976; Figure 5-1). Green rusts are formed by a number of abiotic and biotic processes under circumneutral to alkaline conditions in suboxic environments (Génin et al., 1998; Refait et al., 1998; Kumar et al., 1999). Recently, a mineral extracted from hydromorphic soils was identified as a GR (Troland et al., 1997; Génin et al., 1998; Génin et al., 2001). Due to

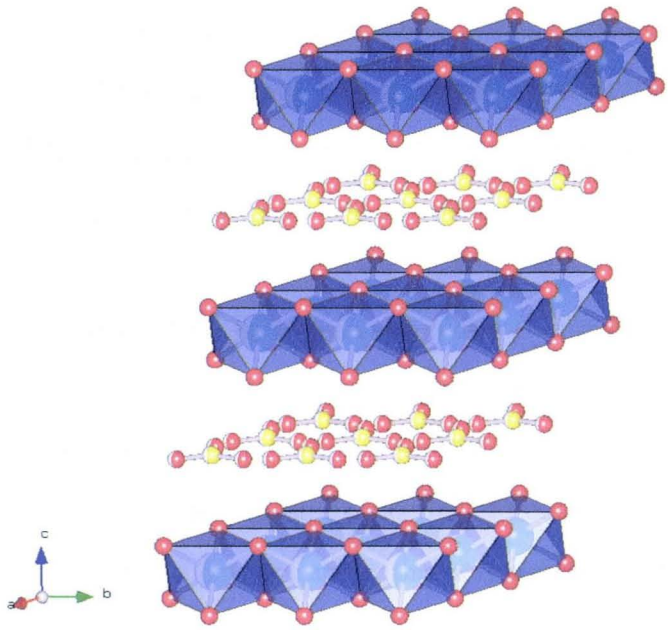

Figure 5-1. Crystallographic structure of green rusts.

its high reactivity with a large reducing potential, GR may have strong influences on the fate and transport of environmental toxins such as the Sb in suboxic environment.

A number of studies for GR interaction with inorganic contaminant were recently reported, showing that GR are capable of reducing many inorganic contaminants including chromate (Loyaux-Lawniczak et al., 1999; Loyaux-Lawniczak et al., 2000; Williams and Scherer, 2001), selenate (Myneni et al., 1997; Refait et al., 2000), selenite (Scheidegger et al., 2003), uranyl (Roh et al., 2002; Dodge et al., 2002; O'Loughlin et al., 2003), nitrate (Hansen et al., 1996; 1998; 2001), and nitrite (Hansen et al., 1994). In comparison, arsenate cannot be reduced by GR (Su and Puls, 2004; Randall and Sherman, 2001; Lin and Puls; 2003). In addition to the reducing potential and the kinetics, the sorption structure on GR surface, which is necessary to understand the reducing and sorption reaction fully, has also been examined for many metal species by spectroscopic methods (Myneni et al., 1997; Randall and Sherman, 2001; Bond and Fendorf, 2003; O'Loughlin et al., 2003).

As far as we know, there have been no studies on the interaction of Sb and GR except for our preliminary work (Mitsunobu et al., 2008). The study indicated that sulphate green rust ($GRSO_4$) has high affinity for Sb(V) and that Sb(V) is partly reduced to Sb(III) by $GRSO_4$. However, the study has focused only on the reducing potential of GR on Sb, and thus little is known about the sorption mechanism and the binding structure of Sb on any GR. Thus, first objective of the present study is to investigate the sorption mechanism of Sb on GR using batch sorption experiments and to determine the binding structure of Sb related to affinity of Sb to GR by extended X-ray absorption fine structure (EXAFS). Consequently, we examine how the sorption mechanism and structure affect Sb reduction by GR.

In addition, though metastable GR gradually transforms to magnetite and $Fe(OH)_2$ even under anoxic conditions, the kinetics of the transformation slows down if phosphate (PO_4^{3-}) ion is present (Benali et al., 2001). Thus, this result suggests that GR is stabilized by the adsorption of phosphate. Similar stabilization effects were observed in other multi-valent oxyanions (AsO_4^{3-} and SiO_3^{2-}) (Su and Puls, 2004; Ruby et al., 2006), but any similar findings were not reported for Sb, while Sb(V) species

dominantly occurs as a monovalent hydroxide anion, $Sb(OH)_6^-$, at pH > 2.5 (Baes and Mesmer, 1976; Filella et al., 2002a). In this study, we also investigated Sb stabilization effect for GR as a second purpose. Moreover, if Sb has a stabilization effect on GR, how the Sb adsorption complex and the binding site on GR crystal are related to the GR transformation mechanism is an important subject.

Materials and Methods

Synthesis and Characterization of $GRSO_4$. The $GRSO_4$ was synthesized by air oxidation of ferrous sulphate solution at neutral pH (Schwertmann and Fechter, 1994). $FeSO_4 \cdot 7H_2O$ (27.80 g) was dissolved in 500 mL of deoxygenated Milli-Q water with magnetic stirring under ambient condition. After the complete dissolution of the ferrous salt, CO_2-free 1 M NaOH was constantly added to the solution by a titrator to maintain pH 7.0. The suspension of the dark blue-green precipitate was vacuum-filtered through 0.22-μm membrane filter under N_2, washed with deoxygenated water, and freeze-dried. The freeze-dried $GRSO_4$ was sieved (< 250-μm) to obtain a uniform particle size. The solid was then sealed and stored in a glass serum vial under N_2 atmosphere in the glovebox.

The Fe(II)/Fe(III) ratio of the prepared $GRSO_4$ was determined to be 1.99 by Mössbauer spectrometry. This ratio close to 2.0 is in good agreement with findings of Génin et al. (Génin et al., 1996), showing that the $GRSO_4$ formula synthesized here is close to $[Fe^{II}_4Fe^{III}_2(OH)_{12}]^{2+} \cdot [SO_4 \cdot nH_2O]^{2-}$.

Batch Experiments. All batch experiments were carried out in an anoxic glovebox purged with 99.999% N_2 (g). Freeze-dried $GRSO_4$ of 20 mg was added to 50 mL centrifuge tube. Appropriate amounts of stock solution of 3.3 mM potassium antimonate ($KSb^V(OH)_6$) were added to make the targeted initial concentration of Sb(V). The total volume of solution was 30 mL. To avoid unexpected interaction, buffer was not used in all batch experiments. Experiments were performed in triplicate with initial and final pH values of 8.0 ± 0.2. The tubes were capped and wrapped with aluminum foil to prevent light exposure. After shaking by a wave-motion shaker for 24 h at 25 ± 0.5°C, solid and water samples were collected by vacuum filtration using 0.22-μm PTFE filter for further

analyses.

Solid and Solution Analyses. The Sb and SO_4^{2-} concentrations in filtered solution samples were measured using ICP-MS (VG; PQ-3) and anion chromatography (Shodex IC I-524A), respectively.

Mineral phase was characterized by X-ray diffractometer (XRD; Rigaku Multiflex) with a Cu Kα radiation source (λ = 1.54056 Å) operating at 40 kV and 40 mA current. Samples were prepared in a glovebox by admixing with glycerol to form a paste that was smeared onto the sample slide, similar to the approach described by Hansen and Poulsen (1999). The glycerol paste was used to prevent oxidation during XRD analysis.

Surface area of solid was determined using a N_2 BET analysis by a BELSORP-mini (BEL Japan). Samples were dried in the glovebox by vacuum desiccation for 24 h at room temperature prior to the analysis (Clausen and Fabricius, 2000). Exposure to air during transfer to the instrument was minimal as evidenced by the lack of color change.

Antimony and Fe K-edge X-ray absorption fine structure (XAFS) spectra were measured at the beamline BL01B1 at SPring-8 (Hyogo, Japan) with a Si(311) (for Sb) and Si(111) (for Fe) double-crystal monochromator and two mirrors. The spectra of the samples and standards were collected in the fluorescence mode using a 19-element Ge semiconductor detector and in the transmission mode using an ionization chamber, respectively. All measurements of solid samples were conducted at 100 K using a cryostat with a closed cycle refrigerator system to prevent unexpected oxidation due to the X-ray radiation effect. The energy calibration was made by the white-line peak maximum of Sb_2O_3 at 30.486 keV for Sb and pre-edge peak maximum of hematite fixed at 7.113 keV for Fe.

The EXAFS data were analyzed by REX2000 (Rigaku Co. Ltd.). EXAFS oscillation was extracted from the original spectrum by a spline smoothing method. E_0 was set at the edge inflection point for all the samples studied. The Fourier transformation of the $k^3\chi(k)$ EXAFS function from k space to r space was performed in a range 3.0-11.0 $Å^{-1}$ to obtain a radial structural function (RSF). The inversely Fourier filtered data were analyzed with a usual curve fitting method. Theoretical phase shifts

and amplitude functions employed in this fitting procedure were extracted from FEFF 7.0 (Zabinsky et al., 1995), in which the structure of tripuhyite ($FeSb^{V}O_4$) was used as an input data to run FEFF for Sb-O and Sb-Fe shells (Berlepsch et al., 2003).

Results

Sorption Experiments. The relationship between initial Sb concentration ($[Sb]_0$) and amount of Sb adsorption in the Sb-$GRSO_4$ sorption experiment was shown in Figure 5-2. Adsorbed amount of Sb monotonically increased within the lower $[Sb]_0$ region ($[Sb]_0$ < 1000 μM), but decreased in the higher $[Sb]_0$ range ($[Sb]_0$ > 1000 μM). This decrease of Sb adsorption indicates that another phase consisting of Sb and Fe by surface precipitation or co-precipitation was not formed on the surface of solids, since mineral precipitation by saturation generally accompanies the increase of adsorption (42). Thus, it was suggested that Sb exists as an adsorption complex on the solid at any $[Sb]_0$. A similar trend was also observed in the concentration of released SO_4^{2-}, namely $[SO_4^{2-}]_{aq}$, which had a maximum in the range of 500 μM < $[Sb]_0$ < 1000 μM and decreased in higher $[Sb]_0$ range (Figure 5-2). This result suggests that the adsorption of Sb on $GRSO_4$ solid is composed of an anion exchange reaction with SO_4^{2-} in the mechanism.

XRD and Fe XANES Analyses for Solid Phase Speciation. Figure 5-3 shows the XRD patterns of the solid samples formed in the presence and absence of Sb. In the control (sample without Sb), peaks of magnetite and $Fe(OH)_2$ (magnetite: 2θ = 30°, 35°, 43°; $Fe(OH)_2$: 2θ = 19°, 38°) were observed in addition to those of $GRSO_4$ peaks, which indicates the $GRSO_4$ transformation into a mixture of $Fe(OH)_2$ and magnetite during experiment. It is reported that carbonate GR is transformed into $Fe(OH)_2$ and magnetite under anoxic condition (Benali et al., 2001). Because the transformed products observed in this study were also magnetite and $Fe(OH)_2$, GR transformation can be described by following reaction.

$$Fe^{II}_4Fe^{III}_2(OH)_{12}SO_4 + 2OH^- \Leftrightarrow Fe^{II}Fe^{III}_2O_4 + 3Fe^{II}(OH)_2 + SO_4^{2-} + 4H_2O \quad (A)$$

This is in agreement with previous thermodynamic predictions (Refait et al., 2003) that magnetite is more stable than $GRSO_4$.

In Sb-$GRSO_4$ system, though magnetite and $Fe(OH)_2$ peaks were also observed

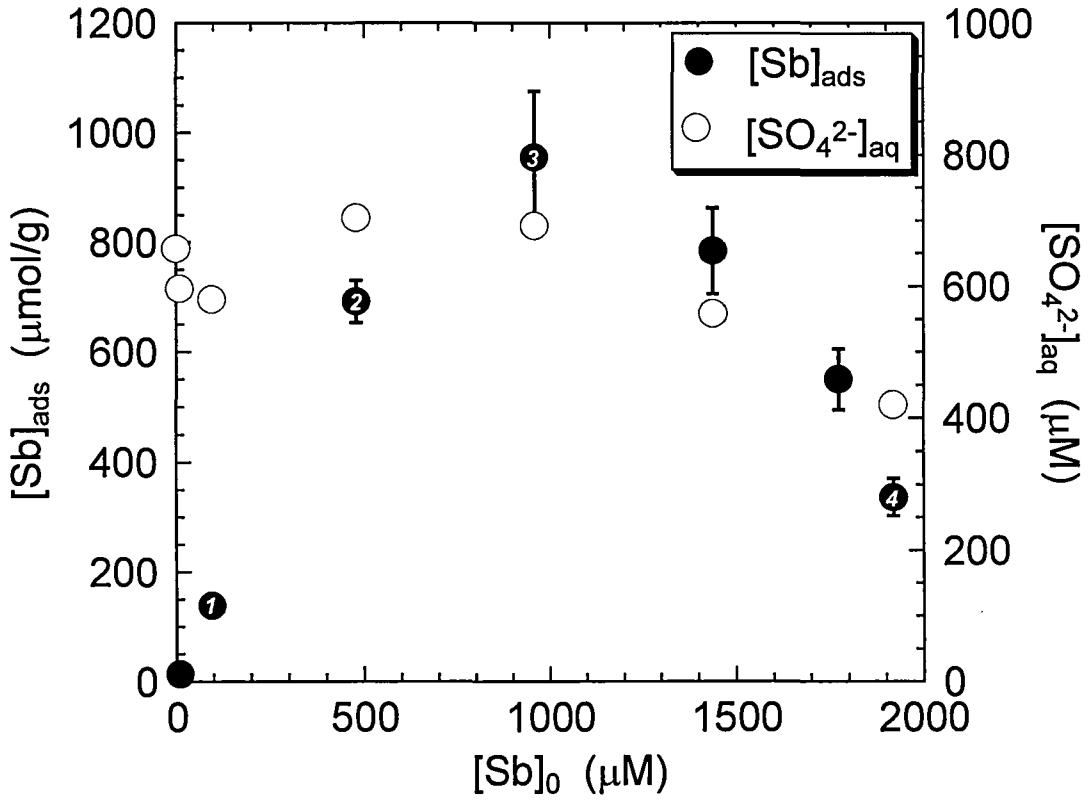

Figure 5-2. Solution chemistry of the reacted solution with initial Sb concentration ($[Sb]_0$). Relationship between adsorbed amount of Sb on solid phase ($[Sb]_{ad}$) and concentration of sulphate ions ($[SO_4^{2-}]_{aq}$) with $[Sb]_0$. Numbers in markers correspond to those in other Figures.

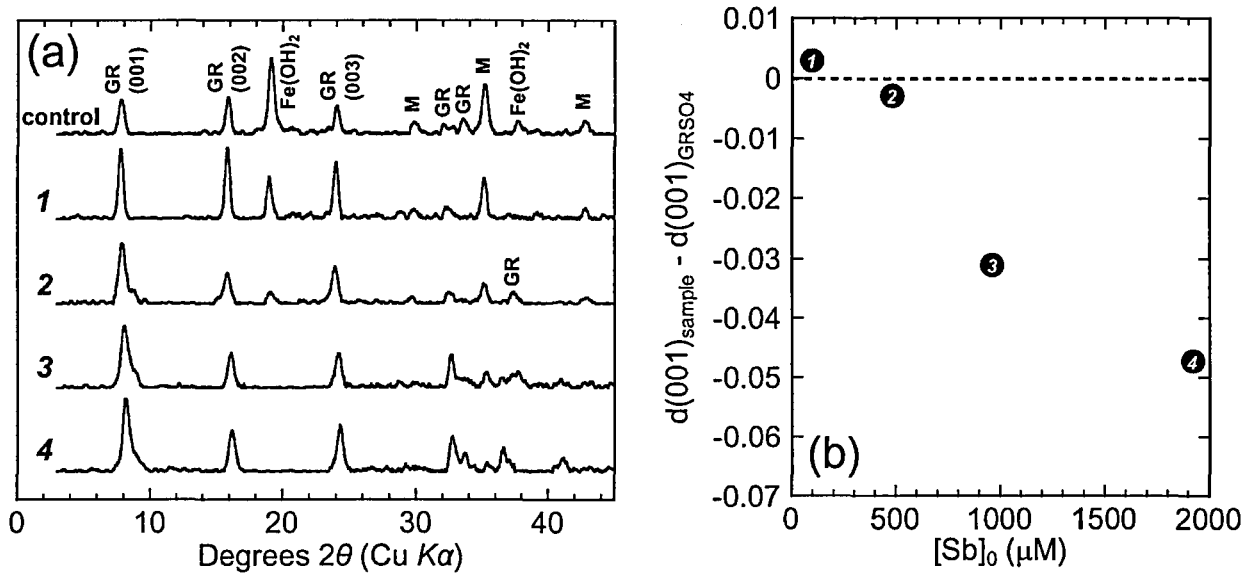

Figure 5-3. (a) XRD patterns of collected solid from Sb-$GRSO_4$ system (Sample 1-4) and control (system without Sb). In (a), a word of 'M' shows magnetite. (b) Change of d(001) values obtained from XRD patterns for the $GRSO_4$ that Sb is adsorbed with initial Sb concentration ($[Sb]_0$). In (b), $d(001)_{GRSO4}$ and $d(001)_{sample}$ represent d(001) value of $GRSO_4$ used and the samples in $GRSO_4$-Sb system, respectively. Patterns in (a) and data points in (b) are labeled with sample numbers shown in Figure 1. Dotted linear line in (b) shows $d(001)_{GRSO4}$ (= 11.18 nm).

clearly in the XRD patterns of low $[Sb]_0$ samples (Samples 1-2), these peaks were less intense compared with those for the control sample. The magnetite and $Fe(OH)_2$ peaks gradually became lower at higher $[Sb]_0$ and most of these peaks were not observed finally in Sample 4 with the highest $[Sb]_0$, indicating that the solid mainly consists of $GRSO_4$. In addition, the $GRSO_4$ peaks in Samples 1-4 became more intense and sharper than those in the control. These results show that the proportion of $GRSO_4$ in solid was enhanced by the presence of Sb and gradually increased with higher $[Sb]_0$. Similar results are shown in Fe K-edge X-ray absorption near edge structure (XANES) spectra of collected samples (Figure 5-4). Simulation of Fe XANES was conducted to determine the $GRSO_4$ fraction in solid sample (Figure 5-4b). At any $[Sb]_0$, fraction of $GRSO_4$ in Sb-$GRSO_4$ system (> 57%) was significantly larger than that of control (= 40%), which gradually increased with $[Sb]_0$. Finally, the fraction reached a maximum (= 80%) in Sample 4 (highest $[Sb]_0$) in the $[Sb]_0$ range of this study. These findings are well consistent with the XRD results. Therefore, these XRD and Fe XANES results suggest that Sb has a stabilization effect for $GRSO_4$ transformation to magnetite and $Fe(OH)_2$. It is also suggested that the stability depends on the Sb concentration in the range of present study ($[Sb]_0 < 1920$ μM).

In the XRD patterns of all the samples in Sb-$GRSO_4$ system, the peaks other than $GRSO_4$, magnetite, and $Fe(OH)_2$ were not observed. Thus, it is suggested that other Sb and Fe hosting phases like the Fe antimonate, tripuhyite, are not formed at any $[Sb]_0$. Therefore, these results suggest that Sb in solid phase does not occur as co-precipitated or precipitated phase but as the species adsorbed on $GRSO_4$ and the transformed products (magnetite and $Fe(OH)_2$). This finding is also consistent with the fact examined in sorption experiment in which the adsorbed amount of Sb decreases at a higher $[Sb]_0$ (Figure 5-2).

Sb XAFS Analysis. Figure 5-5 shows the normalized Sb K-edge XANES spectra of reference materials (Sb_2O_3 and $KSb(OH)_6$) and the samples collected from Sb-$GRSO_4$ system. It is obvious from the spectra of reference materials that the absorption edge shifts to higher energy at the higher oxidation state of Sb. This suggests that the position of the XANES peak can be used to distinguish Sb(III) and Sb(V). The absorption edges

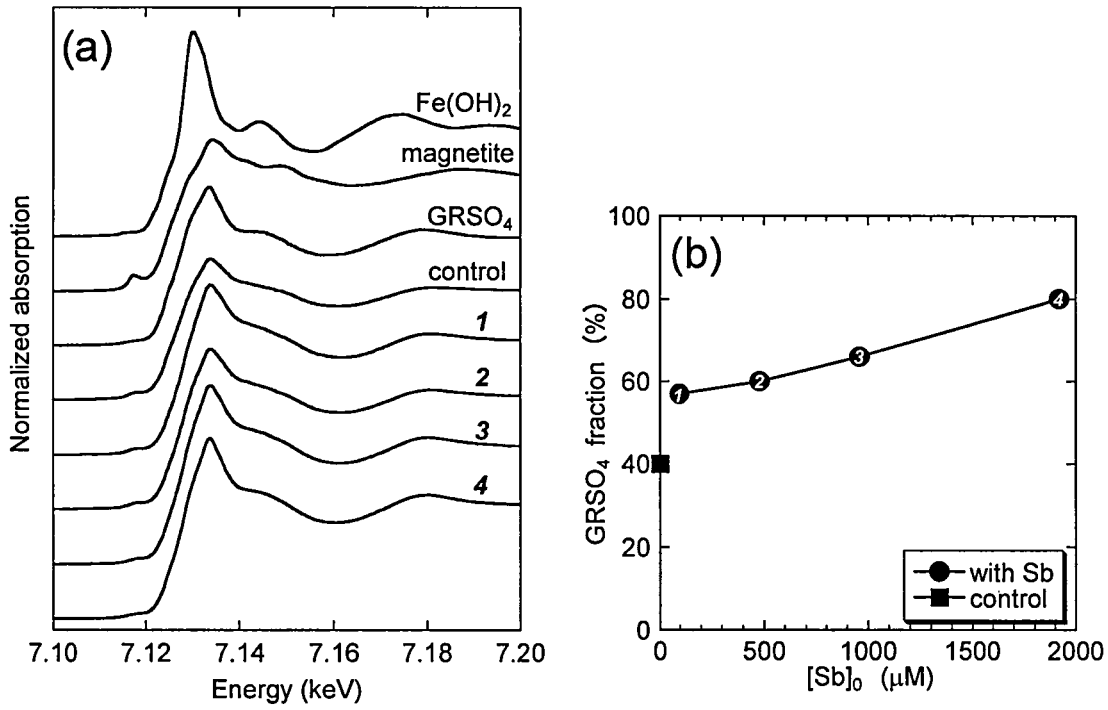

Figure 5-4. (a) Normalized Fe K-edge XANES spectra of the reference materials (Fe(OH)2, magnetite, and GRSO4) and collected solids in Sb-GRSO4 systems (Samples 1-4) and control. Spectra of solids that Sb is adsorbed are labeled with sample numbers shown in Figure 1. (b) GRSO4 fraction of collected solids from Sb-GRSO4 system and control samples obtained by simulation of Fe K-edge XANES using spectra of GRSO4, magnetite, and Fe(OH)2 as end-members.

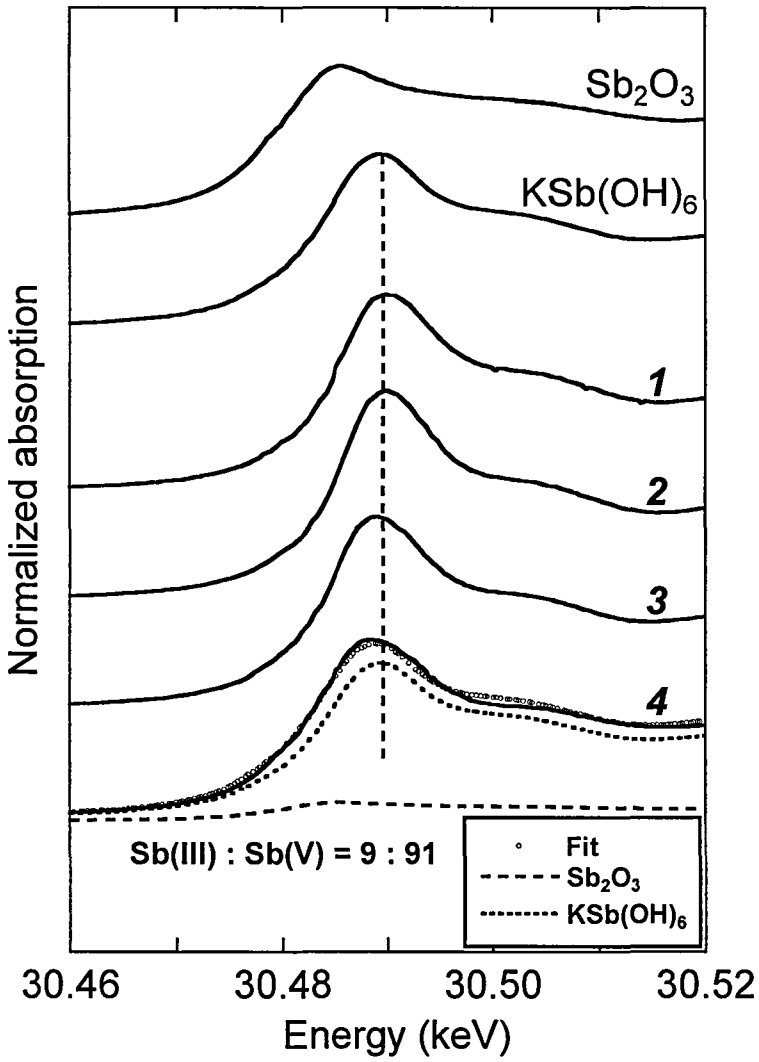

Figure 5-5. Normalized Sb K-edge XANES spectra of the reference materials (Sb_2O_3 and $KSb(OH)_6$) and collected solids that Sb is adsorbed (Samples 1-4). Spectra of solid in Sb-$GRSO_4$ system are labeled with sample numbers shown in Figure 1. A dotted line is drawn to indicate the absorption maximum of Sb(V), $KSb(OH)_6$.

of Sb for low-middle $[Sb]_0$ samples (Samples 1-3) in sorption experiments were similar to that of $KSb(OH)_6$, indicating that Sb in the sample is dominantly Sb(V). On the other hand, the absorption edge of Sb was slightly shifted to lower energy in the spectrum of Sample 4 with the highest $[Sb]_0$, indicating that some Sb(III) are included in the Sample 4. Following Mitsunobu et al. (2006), least-square fitting of Sb XANES spectra was conducted for collected samples using the spectra of the reference materials (Sb_2O_3 and $KSb(OH)_6$). In the simulation results, the presence of Sb(III) was not clearly observed in the Samples 1-3. However, about 9% Sb is present as Sb(III) at the highest $[Sb]_0$, Sample 4 (Figure 5-5). Thus, it is indicated that Sb adsorbed is completely present in the oxidized form, Sb(V), in low-middle $[Sb]_0$ range, whereas Sb(V) is partially reduced to Sb(III) at the highest $[Sb]_0$ by $GRSO_4$. This partial reduction is consistent with the previous work (Mitsunobu et al., 2008).

Local structure of Sb was examined by EXAFS to obtain information on the surface complex of Sb adsorbed on $GRSO_4$ based on the spectrum for Sample 4. Fraction of $GRSO_4$ among all the Fe species including magnetite and $Fe(OH)_2$ reached the maximum in Sample 4 as shown by XRD and Fe XANES. Thus, we can discuss the Sb-$GRSO_4$ complex based on the EXAFS analysis for Sample 4 with minimal influence of the transformed products. Figures 5-6a and b show k^3-weighted EXAFS spectra and Fourier transformations for the Sample 4 and model compounds (tripuhyite and Sb(V) adsorbed on lepidocrocite). In the Fe antimonate tripuhyite, two backscattering peaks were observed in Fourier transform at about 2.6 Å and 3.1 Å (uncorrected for phase shift), and Sb is coordinated with Fe at the distance of 3.08 and 3.63 Å and with Sb at the distance of 3.09 and 3.62 Å based on the fit result (Table 1 in SI). These distances and the coordination numbers obtained are in agreeable with published XRD data (Berlepsch et al., 2003). Figure 5-6c shows that Fourier-filtered EXAFS spectra of the Sb-O, Sb-Fe_1, and Sb-Fe_2 shells for Sample 4 in Figure 5-6b and a subtraction of the contribution of Sb-O shell from the filtered EXAFS spectrum for Sample 4, (Sample 4) – (Sb-O). The subtraction spectrum is not simple wave, which cannot be simulated by a single EXAFS function of a Sb-Fe shell (Figure 5-6c), indicating that the subtraction spectrum contains several components. This fact suggests that more than two Sb-Fe

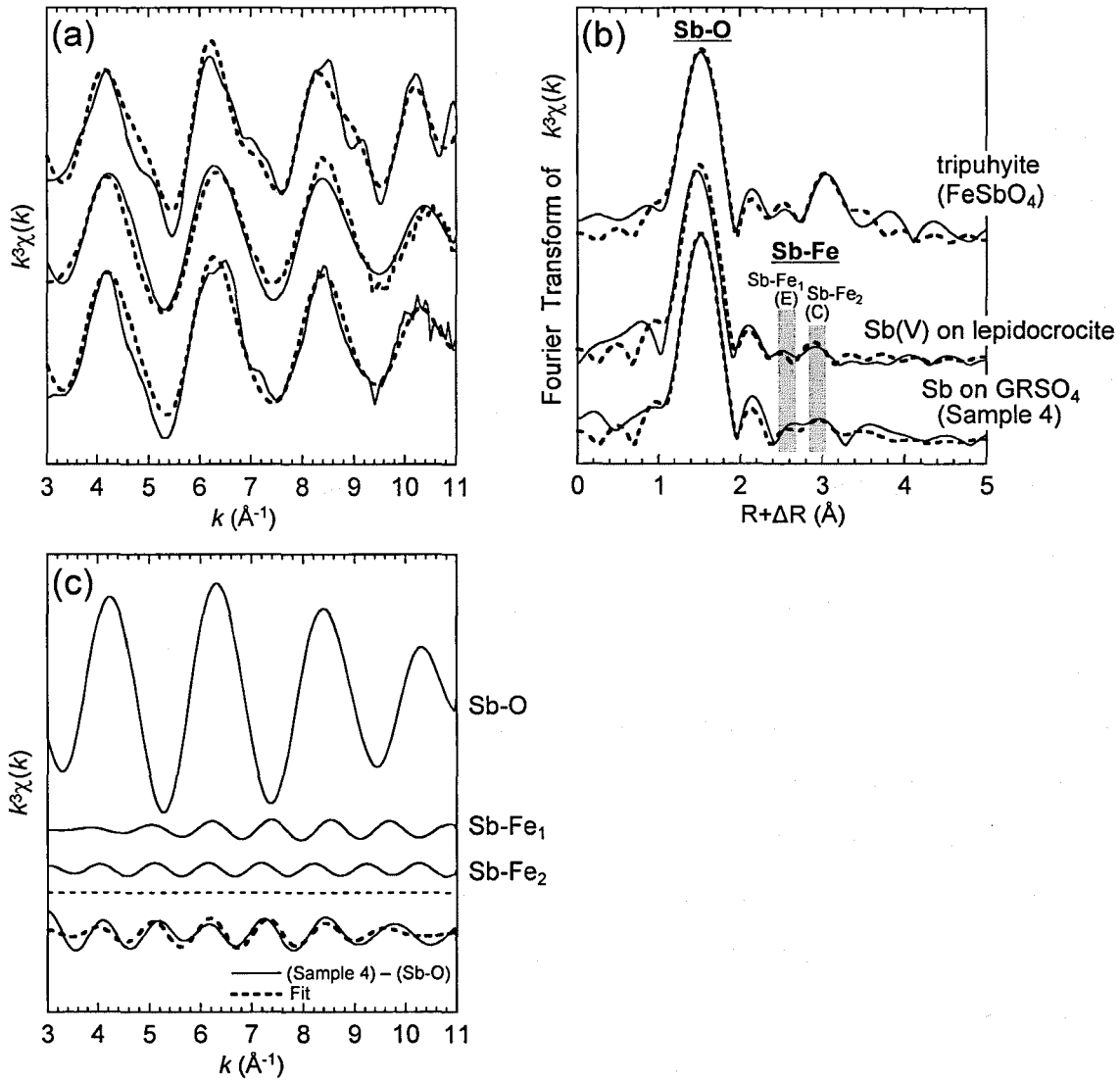

Figure 5-6. (a) Normalized k^3-weighted EXAFS spectra at the Sb K-edge and (b) Fourier-transformed EXAFS spectra of Sb adsorbed on collected solid at the highest initial Sb concentration (Sample 4 labeled in Figure 1) and in model compounds (tripuhyite and Sb adsorbed on lepidocrocite). Radial distances are not corrected for the phase shift. Two gray areas in (b) show the edge- (E) and corner- (C) sharing peaks, respectively. In (a) and (b), solid and dotted lines show experimental functions and calculated curves, respectively. (c) Fourier-filtered EXAFS spectrum of the Sb-O, Sb-Fe_1, and Sb-Fe_2 shells for Sample 4 in (b) after back transforming and a subtraction of contribution of Sb-O shell from the filtered EXAFS spectra (1.01 Å < R+ Δ R < 3.28 Å) of Sample 4 including Sb-O and Sb-Fe shells.

contribute to the EXAFS oscillation. In fact, two small backscattering peaks were also observed in Fourier transform of Sample 4 and Sb(V) on lepidocrocite at about 2.6 Å and 3.0 Å (uncorrected for phase shift), respectively (Figure 5-6b). First peak at 2.6 Å shown in Sample 4 and the two model compounds was fitted with Fe atom at a distance of 3.08-3.10 Å (Table 1), which is in accordance with an $Sb(OH)_6$ octahedron sharing an edge with an $Fe(OH)_6$ octahedron (Scheinost et al., 2006). Second peak at 3.0 Å shown in Sample 4 and Sb(V) on lepidocrocite, corresponding to a fitted distance of 3.61 and 3.55 Å (Table 1), respectively, suggests formation of a bidentate, double corner-sharing complex with Fe octahedron (Mitsunobu et al., 2006). Thus, Sb is adsorbed to $GRSO_4$ and lepidocrocite through the formation of a mixture of edge- and corner-sharing complexes (Figure 5-7). Ideally, the Fe coordination number must be 1 and 2 for the edge and corner sharing surface complexes, respectively. If the surface complex is a 1:1 mixture of both complexes, the coordination number obtained by EXAFS simulation should be apparently 0.5 and 1.0, respectively (Scheinost et al., 2006). Iron shell coordination numbers of 0.5 and 1.2 obtained in this study are close to these values, suggesting that Sb is adsorbed to $GRSO_4$ by forming surface complexes in Sample 4, but not as a co-precipitated and/or solid solution with Fe. This finding is also supported by the sorption isotherm, XRD, and Fe XANES results. The Sb(III) and Sb(V) are coordinated to O with trigonal and octahedral, respectively (Svesson, 1975; Sherman et al., 2000). From Sb XANES analysis, it is suggested that Sample 4 contains a small amount of Sb(III) (~9%) resulting from reduction by $GRSO_4$. However, Sb-O coordination number fitted is 5.5 (Table 1) and close to 6, confirming that Sb detected in EXAFS was mainly Sb(V) in spite of the slight occurrence of Sb(III).

Discussion

Stabilization of $GRSO_4$ in the Presence of Sb. From XRD and Fe XANES results, the transformation of $GRSO_4$ observed in the control system during 24 hours is mitigated in the presence of Sb, showing a stabilization effect of Sb in $GRSO_4$ transformation. Similar effect was observed for phosphate (PO_4^{3-}) and silicate (SiO_3^{2-}) anions for GR (Bocher et al., 2004; Ruby et al., 2006). They suggested that the stabilization effect

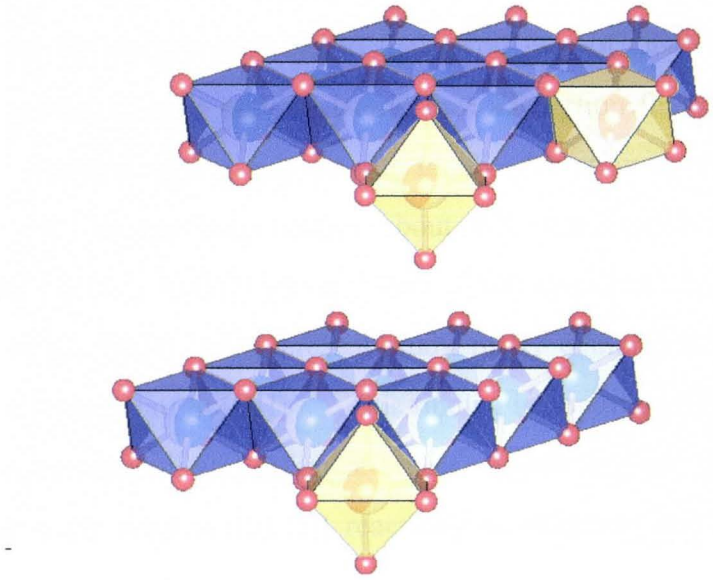

Figure 5-7. Schematic figure of surface complexof Sb adsorbed on green rust.

can be explained by the adsorption of anions to the lateral faces of GR crystal, where the anion adsorbed prevents release of interlayer anions (CO_3^{2-} and SO_4^{2-}) by acting as physical barrier slowing down the kinetics of transformation. The Sb(V) is dissolved as a monovalent hydroxide anion, $Sb(OH)_6^-$, in the solution at pH of this study (Filella et al., 2002). In this study, each fraction of Sb adsorbed on $GRSO_4$ and the transformed products, magnetite and $Fe(OH)_2$, cannot be precisely estimated, because the solid phase does not consist of only one mineral at all $[Sb]_0$. Moreover, the re-adsorbed amount of SO_4^{2-} once released by transformation upon the transformed products is also unknown. Hence, unfortunately, it is difficult to determine quantitatively the Sb amount adsorbed to the lateral face of $GRSO_4$ in this study by balancing the anion exchange and the lateral face adsorption for Sb. However, it is speculated that Sb stabilization may be due to Sb adsorption on the lateral faces of $GRSO_4$ based on the previous studies about GR stabilization with multi-valent oxyanions (PO_4^{3-}, SiO_3^{2-}, AsO_4^{3-}) (Su and Puls, 2004; Benali et al., 2001; Ruby et al., 2006; Bocher et al., 2004). The present study firstly demonstrates that GR can be stabilized in the presence of $Sb(OH)_6^-$. This finding is important for understanding the GR behavior in natural soil and sediment where various ions are present, since these studies and our study suggest that GR reactivity as adsorbent and reductant strongly depends on the stability in the environment.

Change of Character as Sorbent by GR Transformation. Figure 5-8 shows BET surface area of solids collected in Sb-$GRSO_4$ system. The surface areas of the solids have a maximum at the lowest $[Sb]_0$ (Sample 1) and gradually decrease at higher $[Sb]_0$. On the other hand, in the low $[Sb]_0$ range, the fraction of transformed products is significantly large compared within higher $[Sb]_0$ region based on XRD and Fe XANES results. These findings suggest that the increase in surface area at a lower $[Sb]_0$ can be explained by the formation of transformed products, magnetite and $Fe(OH)_2$, that have larger surface areas, if the surface area of $GRSO_4$ fraction is constant during sorption experiment. This assumption may be valid, because the surface area of the samples gradually became close to that of $GRSO_4$ used (= 26.6 m^2/g) at higher $[Sb]_0$ (Figure 5-8). As stated in above part, the presence of Sb slows down the kinetics of GR transformation

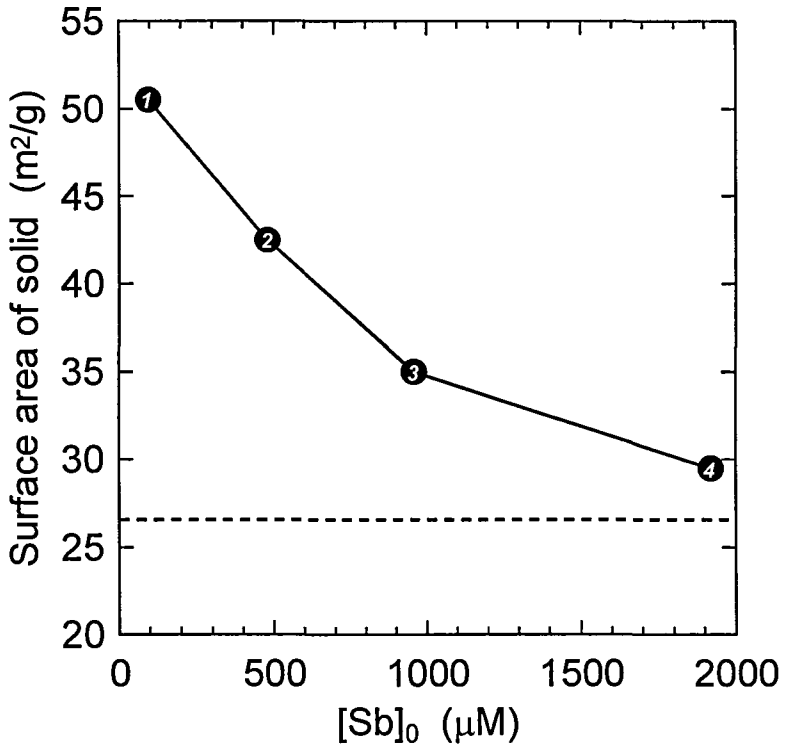

Figure 5-8. Change of BET surface area of collected solids with initial Sb concentrations ($[Sb]_0$). Data points are labeled with sample numbers shown in Figure 1. Dotted line shows surface area of $GRSO_4$ used (= 26.6 m^2/g).

expressed by Equation (A). Thus, this finding suggests that the transformation rate of GR at higher $[Sb]_0$ is slower than that at lower $[Sb]_0$, due to the stabilization of GR by Sb. The particle size of Fe hydroxide generally changes depending on the formation rate. Iron hydroxide formed at faster rate has a smaller particle size, which leads to a larger surface area of the Fe hydroxide (Cornell and Schwertmann, 1991). These facts suggest that transformation of $GRSO_4$ with faster rate at lower $[Sb]_0$ forms the transformed products (magnetite and $Fe(OH)_2$) with smaller particle size and larger surface area. The surface area is one of the crucial factors controlling the reactivity of Fe oxide, and the Fe oxides with larger surface area have a higher potential as adsorbent. Therefore, it is suggested that the decline in the amount of adsorbed Sb observed at higher $[Sb]_0$ is due to the decrease in adsorption capacity accompanied by GR stabilization, and that GR transformation strongly affects the sorption property of solids also in the case of many other anions as well as Sb.

Reduction of Sb(V) by $GRSO_4$. The d(001) values of solid samples obtained by XRD analysis decrease monotonically with $[Sb]_0$ (Figure 5-3b). This change demonstrates that $Sb(OH)_6^-$ exchanges with SO_4^{2-} in the interlayer (Hansen and Poulsen, 1999). Thus, this result suggests that Sb abundance in interlayer of $GRSO_4$ gradually increases with $[Sb]_0$. Since adsorbed amount of Sb decreases in Sample 4 (Figure 5-2), it is also suggested that fraction of Sb being in interlayer of GR to the total adsorbed amount reached a maximum in Sample 4. This fact may contribute to the partial reduction observed only in Sample 4. These findings suggest that Sb accessibility into $GRSO_4$ interlayer would be one of important factors in Sb reduction by $GRSO_4$. The reducing activity of GR changes depending on a kind of interlayer anion (Cl^-, SO_4^{2-}, CO_3^{2-}, etc.), and thus the reducing reaction by GR occurs in the interlayer site more efficiently (26,31), which supports our suggestion for the importance of Sb accessibility in Sb reduction by $GRSO_4$.

On the other hand, GR fraction in solid phase increases at a higher $[Sb]_0$, whereas transformed product of GR increases at a lower $[Sb]_0$. Thus, it is suggested that fraction of Sb adsorbed on $GRSO_4$ to total adsorbed Sb in Sample 4 is the largest among the samples. Bond and Fendorf (2003) reported that the reduction rate of Cr(VI) by GR far

exceeds other reductants such as magnetite, aqueous Fe(II), and sulphate reducing bacteria (e.g., *Desulfovibrio vulgaris*) by comparing each reduction rate, showing that GR has much higher reducing potential. In addition, the rate of reduction of Cr(VI) by GR is 10^3 times faster than that by magnetite (Bond and Fendorf, 2003), which is one of transformed minerals of $GRSO_4$ in this study. Therefore, the reduction observed in Sample 4 is also due to Sb being adsorbed more richly to $GRSO_4$, which is a strong reducer.

Conclusions

In this study, interaction of Sb with $GRSO_4$ was successfully investigated in detail using a multi-technique approach, EXAFS, XANES, XRD, and BET analyses, to the $GRSO_4$ solid adsorbing Sb. It was shown that Sb(V) is adsorbed to $GRSO_4$ with an inner-sphere complex on the surface, and that the surface complex species is a mixture of edge- and corner-sharing complexes based on EXAFS analysis. Stabilization of "metastable" $GRSO_4$ by the presence of Sb is firstly observed, moreover $GRSO_4$ stability gradually increased with $[Sb]_0$ in the range of this study. This stabilization effect for GR is also reported on other oxyanions that is adsorbed to GR with the formation of an inner-sphere complex such as phosphate, arsenate, and silicate. Thus, the Sb inner-sphere complex to $GRSO_4$ also contributes to the $GRSO_4$ stabilization by Sb. The transformed products of $GRSO_4$ have a larger surface area and higher potential as adsorbent than $GRSO_4$, which strongly affects the sorption of Sb to solid phase. In addition, the surface area of the solid systematically increases with the advance of transformation. Thus, the transformation of GR is important for evaluating GR activity not only as a reductant but also as an adsorbent of inorganic species in natural environment. In a sample where a large amount of Sb was adsorbed in interlayer, partial reduction of Sb(V) to Sb(III) was observed, suggesting that Sb accessibility into the interlayer of GR may be one of the important keys for Sb(V) reduction. Therefore, the binding complex and the site of Sb adsorbed on GR are of importance in understanding of reaction between Sb and GR, including adsorption and reduction in an aquatic environment.

References

Baes, C. F.; Mesmer, R. E. The Hydrolysis of Cations; Wiley: New York, 1976.

Berlepsch, P.; Armbruster, T.; Brugger, J.; Griddle, A. J.; Graeser, A. J. 2003. Tripuhyite, $FeSbO_4$, revised. Mineral. Mag. 67, 31-46.

Benali, O.; Abdelmoula, M.; Refait, P.; Génin, J. -M. R. 2001. Effect of orthophosphate on the oxidation products of Fe(II)-Fe(III) hydroxycarbonate: The transformation of green rust to ferrihydrite. Geochim. Cosmochim. Acta 65, 1715-1726.

Bocher, F; Génin, A.; Ruby, C.; Ghanbaja, J.; Abdelmoula, M.; Génin, J.- M. R. 2004. Coprecipitation of Fe(II-III) hydroxycarbonate green rust stabilized by phosphate adsorption. Solid State Sci. 6, 117-124.

Bond, D. L.; Fendorf, S. 2003. Kinetics and structural constraints of chromate reduction by green rusts. Environ. Sci. Technol. 37, 2750-2757.

Brindley, G. W.; Bish, D. L. 1976. Green rust – pyroaurite type structure. Nature 263, 353.

Chen, Y.-W.; Deng, T.-L.; Filella, M.; Belzile, N. 2003. Distribution and early diagenesis of antimony species in sediments and pore water of freshwater lakes. Environ. Sci. Technol. 37, 1163-1168.

Clausen, L.; Fabricius, I. 2000. BET measurements: outgassing of minerals. J. Colloid Interface Sci. 227, 7-15.

Cornell, R. M.; Schwertmann, U.; The iron oxides: Structure, Properties, Reactions, Occurrences and Uses 2nd ed.; Wiley-VCH: Weinheim, 1991.

Council of the European Communities. Council Directive 76/ Substances Discharged into Aquatic Environment of the Community; Official Journal L 129, 1976; pp 23-29.

Dodge, C. J.; Francis, A. J.; Gillow, J. B.; Halada, G. P.; Eng, C.; Clayton, C. R. 2002. Association of uranium with iron oxides typically formed on corroding steel surfaces. Environ. Sci. Technol. 36, 3054-3511.

Filella, M.; Belzile, N.; Chen, Y.-W. 2002a. Antimony in the environment: a review focused on natural waters. I. Occurrence. Earth-Sci. Rev. 59, 265-285.

Filella, M.; Belzile, N.; Chen, Y.-W. 2002b. Antimony in the environment: a review focused on natural waters. II. Relevalent solution chemistry. Earth-Sci. Rev. 57, 125-176.

Génin, J.-M. R.; Bourrié, G; Trolard, F; Abdelmoula, M.; Jaffrezic, A.; Refait, Ph.; Maitre, V.; Humbert, B.; Herbillon, A. 1998. Thermodynamic equilibria in aqueous suspensions of synthetic and natural Fe(II)-Fe(III) green rusts: Occurrences of the mineral in hydromorphic soils. Environ. Sci. Technol. 32, 1058-1068.

Génin, J.-M. R.; Refait, Ph.; Bourrié, G; Abdelmoula, M.; Trolard, F. 2001. Structure and stability of the Fe(II)-Fe(III) green rust "fougerite" mineral and its potential for reducing pollutants in soil solutions. Appl. Geochem., 16, 559-570.

Génin, J.-M. R.; Olowe, A. A.; Refait, Ph.; Simon, L. 1996. On the stoichiometry and Pourbaix diagram of Fe(II)-Fe(III) hydroxy-sulphate or sulphate-containing green rust 2; an electrochemical and Mössbauer spectroscopy study. Corro. Sci. 38, 1751-1762.

Hansen, H. C. B.; Poulsen, I. F. 1999. Interaction of synthetic sulphate "green rust" with phosphate and the crystallization of vivianite. Clay Clay Miner. 47, 312-318.

Hansen, H. C. B.; Koch, C. B.; Nanche-Krogh, H.; Borggaard, O. K.; Sorensen, J. 1996. Abiotic nitrate reduction to ammonium: Key role of green rust. Environ. Sci. Technol. 30, 2053-2056.

Hansen, H. C. B.; Koch, C. B. 1998. Reduction of nitrate to ammonium by sulphate green rust: activation energy and reaction mechanism. Clay Miner. 33, 87-101.

Hansen H. C. B.; Guldberg, S.; Erbs, M.; Koch, C. B. 2001. Kinetics of nitrate reduction by green rusts-effect of interlayer anion and Fe(II):Fe(III) ratio. Appl. Clay Sci. 18, 81-91.

Hansen, H. C. B.; Borggaard, O. K.; 1994. Sorensen, J. Evaluation of the free-energy of formation of Fe(II)-Fe(III)Hydroxide-sulphate (green rust) and its reduction of nitrate. Geochim. Cosmochim. Acta 58, 2599-2608.

Krachler, M.; Emons, H.; Zheng, J. 2001. Speciation of antimony for the 21th century: promises and pitfalls. Trends Anal. Chem. 20, 79-90.

Kumar, A. V. R.; Singh, R.; Nigam, R. K. 1999. Mössbauer spectroscopy of corrosion products of mild steel due to microbiologically influenced corrosion. J. Radioanal. Nucl. Ch. 242, 131-137.

Langmuir, D. In Aqueous Environmental Geochemistry; Prentice–Hall; Upple Saddle River, NJ, 1997.

Lin, Z.; Puls, R. W. 2003. Potential indicators for the assessment of arsenic natural attenuation in the subsurface. Adv. Environ. Res. 7, 825-834.

Loyaux-Lawniczak, S.; Refait, P.; Ehrhardt, J. J.; Lecomte, P.; Genic, J. –M. R. 1999. Trapping of Cr by formation of ferrihydrite during the reduction of chromate ions by Fe(II)-Fe(III) hydroxysalt green rusts. Environ. Sci. Technol. 34, 438-443.

Mitsunobu, S.; Harada, T.; Takahashi, Y. 2006. Comparison of antimony behavior with that of arsenic under various soil redox conditions. Environ. Sci. Technol., 40, 7270-7276.

Mitsunobu, S.; Takahashi, Y.; Sakai, Y. 2008. Abiotic reduction of antimony(V) by green rust ($Fe_4(II)Fe_2(III)(OH)_{12}SO_4 \cdot 3H_2O$). Chemosphere, 70, 942-947.

Myneni, S. C. B.; Tokunaga, T. K.; Brown, Jr. G. E. 1997. Abiotic selenium redox transformations in the presence of Fe(II, III) oxides. Science 278, 1106-1109.

O'Loughlin, E.; Kelly, S. D.; Cook, R. E.; 2003. Csencsits, R.; Kemner, K. M. Reduction of uranium(VI) by mixed iron(II)/iron(III) hydroxide (green rust): formation of UO_2 nanoparticles. Environ. Sci. Technol. 37, 721-727.

Randall, S. R.; Sherman, D. M.; Ragnarsdottir, K. V. 2001. Sorption of As(V) on green rust ($Fe_4(II)Fe_2(III)(OH)_{12}SO_4 \cdot 3H_2O$) and lepidocrocite (γ-FeOOH): surface complexes from EXAFS spectroscopy. Geochim. Cosmochim. Acta 65, 1015-1023.

Refait, P.; Abdelmoula, M.; Génin, J. –M. R. 1998. Mechanisms of formation and structure of green rust one in aqueous corrosion of iron in the presence of chloride ions. Corros. Sci. 40, 1547-1560.

Refait, Ph.; Génin, A.; Abdelmoula, M.; Génin, J.- M. R. 2003. Coprecipitation thermodynamics of iron(II-III) hydroxysulphate green rust from Fe(II) and Fe(III) salts. Corros. Sci., 45, 659-676.

Refait, P; Simon, L.; Genin, J.-M. R. 2000. Reduction of SeO_4^{2-} anions and anoxic formation of iron(II)-iron(III) hydroxy selenate green rust. Environ. Sci. Technol., 34, 819-825.

Roh, Y.; Lee, S. Y.; Elless, M. P.; Foss, J. E. 2000. Incorporation of radioactive contaminants into pyroaurite-like phases by electrochemical synthesis. Clay Clay Miner. 48, 266-271.

Ruby, C.; Génin, A.; Aissa, R.; Ghanbaja, J.; Abdelmoula, M.; Génin, J.- M. R. 2006. Chemical stability of hydroxysulphate green rust synthesized in the prensence of foreign anions: carbonate, phosphate and silicate. Hyperfine Interact. 167, 803-807.

Scheidegger, A. M.; Grolimund, D.; Cui, D.; Devoy, J.; Spahiu, K.; Wersin, P.; Bonhoure, I.; Janousch, M. 2003. Reduction of selenite on iron surfaces: A micro-spectroscopic study. J. Phys. IV 104, 417-420.

Scheinost, A. C.; Rossberg, A.; Venelon, D.; Xifra, I.; Kretzschmar, R.; Leuz, A.-K.; Funke, H.; Johnson, C. A. 2006. Quantitative antimony speciation in shooting-range soils by EXAFS spectroscopy. Geochim. Cosmochim. Acta 70, 3299-3312.

Schwertmann, U.; Fechter, H. 1994. The formation of green rust and its transformation to lepidocrocite. Clay Miner. 29, 87-92.

Sherman, D. M.; Rangnarsdottir, K. V.; Oelkers, E. H.; 2000. Antimony transport in hydrothermal solutions: an EXAFS study of antimony(V) complexation in alkaline sulfide and sulfide-chloride brines at temperatures from 25°C to 300 °C at P_{sat}. Chem. Geol. 167, 161-167.

Su, C. M.; Puls, R. W. 2004. Significance of iron(II,III) hydroxucarbonate green rust in arsenic remediation using zerovalent iron in laboratory column test. Environ. Sci. Technol., 38, 5224-5231.

Svensson, C. 1975. Refinement of the crystal structure of cubic antimony trioxide, Sb_2O_3. Acta Crystallogr. B, 31, 2016-2018.

Trolard, F.; Génin, J.-M. R.; 1997. Abdelmoula, M.; Bourrié, G.; Humbert, B.; Herbillon, A. J. Identification of a green rust mineral in a reductomorphic soil by Mössbauer and Raman spectroscopies. Geochim. Cosmochim. Acta, 63,

1107-1111.

United States Environmental Protection Agency. Water Related Fate of the 129 Priority Pollutants; Doc. 745-R-00-007; USEPA: Washington, DC, 1979; Vol. 1.

Williams, A. G. B.; Scherer, M. M. 2001. Kinetics of Cr(VI) reduction by carbonate green rust. Environ. Sci. Technol. 35, 3488-3494.

Zabinsky, S. I.; Rehr, J. J.; Ankudinov, A.; Albers, R. C.; Eller, M. J. 1995. Multiple-scattering calculations of X-ray-absorption spectra. Phys. Rev. B 52, 2995-3009.

CHAPTER 6 Conclusions

In this study, the speciation of Sb and As in both solid and water phases were successfully conducted understand the reaction of Sb in aquatic environment in detail and to compare the Sb behavior with As examined in mine tailings in a natural system and in a solid-water system simulated in laboratory. This work particularly focused on the "chemical form" of Sb or As controlling the mobility and toxicology. X-ray and Mössbauer spectroscopies and chromatographic analysis such as HPLC were used for speciation methods in both solid and water phases and the findings using these methods were helpful to reveal the Sb, As, Fe species. Since the soil-water system around Ichinokawa mine yielding stibnite (Sb_2S_3) is highly contaminated by Sb and As compared with natural environment and the source is the polluted water from Sb mine tailing, the environment similar to this site is especial and may not often occur in the real environment. However, the knowledge obtained in this study contains many important information to understand the Sb behavior in aquatic environment under various redox conditions, which the information has not been reported previously. The findings obtained in each chapter are summarized in following section.

In Chapter 2, the oxidation states and host phases of Sb and As in soil samples around Sb mine tailing (Ichinokawa mine, Ehime, Japan) and in laboratory soil-water system were investigated using XAFS and HPLC-ICP-MS combined with the partition behaviors of Sb and As in soil-water system (Figure 6-1):

(1) Ichinokawa soil was heavily contaminated by Sb and As and the bulk XRF analyses showed that the abundances of Sb and As range 8870-11200 mg/kg and 1160-1960 mg/kg in the soil collected, respectively. EPMA and XRD analyses indicate that stibnite was not present in all the soil samples, which suggests that the source of Sb concentrated in soil is not the stibnite but the Sb secondarily leached into aqueous phase from stibnite, and that the information on secondary behavior for Sb can be obtained from this soil-water system.

(2) In the Ichinokawa soil and water systems, Sb was present dominantly as the oxidized

form, Sb(V), over a wide redox range (from Eh = 360 to –140 mV, pH 8), while As was present as a mixture of As(III) and As(V). This finding was confirmed in the laboratory experiments. These results suggest that Sb(V) is a very stable form in the environment and that Sb is oxidized under more reductive condition than As.

(3) Combining the results of Fe and Mn XAFS analyses with a positive correlation among Sb, As, and Fe abundances in the soil, it is suggested that the host phases of Sb and As are amorphous Fe(III) hydroxide under all redox conditions. Direct speciation by Sb and As EXAFS analyses are also consistent with this finding.

(4) Under more reducing condition, the concentration of As in the soil water increased in both the Ichinokawa and laboratory systems. The speciation of As in soil and water phases suggests that the leaching of As under reducing condition depends on (i) the reductive dissolution of Fe(III) hydroxides, host phase for As in soil and (ii) the reduction of As(V) to As(III), since As(III) is liable to partition to the aqueous phase more readily than As(V) (Bowell, 1994; Smedley and Kinniburgh, 2002).

(5) On the other hand, the concentration of Sb in soil water decreased under reducing condition. Since Sb oxidation states in present system was mainly Sb(V) and did not change with redox condition, changing of Sb species is not the controlling factor of the Sb decrease in water phase. Under reducing condition, (i) dissolution reaction due to the reduction of Fe(III) to Fe(III) and (ii) reprecipitation reaction with the oxidation to Fe(III) hydroxide may be dynamically occurring in the system. When a structural order of Fe(III) hydroxides decrease, the Fe(III) hydroxides have a larger surface area and stronger adsorptive potential (Richmond et al., 2003). It is speculated that the larger surface area of disordered Fe(III) hydroxides under more reducing condition leads to the larger partition ratio of Sb to soil. To reveal this hypothesis, detail speciation of Fe hydroxides in soil was done in following chapter, Chapter 3.

In Chapter 3, characterization of Fe(III) hydroxides, host phases of Sb and As, in the Ichinokawa soil collected under various redox conditions was conducted in detail, and the effect of the change of redox condition on the morphology of Fe(III) hydroxides such

as particle size, crystallinity, and surface area was examined (Figure 6-2):

(1) Iron is mainly present as Fe(III) hydroxides, like ferrihydrite, over a wide redox range (from Eh = 360 to −140 mV) based on the XAFS and Mössbauer analyses.

(2) The crystallinity of ferrihydrite in soil slightly decreased under reducing condition (at deeper part). This fact suggests that in the redox range of this study, the Fe species remains as ferrihydrite under the redox condition, but the morphology of amorphous Fe(III) hydroxides such as the particle size and the structural order can change with the progress of reducing condition.

(3) This finding obtained in the present study is important for understanding the behaviors of As and other elements in soil-water system. In the natural soil-water system examined here where As concentration and As(III)/As(V) ratio in soil water increased with the progress of reducing condition, it was shown that Fe(III) hydroxides phase keeps its potential, or even has a larger potential with depth as a host phase of As. Therefore, we can conclude that As release from the soil largely depends on the higher mobility of As(III) than As(V), rather than reductive dissolution of Fe(III) hydroxides.

(4) Although the structural order of Fe(III) hydroxide decreases under reducing condition, the extent of the variation is low. Thus, increase in the adsorptive potential of Fe(III) hydroxides with the decrease of the structural order is also too low to explain the larger partition of Sb into soil under more reducing condition observed. Another factor controlling the Sb partition behavior under reducing condition should be reconsidered.

In Chapter 4, microscopic speciation and characterization for Sb and Fe in Ichinokawa soil grain were investigated by EPMA and μ-XAFS analyses to observe the local elemental distributions of Sb, As, Fe, Mn, Ca, and Si in soil and to understand why Sb partition into soil phase in soil-water system is enhanced under reducing condition (Figure 6-3):

(1) The abundances of Sb and As correlate with that of Fe in all Sb hot-spots in soil. In addition, Fe μ-XANES showed the Fe species in Sb hot-spot is Fe(III) hydroxides.

Thus, these findings indicate that host phases of Sb and As in soil are Fe(III) hydroxide. This is agreeable with the bulk Sb and As EXAFS analyses shown in Chapter 2.

(2) Iron and Sb hosting mineral ($Fe^{III}Sb^{V}O4$, tripuhyite) was found in a soil grain in Ichinokawa soil based on both EPMA quantitative analysis and μ-XANES analysis. It is suggested that this mineral is authigenically deposited from aqueous phase during soil sedimentation. This is first report of authigenic tripuhyite mineral in the soil.

(3) In other Sb hot-spots, Sb exists as coprecipitated or adsorbed form with Fe hydroxides based on the quantitative analyses.

(4) Elemental distributions in X-ray maps shows that detrital grains such as quartz and biotite in Sb hot-spots were covered with Fe hydroxides and Sb was concentrated in the Fe hydroxides part of the grain. Moreover, significant Sb(III) (Sb(III) = 15-22%) was locally observed at the rim of the Fe hydroxides part, while Sb(III) was not exclusively observed at the center part. It is reported that the solubility of Sb(III) is much lower than that of Sb(V) (Filella et al., 2002), and the Sb(III) was also slightly observed in both soil and soil water phases under reducing condition in bulk analysis (Chapter 2). Therefore, the findings obtained by the microscopic analysis suggest that Sb reduced to Sb(III) was precipitated on the mineral surface due to its low solubility and that the precipitates containing Sb(III) like Sb_2O_3 may cause the fixation of Sb to solid phase under reducing condition.

In Chapter 5, interaction of Sb(V) with Fe(II)/Fe(III) hydroxide (green rust, GR) was investigated to examine whether green rust can be as a reducer of stable Sb(V), which the green rust occurs in many suboxic soil and sediment and are considered to be strong abiotic reducer of many inorganic contaminants (Figure 6-4).

(1) Sb(V) is partly reduced by sulphate green rust, suggesting that green rust can be one of the important reducing agents for Sb(V), and that GR can influence the Sb mobility in suboxic environments where green rust is formed.

(2) It was shown that Sb(V) is adsorbed to GR with an inner-sphere complex on the surface, and that the surface complex species is a mixture of edge- and corner-sharing

complexes based on EXAFS analysis.

(3) Stabilization of "metastable" GR by the presence of Sb is firstly observed, moreover GR stability gradually increased with Sb concentration in aqueous phase in the range of this study. This stabilization effect for GR is also reported on other oxyanions that is adsorbed to GR with the formation of an inner-sphere complex such as phosphate, arsenate, and silicate. Thus, the Sb inner-sphere complex to GR also contributes to the GR stabilization by Sb.

(4) In a sample where a large amount of Sb was adsorbed in interlayer, partial reduction of Sb(V) to Sb(III) was observed, suggesting that Sb accessibility into the interlayer of GR may be one of the important keys for Sb(V) reduction. Therefore, the binding complex and the site of Sb adsorbed on GR are of importance in understanding of reaction between Sb and GR, including adsorption and reduction in an aquatic environment.

Integrating the findings obtained from all the chapters, it is finally concluded that the change of Sb solubility accompanied with change of the oxidation state would control the partition behavior in soil-water system under various redox conditions, since the solubility and complexation properties strongly depend on the oxidation state for Sb. Therefore, to comprehend the fate and transport of Sb in aquatic environment, the "determination of the species", particular oxidation states, is much important. In addition, the different redox properties of Sb and As observed in present study is of great importance to an understanding of the behaviors of As and Sb and their fractionation in natural aquifer.

In Appendix 1, a simple method for the observation of the kinetics of the reactions at the solid-water interface was developed using quick XAFS (X-ray absorption fine structure) combined with a column reactor. We applied the method to the oxidation reaction of As(III) by Mn oxide (δ-MnO_2), a strong oxidizer in natural systems. A reliable reaction rate constant k', 3.86×10^{-4} $\%^{-1}min^{-1}$ at pH 7.1, was obtained, where the effect of photooxidation under X-ray beam can be eliminated. Considering the average Mn/As

molar ratio in the system, the value is reasonable compared with other reported values. Since this method is very simple, we will apply it to various elements and reaction systems at the solid-water interface as a tool to understand the kinetics of various reactions including various reactions of Sb in the future.

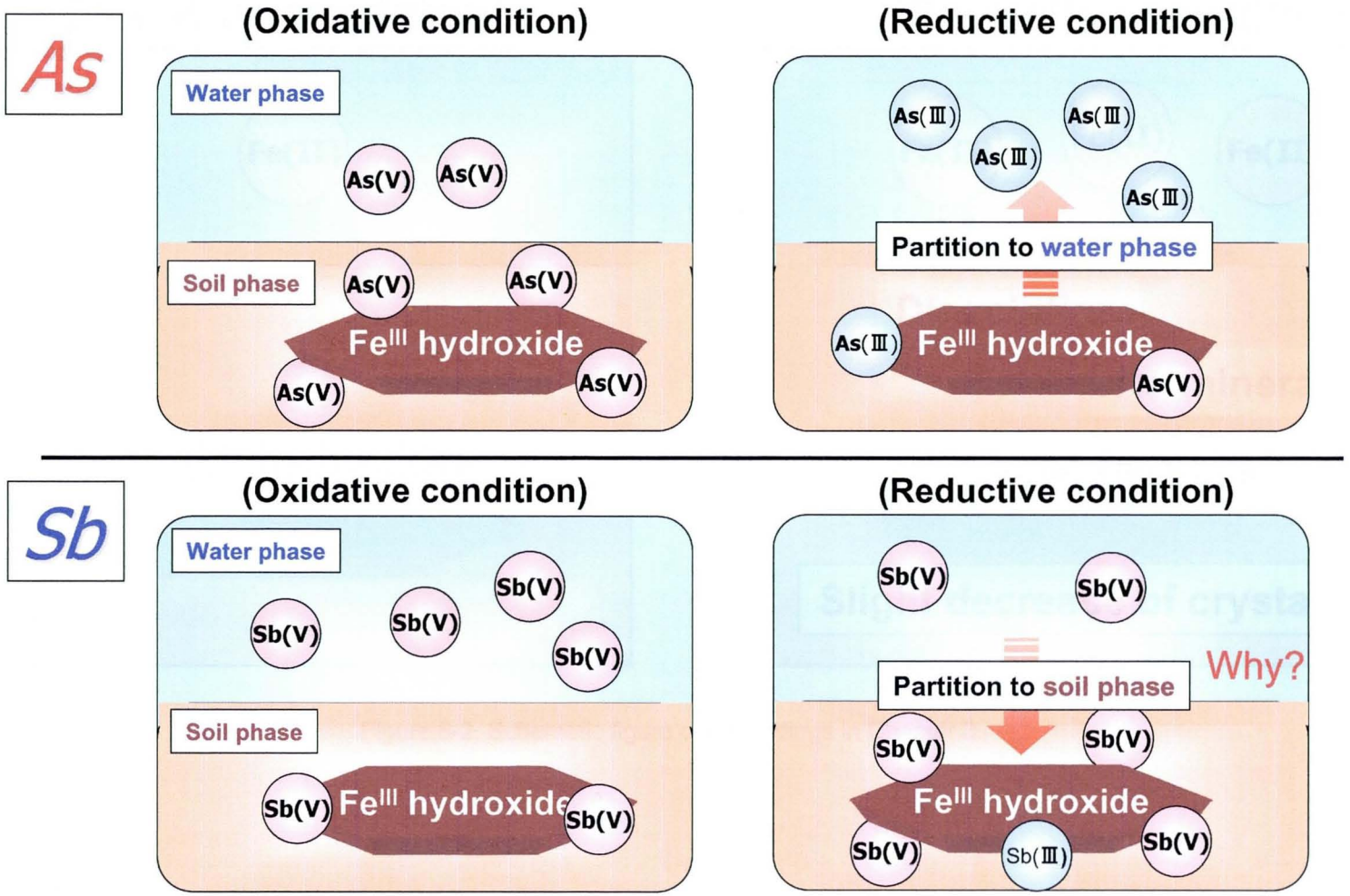

Figure 6-1. Schematic figure of the findings described in Chapter 2.

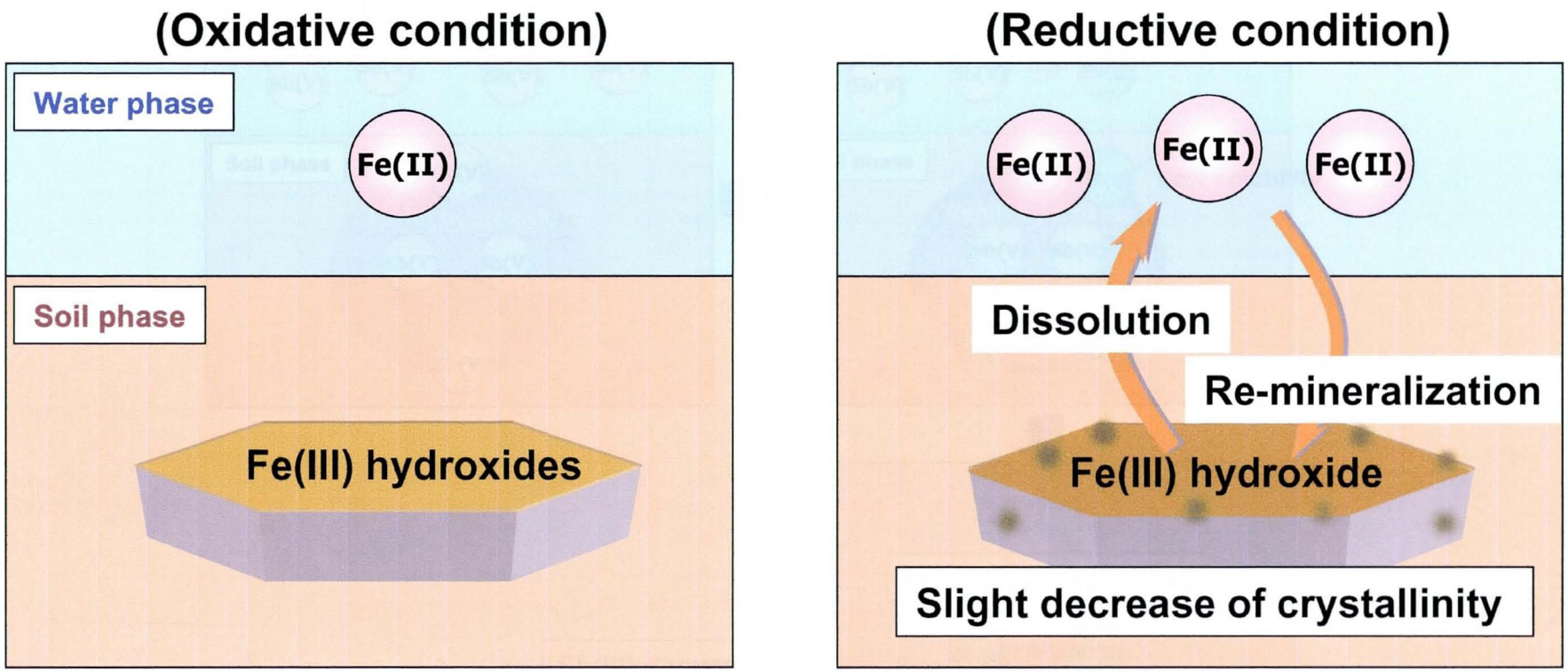

Figure 6-2. Schematic figure of the findings in Chapter 3.

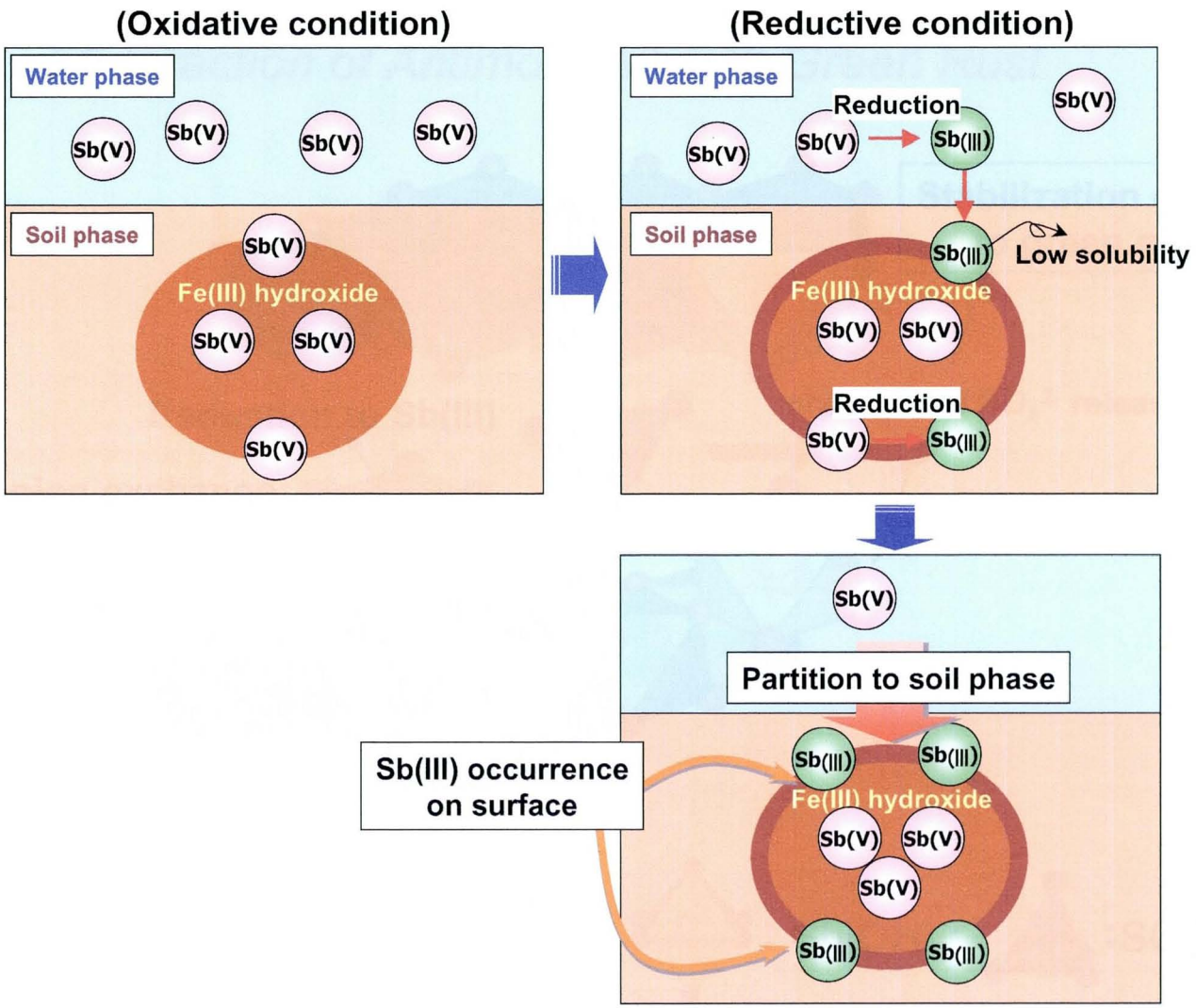

Figure 6-3. Schematic figure of the findings in Chapter 4.

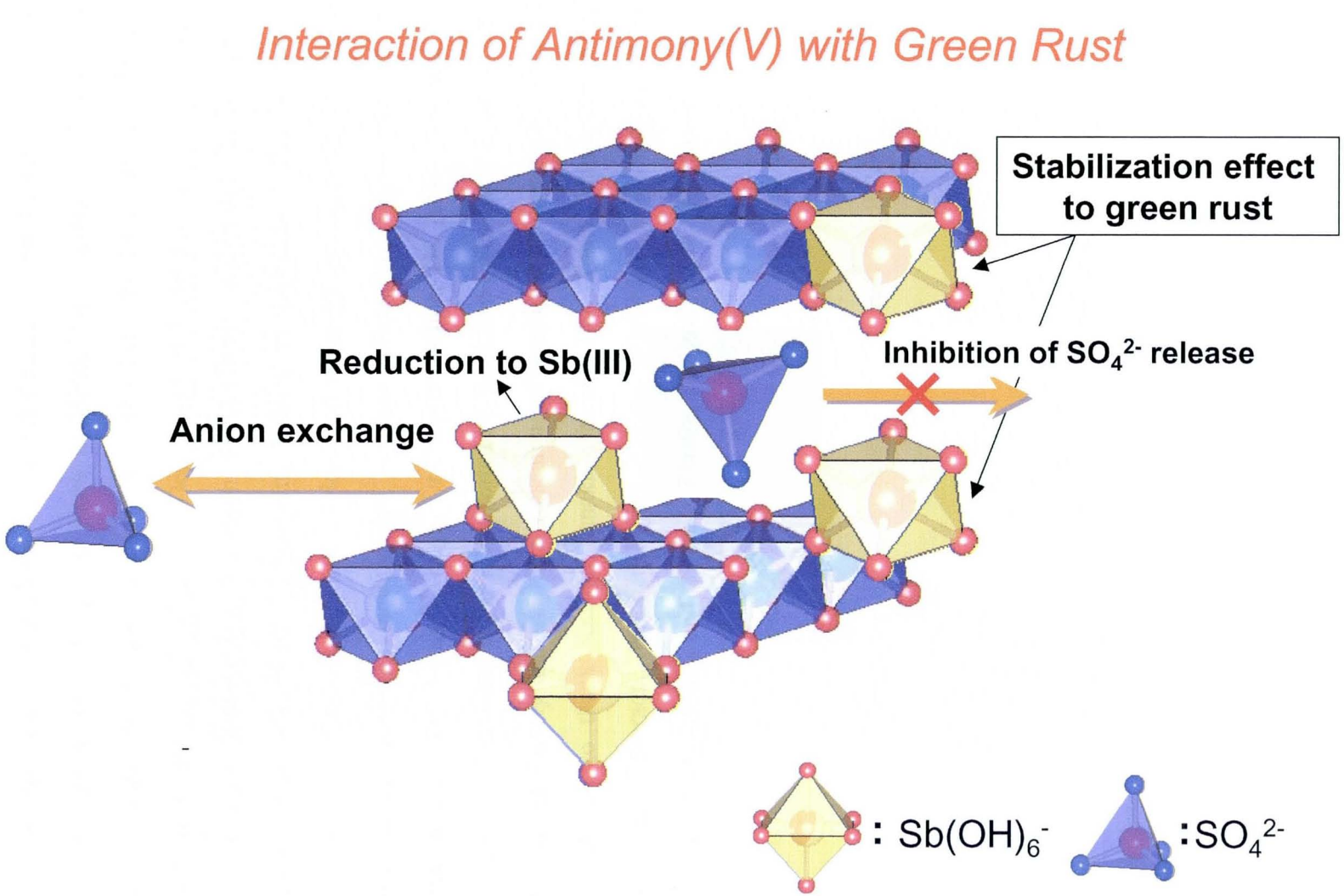

Figure 6-4. Schematic figure of the findings in Chapter 5.

Acknowledgement

I would like to deeply thank Dr. Yoshio Takahashi and Prof. Hiroshi Shimizu for their patient supervision during six years in Hiroshima University. Thanks are extended to helpful instructions and reviewing the thesis by Profs. Fumiko Tajima, Ryuji Kitagawa, and Hiroshi Hidaka in Department of Earth and Planetary Systems Science, Hiroshima University. Dr. Yoichi Sakai (Daido Institute of Technology in Nagoya) provided significant supports in Mössbauer analyses. The following colleagues are also thanked for their advices and technical assistance in Hiroshima University and at synchrotron facilities: Mr. Yasuhiro Shibata, Mr. Hayami Ishisako, Dr. Masaharu Nomura, Dr. Tomoya Uruga, Dr. Hajime Tanida, Dr. Atsuo Iida, and Dr. Yasuko Terada. This work is partly supported by Sasakawa Scientific Research Grant from The Japan Society and the JSPS Research Fellowships for Young Scientists. I also would like to thank Kazuya Tanaka, Takaaki Itai, Yuhei Yamamoto, Kenji Furukawa, Teppei Harada, Tomonari Fujimoto, Yoko Shimamoto, and the others in our laboratory for many advices and cheers. Finally, I'm grateful to my parents for their supports.

Appendix 1

A new method to observe the reactions at solid-water interface

Introduction

Recently, the environmental and human health impacts of elevated concentrations of arsenic (As) in groundwater have received increased attention because of its toxicity (WHO, 1997; Dhar et al., 1997; Bhattacharya et al., 1997). The predominant forms of As in the environment are as inorganic arsenate (As(V)) and arsenite (As(III)) (Aurillo et al., 1994; Hansen et al., 1992; Masscheleyn et al., 1991; Tye et al., 1985). As a water contaminant, As(III) is more problematic than As(V). Unlike the arsenate anions $H_2AsO_4^-$ and $HAsO_4^{2-}$, the dominant As(III) species up to pH 8 is the nonionic H_3AsO_3, which does not adsorb onto mineral surface as strongly as As(V) (Manning and Goldberg, 1997a-b). The As(III) species is substantially more toxic than As(V) (Knowles and Benson, 1983; Coddington, 1986). Therefore, it is important for the geochemistry and toxicology of As to determine its oxidation state. In natural systems, Mn oxide can be the strong oxidizer and sorbent for various trace elements including As because of its high oxidative capability, high adsorptive capacity, and large abundance in the environment. Considering the environmental fate of As, the oxidation of As(III) by Mn oxide is an important reaction. Although details about the chemical mechanism of As(III) by amorphous Mn oxide have been reported (Moore et al., 1990; Nesbitt et al., Scott and Morgan, 1995; Oscarson et al., 1983), more information is needed for the kinetics of the oxidation of As(III) to As(V).

In this study, to observe the kinetics and dynamics in the oxidation process of As(III) by Mn oxide, we applied a new method that combines a column reactor with the time-resolved measurement of As species at the solid-water interface using quick XAFS (QXAFS) technique (Frahm, 1998). In the conventional XAFS measurement using a step scan for whole energy range, a long time (20 min to 1 h) is required to collect the spectrum. On the other hand, the monochromator is moved continuously in the QXAFS mode. As a result, the quick measurement, less than several seconds to minutes, becomes possible. In particular, a short time scale observation is required for the

observation of As oxidation by Mn oxide, since the oxidation of As(III) by Mn oxide is rapid. In addition, the column reactor enables us to observe directly the reaction at the solid-water interface with minimum interference of the dissolved As in the water phase as compared to a batch reactor. This method directly observes the reaction at the solid-water interface, which is clearly better than other methods measuring As(III) and As(V) dissolved in the aqueous phase or extracted from the solid phase by some leaching agent (such as phosphate) (Manning and Goldberg; 1997a,b) to examine the oxidation at the solid-water interface. The application of this method allows us to gain better understanding of the various reaction processes at the solid-water interface.

Materials and Methods

Synthesis of δ-MnO_2. δ-MnO_2 was prepared by the oxidation of Mn(II) ion by permanganate following the procedures of Murray (Murray, 1974). A 1.0 M $Mn(NO_3)_2$ solution (7 ml) was slowly added to 400 ml of a stirred 35 mM KOH solution, containing 4.2 mmol $KMnO_4$. The X-ray diffractometer diffraction analysis (XRD; MAC Sci., M18XHF) of the dried samples gave broad and diffuse reflection peaks which are the characteristics of δ-MnO_2. The δ-MnO_2 was dried in air for 24 h at 50°C and passed through a 250-μm sieve prior to use.

Column Reactor. A small disposable polystyrene column with an inner diameter of 10 mm was used as the reactor to investigate the oxidation of As(III) with Mn oxide (Figure A-1). As the amorphous Mn oxide, 0.025 g (dry weight) δ-MnO_2 was packed into the column (height of δ-MnO_2 layer: 5 mm). A 1 ml of a 1050 mg kg^{-1} As(III) solution was introduced into a column reactor with the outflow port closed. Using a peristaltic pump (EYELA, MP-1100) connected to the outlet of the column, the As(III) solution started to flow into the δ-MnO_2 layer, initiating the oxidation reaction. The switch of the pump was operated by remote control to investigate the reaction outside of the experimental hutch at the beamline. The oxidation experiment was conducted at 27 ± 2°C. The pH value in the column was obtained by measuring the pH in the filtrate with a glass electrode (Horiba, D-51). The total As sorbed on the solid was estimated by determining the concentration of As in the filtrate by inductively coupled

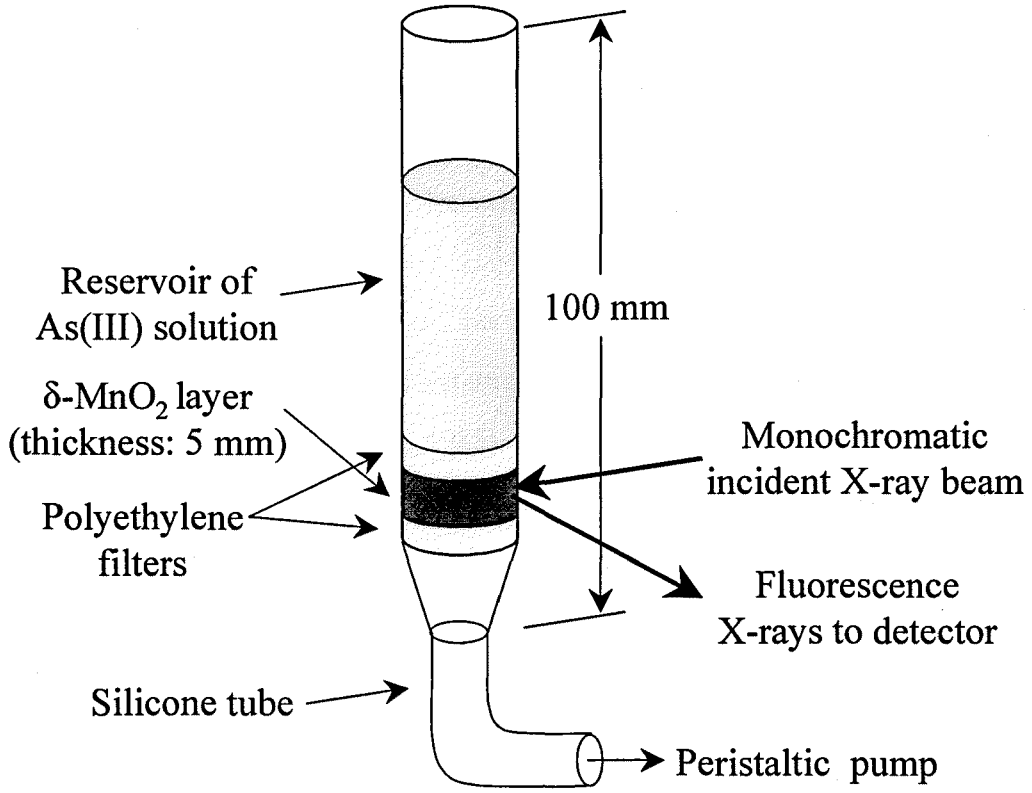

Figure A-1. Schematic figure of the column reactor.

plasma-mass spectrometry (ICP-MS; VG, PQ-3). The result shows the average Mn/As molar ratio of 730 in the δ-MnO_2 layer. Concentrations of Mn and As at the exact point exposed to X-ray beam can be determined *in situ* by measuring the intensities of fluorescence X-rays by this method, though this was not conducted in the present study.

Quick XAFS measurement and analysis. Quick XAFS measurements were performed at the BL01B1 in the SPring-8 (Hyogo, Japan). A Si(111) double crystal monochromator was used to obtain a monochromatic X-ray beam. Quick XAFS measurements of the As K-edge were carried out in fluorescense mode using a Lytle detector. The Si(111) monochromator was moved from 9.63° (11.836 keV) to 9.00° (12.638 keV) in 1 min. The beam size was 4 mm (horizontal) × 0.2 mm (vertical) at the sample position. The energy of X-ray was calibrated with As_2O_3 as a reference. The measurements were conducted at 27 ± 2°C under ambient air condition. For the EXAFS analysis, the EXAFS oscillation was extracted from the measured spectra by a spline smoothing method (Zon et al., 1985). The Fourier transformations of the $k^3\chi(k)$ EXAFS oscillation from k space to r space were performed in a range 3.0 – 10.3 $Å^{-1}$ to obtain a radial structural function (RSF) for As in all spectra. Simulations of XANES spectra of the sample using the As(III) ($KAsO_2$) and As(V) (KH_2AsO_4) solutions were conducted following the procedure done by Takahashi et al (2003). This fitting procedure was performed with the range of 11.860 – 11.873 keV.

Results and Discussion

Figures A-2A and -2B show the time-resolved As K-edge XANES spectra of As(III) solution (pH 7.0) and of As(III) on δ-MnO_2, respectively. Without δ-MnO_2, no appreciable shift of As absorption edge was observed during X-ray exposure for 40 min (Figure A-2A). On the other hand, in the As(III)/δ-MnO_2 system, the absorption edge of As shifted to higher energy with time (Figure A-2B), showing the rapid oxidation of As(III) by δ-MnO_2. These results suggest that the formation of As(V) due to the oxidation induced by oxygen and incident X-ray is a minor fraction (4%) in this time scale in our system. The ratio of dissolved As to the As sorbed on δ-MnO_2

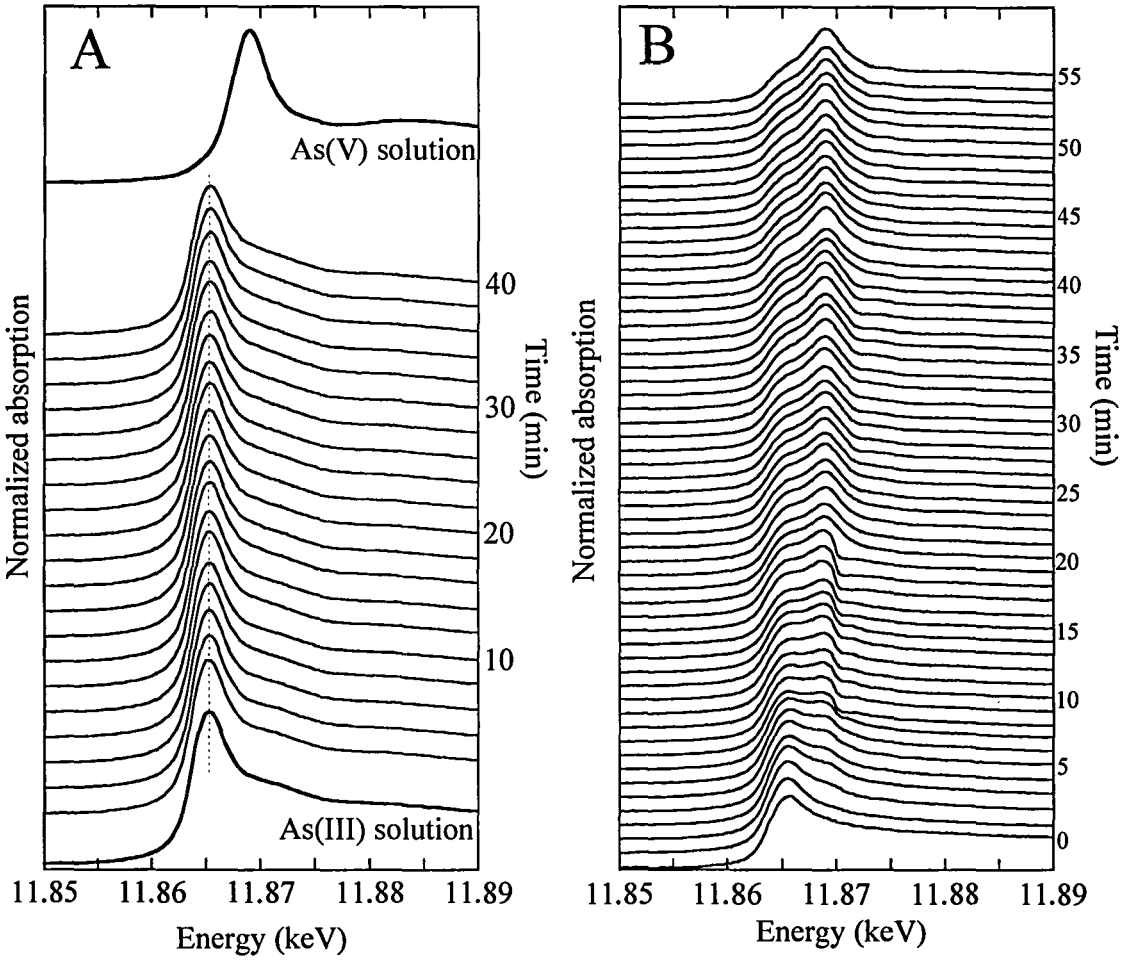

Figure A-2. Arsenic K-edge XANES spectra of (A) As(III) solution in the absence of δ-MnO_2 and (B) As(III)/δ-MnO_2 system. A line is drawn to indicate the maximum absorption of As(III) in Fig. A-2A.

at the point exposed to the incident X-ray beam was less than 1%, estimated from the water content in the slurry of δ-MnO_2 and As concentration in the outflow solution. This fact shows that the XANES spectra reflects the As species at the solid-water interface.

Figure A-3A shows the As(III) and As(V) ratio obtained by the simulation of XANES spectra during the oxidation reaction of As(III). Initial ratios of As(III) and As(V) are 100% and 0%, respectively. Arsenic(III) was rapidly oxidized by δ-MnO_2, and about 50% of the original As(III) added was oxidized to As(V) for 20 min (Figure A-3A). Many reserchers reported that the net stoichiometry of the oxidation of As(III) by δ-MnO_2 is (Moore et al., 1990; Nesbitt et al., 1998; Scott and Morgan, 1995; Oscarson et al., 1983)

$$MnO_2 + H_3AsO_3 + 2H^+ = Mn^{2+} + H_3AsO_4 + H_2O \quad (1)$$

The decrease of As(III) in this study follows a second order reaction kinetic, as shown by the linear relation in the time dependence of 1/As(III) – 1/As(III)$_0$ (As(III): the percentage of As(III) fraction) in Figure A-3B. Heterogeneous reactions such as the reaction of ions with amorphous solid generally follow a first order or pseudo first oder kinetics, since it is postulated that the number of the reaction sites is excessive compared with that of As(III). However, it is possible that the masking of reaction sites by the reaction products reduces the number of the site, which results in a fast initial decrease of As(III), followed by a slower rate. This leads to a second order reaction for this system as reported in other study,[20] the model of which is also employed in this study.

The rate constant (k') value based on the second order reaction is 3.9×10^{-4} $\%^{-1}$ min^{-1} at pH 7.1, which was obtained by the least-squares fitting of the plot, as shown in Figure A-3B. Several data points before 12 min are not on the regression line. Although the details of the reason are not clear at present, it is possible that the As(III) oxidation was induced by X-ray beam at an initial time range. Ona-Nguema et al. reported that the As(III) sorbed on the Fe oxide was partly oxidized by incident X-ray and the oxidation terminated at a certain As(III)/As(V) ratio within a short time (< 30 min).[21] In this study, the As(V) ratio in the absence of δ-MnO_2 slightly increased upto

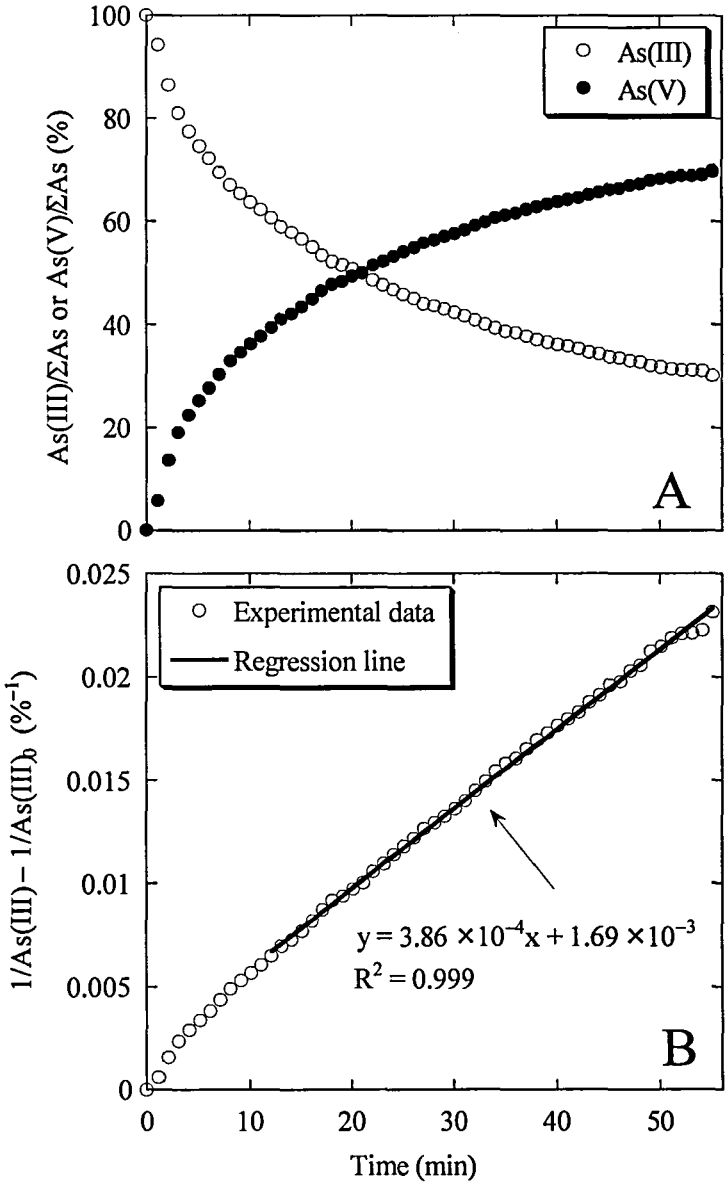

Figure A-3. (A) Decrease of As(III) and formation of As(V) during the oxidation of As(III) by δ-MnO_2. (B) Relationship between elapsed time and 1/As(III) – 1/As(III)$_0$ (As(III): percentage of As(III) fraction; As(III)$_0$ = 100%).

4% within 10 min and reached an equiliburium. Subsequently, the abundance of As(V) became constant during the measurement in the absence of δ-MnO_2 (data not shown). These results suggest that the steep slope during initial time range in the As/δ-MnO_2 system (Figure A-3B) is likely caused by the incident X-ray. Despite the effect at the initial time range, the obtained *k'* value does not change within 4.2% by including several data points in the least-squres fitting. We did the whole experiment twice independently, showing that the difference of the duplicate data of *k'* value was within 10%.

The validity of our *k'* value is discussed by means of comparison with other reports. The reported *k'* values calculated according to the second order reaction range from 2.9×10^{-5} to 2.6×10^{-3} $\%^{-1}$ min^{-1} (note that some values are recalculated here based on the second order reaction).[12,20,22] Our *k'* value is within the range, showing that the present *k'* value may be valid considering other reported data. The results suggest that the effect of incident X-ray beam which may apparently increase the *k'* value is not important in our system.

In many previous works, the oxidation rate is determined indirectly by measuring concentrations of As(III) and As(V) dissolved in aqueous phase (Driehaus et al., 1995; Manning et al., 2002). The rate constant obtained by this method includes the sorption/desorption processes of As(III) and As(V). Since the sorption coefficient of As(III) and As(V) are different, the *k'* value obtained by such method may include some ambiguities. On the other hand, the *k'* value obtained in our system reflects only the oxidation of As(III) by δ-MnO_2 at the solid-water interface. This point is a highlight of the method based on the observation of the oxidation kinetics using QXAFS.

The oxidation kinetics has also been reported based on the speciation of As on the solid using some extractants. In this case, the concentration of adsorbed species was quantified by measuring the increase in the concentration of As(III) and As(V) species in the solution after diplacement with a competing adsorbate or exhaustive digestion (i. e., dissolution) of the solid (Moore et al., 1990; Manning and Goldberg, 1996; Manning and Goldberg, 1997a,b; Chiu and Hering, 2004). Excess phosphate

has been used to desorb As(III) and As(V) from sediments, fly ash, and soils and to assess the extent of As(III) oxidation at the surface of clay minerals, but the displacement is slow and often incomplete (Manning and Goldberg, 1996; 1997a,b). Digestion with hot 4 M HCl has been used to extract As(III) and As(V) from lacustrine sediments (Ficklin, 1990) and to follow the oxidation process of As(III) by δ-MnO_2 (Moore et al., 1990), but the method is not applicable for the oxidation kinetics on the time scale of minutes to hours. The method developed in the present study using QXAFS is simple without any pretreatments. It also enables us to follow the As(III) oxidation in a short time scale from several seconds to minutes.

Time-resolved Fourier Transform of the $k^3\chi(k)$ EXAFS for As(III)/δ-MnO_2 system is presented in Figure A-4. The RSFs of As sorbed on δ-MnO_2 have one prominent peak near 1.25 Å (phase shift uncorrected) due to oxygen coordinating to As atom and another prominent peak of the second coordination shell near 2.7 Å due to As-Mn coordination (Farquhar et al., 2002; Foster et al., 2003), respectively. The first shell due to As-O shifts slightly to shorter distance with time due to the bond length of As(V)-O that is smaller than that of As(III)-O (Farquhar et al., 2002). The magnitude of As-O shell in Figure A-4 increases with time. This result suggests that the coordination number of oxygen increases due to the oxidation of As(III) to As(V). Although the variation of EXAFS spectra in Figure A-4 is simply due to the increase of the As(V)/As(III) ratio with time, the present results show that the method can be applied not only to the kinetic study but also to the characterization of local structure during reaction by EXAFS analysis.

Conclusions

A simple method for *in situ* observation of the oxidation of As(III) by QXAFS combined with the column reactor has been developed in this study. This method has been shown to have multi-merits in that (1) the obtained rate constant *k'* reflects only the oxidation reaction at the solid-water interface, while other indirect methods measuring the species in the solution include sorption/desorption processes to observe the redox reactions at the interface, (2) the use of column reactor minimizes the

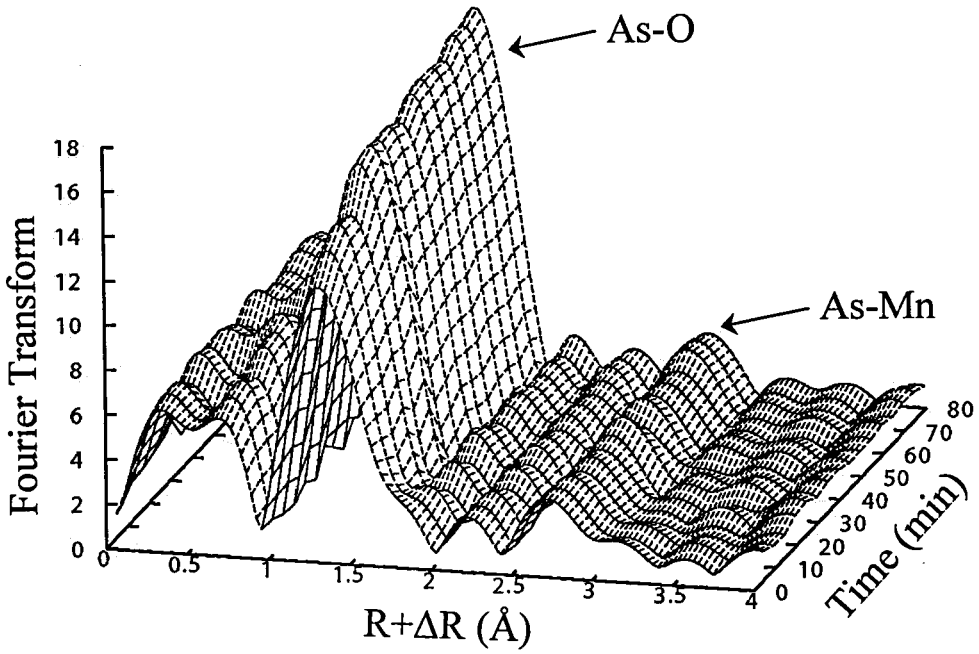

Figure A-4. Radial structure functions (phase shift is uncorrected) for As during the oxidation of As(III) by δ-MnO_2.

interference of dissolved species with the XAFS measurement, (3) time-resolved XANES and EXAFS analyses enable us to study redox reactions and structural change during the reaction. Moreover, since this method is very simple, we can apply it to various elements and reaction systems at the solid-water interface.

References

Arsenic contamination of groundwater and its remedial action plan in West Bengal. AIIH&PH. In Consultation on arsenic drinking water and resulting arsenic toxicity in India and Bangladesh; World Health Organization: New Delhi, India, 1997.

Dhar, R. K.; Biswas, B. K.; Samanta, G; Mandal, B. K.; Chakraborti, D.; Roy, S.; Jahar, A.; Islam, A.; Ara, G.; Kabir, S.; Khan, A. W.; Ahmed, S. A.; Hadi, S. A. 1997. Curr. Sci. 73, 48-59.

Bhattacharya, P.; Chatterjee, D.; Jacks, G. Int. J. 1997. Water Res. Manage. 13, 79-92.

Aurillo, A. C.; Mason, R. P.; Hemond, H. F. 1994. Environ. Sci. Technol. 28, 577-585.

Hansen, S. H.; Larsen, E. H.; Pritzl, G.; Cornatt, C. 1992. J. Anal. At. Spectrom. 7, 629-634.

Masscheleyn, P. H.; Delaune, R. D.; Patrick, W. H., Jr. 1991. J. Environ. Qual. 20, 522-527.

Tye, C. T.; Haswell, S. J.; O'Neil, P.; Bancroft, K. C. C. 1985. Anal. Chim. Acta 169, 195-200.

Manning, B. A.; Goldberg, S. 1997a. Environ. Sci. Technol. 31, 2005-2011.

Manning, B. A.; 1997b. Goldberg, S. Soil Sci. 162, 886-895.

Knowles, F. C.; Benson, A. A. 1983. Trends Biochem. Sci. 8, 178-180.

Coddington, K. 1986. Toxicol. Environ. Chem. 11, 281-290.

Moore, J. N.; Walker, J. R.; Hayes, T. H. 1990. Clays and Clay Miner. 38, 549-555.

Nesbitt, H. W.; Canning, G. W.; Bancroft, G. M. 1998. Geochim. Cosmochim. Acta 62, 2097-2110.

Scott, M. J.; Morgan, J. J. 1995. Environ. Sci. Technol. 29, 1898-1905.

Oscarson, D. W.; Huang, P. M.; Liaw, W. K.; Hammer, U. T. 1983. Soil Sci. Soc. Am. J. 47, 644-648.

Frahm, R. 1988. Nucl. Instrum. and Methods, A270, 578.

Murray, J. W. J. 1974. Colloid Interface Sci. 46, 357-371.

Van Zon, J. B.; Koningsberger, D. C.; Van Blik, H. F. J.; Sayers, D. E. J. 1985. Phys. Chem. 82, 5742.

Takahashi, Y.; Ohtaku, N.; Mitsunobu, S.; Yuita, K.; Nomura, M. 2003. Anal. Sci. 19, 891-896.

Driehaus, W.; Seith, R.; Jekel, M. 1995. Wat. Res. 29, 297-305.

Ona-Nguema, G.; Morin, G.; Juillot, F.; Calas, G.; Brown, G. E., Jr. 2005. Environ. Sci. Technol. 39, 9147-9155.

Manning, B. A.; Fendrf, S. E.; Bostick, B., Suarez, D. L. 2002. Environ. Sci. Technol. 36, 976-981.

Farquhar, M. L.; Charnock, J. M.; Livens, F. R.; Vaughan, D. J. 2002. Environ. Sci. Technol. 36, 1757-1762.

Foster, A. L.; Brown, G. E., Jr.; Parks, G. A. 2003. Geochim. Cosmochim. Acta 67, 1937-1953.

Manning, B. A.; Goldberg, S. 2003. Soil Sci. Soc. Am. J. 60, 121-131.

Ficklin, W. H. 1990. Talanta 37, 831-834.

Chiu, V. Q.; Hering, J. G. 2000. Environ. Sci. Technol. 34, 2029-2034.